Coordinated control of wind power and combined AC-DC grid

Wang, Pengda

Publication date:
2021

Document Version
Publisher's PDF, also known as Version of record

COORDINATED CONTROL OF WIND POWER AND COMBINED AC-DC GRID

Pengda Wang

Kongens Lyngby 2021
CEE-PhD-2021

Coordinated Control of Wind Power and Combined AC-DC Grid

Author:
Pengda Wang

Supervisors:
Senior Scientist: Guangya Yang, CEE, DTU
Associate Professor: Qiuwei Wu, CEE, DTU
Postdoc: Menglin Zhang, CEE, DTU

Center for Electric Power and Energy
Eletrovej, Bygning 325, 1st floor
2800 Kgs. Lygnby
Denmark

Dissertation Examination Committee
Senior Researcher: Henrik W. Bindner
Department of Electrical Engineering, Technical University of Denmark, Denmark

Professor: Vladimir V. Terzija
Center for Energy Science and Technology, Skolkovo Institute of Science and Technology, Russian

Professor: Lie Xu
Department of Electronic and Electrical Engineering, University of Strathclyde, UK

Release date: October 2021

Class: 1 (public)

Edition: 1st Edition

Comment: This dissertation is submitted to the faculty of Department of Electrical Engineering at Technical University of Denmark in partial fulfillment of the requirements for the degree of PhD.

PREFACE

This thesis is prepared at the Department of Electrical Engineering of the Technical University of Denmark in partial fulfillment of the requirements for acquiring the degree of Doctor of Philosophy in Engineering.

This dissertation summarizes the work carried out by the author during his Ph.D. project. It started on 15th October 2018, and it was completed on 14th October 2021. During this period, he was a Ph.D. student at the Center for Electric Power and Energy (CEE), Department of Electrical Engineering, Technical University of Denmark (DTU).

The thesis is composed of 5 chapters and is based on 4 papers.

October 2021

ABSTRACT

With the increasing number and size of wind farms (WFs), the wind power fluctuations and the interaction between large-scale WFs and the power system have introduced several technical challenges. These include voltage profile regulation, optimal power distribution, as well as increased computational and communicational burden of system operators. In addition, due to the physically coupled grid and WFs, and limited coordination among transmission system operator and WF operators, the current transmission system operator and WF operators are almost "blind" to each other's system control and operation. As such, the present voltage control cannot fulfill the system-level goals of grid operation while also achieving optimal voltage regulation of the WF without the loss of global optimality. Thus, this thesis proposes a coordinated optimal voltage control strategy for AC-DC grid with large-scale WFs in order to achieve global optimal voltage management.

The massive amount of wind power generated from remote onshore and offshore WF clusters need to be transported to power system by transmission system. Thus, it is necessary to efficiently coordinate the operation of the transmission system and the individual WFs. Therefore, one focus of this thesis is to propose a distributed active and reactive power control scheme for a strongly coupled transmission system and WFs. The developed optimal power flow (OPF) of the transmission system is relaxed while the branch flow model is applied to the model of the wind power collection system. The proposed scheme can realize the global optimal power control of the whole system to minimize power losses taking into account transmission system operator requirements, while controlling the terminal bus voltages in the WF collection systems.

Due to the large size of modern offshore wind farms (OWFs), they can be seen as a wind power system which includes power generation, collection and transmission. Therefore, the dynamic behavior of wind turbines (WTs) should be taken into consideration to improve voltage control performance in the coordinated control strategy. In this thesis, a distributed optimal voltage control method is developed for

the AC grid with DC connection including large-scale OWFs. First, the model predictive control (MPC)-based OPF approach of the AC grid with DC connection is formulated with convex relaxation. At the same time, the voltage control problem based on the MPC inside OWF is modeled considering the dynamic process of WT. The proposed voltage control method has shown to be capable of enhancing the voltage control performance.

Contemporary voltage control strategy may not be as effective in the grid coupled with WFs in the situations of the cut-out wind speed conditions. To enhance the voltage control performance while considering cut-out wind conditions, the energy storage systems could be used. Therefore, this thesis proposes a distributed optimal voltage control strategy for AC grid with voltage source converter (VSC)-HVDC incorporating OWFs. The OWFs are equipped with distributed energy storage systems and the strategy takes into account the cut-out wind speed, and the dynamic behaviors of WT and energy storage systems. The proposed strategy aims to achieve optimal power distribution in the AC grid with VSC-HVDC, while generating the optimal references among WTs and energy storage systems to achieve optimal voltage regulation inside OWFs. In addition, the large-scale coupled voltage control problem can be decomposed by the alternating direction method of multipliers. Then, the sub-problems of optimal voltage control are solved in parallel guaranteeing the global optimality. Furthermore, the protection of system privacy can be enhanced with respect to the limited communication of coupled grid and OWFs.

Therefore, to summarize, this thesis develops several distributed voltage control strategies for the voltage regulation in coupled AC-DC grid and OWFs.

ABSTRACT (DANISH)

Som følge af det øgede antal og størrelser af vindmølleparker (WF'er) forårsager variationer i vinden og vekselvirkningen mellem store WF'er og elsystemer flere nye tekniske udfordringer, herunder regulering af spændingsprofil, optimal strømfordeling, øget beregnings- og kommunikationsbyrde for systemoperatører. På grund af den fysiske kobling mellem el-nettet og WF'er, samt en begrænset koordinering mellem operatører af transmissionssystemer og vindmølleparker kan systemoperatører og parkoperatører betragtes som næsten "blinde" i forhold til den anden parts systemdrift. Den eksisterende metode til styring af spænding i WF'er kan kun håndtere driften på systemniveau samtidig med spændingsreguleringen inde i WF'en med delvis kompromittering af global optimering. I denne afhandling fremlægges en koordineret optimal strategi for spændingsstyring i AC-DC-net med store WF'er med henblik på at opnå en global optimal spændingsstyring.

På grund af den massive udbygning af vindkraft fra fjerntliggende onshore og offshore WF -klynger, er det ved tilkoblingen til el-systemet nødvendigt at tage hensyn til transmissionssystemet selv. Det er nødvendigt at udvikle en koordineringen mellem transmissionssystem og WF'er for at opnå optimal drift af hele systemet. Et fokus i denne afhandling er at foreslå et distribueret aktivt og reaktivt effektstyringsskema for de stærkt koblede systemer: transmissionssystem og WF'er. Dette opnås ved at slække på betingelserne for det optimale effektflow (OPF) i transmissionssystemet, mens "branch flow" modellen anvendes på opsamlingssystemet for vindkraften. Den foreslåede løsning kan imødekomme det globale optimale effektflow for hele systemet, minimere effekttab under hensyntagen til systemoperatørernes ønsker, mens terminalspændingerne samtidigt håndteres for opsamlingssystemet for vindkraften.

På grund af moderne havmølleparkers (OWF'er) enorme størrelsre, bør de betragtes som et fuldt system der inkluderer både vindproduktion, opsamlingssystem og el-net. Derfor bør den dynamiske karakteristik af vindmøller (WT) tages i betragtning i forhold til at forbedre spændingsstyringen i den

koordinerede kontrolstrategi. I denne afhandling udvikles en metode til distribueret optimal spændingsstyring for AC-nettet inklusiv DC forbindelser til store OWF'er. Først formuleres et model-predictive control (MPC) -baseret OPF-program med konveks ”relaxation” for et AC-net forbundet til DC-forbindelser. Parallelt hermed modelleres spændingsreguleringsproblemet baseret på MPC inde i OWF under hensyntagen til vindmøllernes dynamiske karakteristikker. Den foreslåede metode til spændingsregulering kan forbedre den overordnede spændingsstyring for hele systemet.

Den nuværende strategi for spændingsstyring håndterer ikke kombinationen el-net og WF særligt effektivt i tilfælde af meget lidt vind (under cut-off). Derfor bør energilagringssystemer tilføjes til at forbedre effektiviteten af spændingskontrollen, således at der tages højde for ophold i vinden. Denne afhandling fremlægger en strategi for distribueret optimal spændingsstyrings for et AC-net forbundet med spændingskildekonvertere (VSC) -HVDC, der inkorporerer OWF'er. Det antages at OWF'ene er udstyret med distribuerede energilagringssystemer, der tager lave vindhastigheder samt WT’ens og energilagringssystemets dynamiske karakteristik i betragtning. Den foreslåede strategi sigter mod at opnå optimal effektflow i AC-nettet forbundet med VSC-HVDC, samtidig med at den genererer de optimale referencer for WT'er og energilagringssystemerne for at opnå optimal spændingsregulering indenfor OWF'erne. Derudover kan det store koblede spændingsstyringsproblem i stor skala nedbrydes ved hjælp af vekselretningsmetode for multiplikatorer. Derefter løses delproblemerne med optimal spændingskontrol parallelt, hvilket garanterer den globale optimering. Beskyttelsen af systemets privatliv kan forbedres i henhold til den begrænsede kommunikation mellem koblet net og OWF'er.

Denne afhandling beskriver således flere distribuerede strategier for spændingsstyring koblede AC-DC-net og OWF'er.

ACKNOWLEDGEMENTS

I would like to greatly express my gratitude to my supervisor Associate Prof. Qiuwei Wu for his great supervision, helpful guidance, and lots of patience during these three years. He has always been guiding my academic research, providing me excellent ideas, and caring my dairly life. I am also grateful to Dr. Sheng Huang. I significantly appreciate the academic skills, theoretical knowledge of my research area, which he passed on to me unreservedly. I have been gained a lot from the discussion with Dr. Sheng. I particularly wish to thank my supervisor Senior Scientist Guangya Yang for his helpful supervision, great guidelines of this thesis and administration issue of graduation. I also wish to thank Prof. Zhe Chen and Asistant Prof. Zhou Liu for hosting me during my external stay at Aalborg University. I thank them for the valuable guidelines and great collaboration. I also appreciate the useful discussion and great support from Prof. Canbing Li, Assocaite Prof. Bin Zhou, and Postdoc. Menglin.

I specially thank Associate Prof. Chresten, Dr. Theis and Dr. Chi for their great translation of my abstract into Danish. During these years, I appreciate the valuable discussion with my fellow Ph.D. students Feifan, Jin, Da, Weiyu, Weijuan, Sheng, Congying, Ana, Kanakesh, and Postdoc. Xiaolong.

The Ph.D. study period has been more happiness thanks to my excellent colleagues of my research group, and friends at DTU. Thus, I thank to Ying, Qingtao, Xiaoning, Chen, Yi, Daniel, Mikhail, and other friends for our wonderful experience.

Most importantly, I am deeply thankful to my family, expecially my mother, for their understanding, patience, support and endless love.

TABLE OF CONTENTS

PREFACE i
ABSTRACT i
ABSTRACT (Danish) iii
ACKNOWLEDGEMENTS v
LIST OF TABLES ix
LIST OF FIGURES xi
LIST OF ABBREVIATIONS xiii
CHAPTER 1. Introduction 1
1.1 Background 1
1.2 Literature Review on Grid Control 4
1.3 Literature Review on Wind Farm Control 8
1.3.1 Voltage and Reactive Power Control with Devices 9
1.3.2 Voltage and Reactive Power Control with Control Algorithms 11
1.3.3 Wind Farm Control Schemes 13
1.4 Literature Review on Coordinated Voltage Control for AC-DC Grid with Wind Farms 16
1.5 Motivations and Contributions of the Thesis 18
1.6 Structure of the Thesis 20
1.7 List of Publications 20
CHAPTER 2. Distributed Active and Reactive Power Control for Regional AC Power Grid with Wind Farms 23

2.1 Introduction 23
2.2 Control Strategy Architecture 26
2.2.1 System Configuration 26
2.2.2 Concept of Proposed Strategy 26
2.3 TS Optimization Model 27
2.3.1 Objective Function and Constraints 27
2.3.2 Convex Relaxation of OPF of TS 29
2.4 WF Optimization Model 32
2.5 ADMM Formulation for Whole System 34
2.6 Case Study 37
2.6.1 Test System 37
2.6.2 Control Performance 38
2.7 Summary 45
CHAPTER 3. Distributed Optimal Voltage Control Strategy for AC Grid with DC Connection and Offshore Wind Farms Based on ADMM 47
3.1 Introduction 47
3.2 Control Strategy Architecture 49
3.2.1 System Configuration 49
3.2.2 Strategy Concept 50
3.3 AC Grid with DC Connection Optimization Model 51
3.3.1 MPC-based OPF of AC Grid with DC Connection Formulation 52
3.3.2 Convex Relaxation of AC-DC OPF within MPC 56
3.4 Offshore Wind Farm Control 61
3.4.1 Modeling of Offshore Wind Farm 61
3.4.2 MPC-based Offshore Wind Farm Control 62
3.5 ADMM Formulation for the Whole System 64
3.6 Case Study 67
3.6.1 Test System 67

3.6.2 Control Performance 67
3.7 Summary 74
CHAPTER 4. Distributed Optimal Voltage Control in AC Grid with VSC-HVDC Including Offshore Wind Farms Equipped with Distributed ESSs 75
4.1 Introduction 75
4.2 Optimal Voltage Control Architecture 78
4.2.1 System Configuration 78
4.2.2 Strategy Concept 78
4.3 AC Grid with VSC-HVDC Optimization Model 80
4.3.1 Semidefinite Relaxation of Voltage Control Program of AC Grid with VSC-HVDC 80
4.4 Offshore Wind Farm Formulation 87
4.4.1 Modeling of Distributed ESSs 87
4.4.2 Modeling of OWF Collection System 90
4.4.3 Priority List-based Cutting-in Sequence for WTs 93
4.4.4 Formulation of OPC-based Voltage Control Program for OWF Collection Systems with Distributed ESSs 94
4.5 ADMM-based Solution for DOVC Program 96
4.6 Case Study 99
4.6.1 Test System 99
4.6.2 Control Performance 99
4.7 Summary 108
CHAPTER 5. Conclusions and Future Work 111
5.1 Conclusions 111
5.2 Future Work 113
Appendix A Solution Method 115
Appendix B Simulation Parameters 116
Bibliography 119

LIST OF TABLES

Table A-1 Steps of solution method for the whole system..... 115
Table B-1 The parameters of system……...116
Table B-2 The parameters of the whole system……..117

LIST OF FIGURES

Fig. 1-1 Global installation for onshore and offshore wind power. Source: [1]-[3]. 2
Fig. 1-2 Global new installation for onshore and offshore wind power. Source: [3]. 3
Fig. 1-3 The installed wind capacity in Denmark. Source:[3]..... 3
Fig. 1-4 Overview of OPF-based control methods. Source: [157]. 5
Fig. 1-5 The classical structure of offshore wind farm. Source: [74]..... 8
Fig. 1-6 The wind penetration level in top global wind markets. Source: [72].... 11
Fig. 1-7 The overview of WF control concepts..... 16
Fig. 2-1 Configuration of AC TS connected with WFs..... 26
Fig. 2-2 Structure of proposed strategy. 27
Fig. 2-3 Topology of system communication network. 35
Fig. 2-4 Available wind power of each WF. 38
Fig. 2-5 MV bus voltage in WF1. 39
Fig. 2-6 Terminal voltage of WT32 in WF1. 39
Fig. 2-7 Available wind power of WT1 in WF1. 40
Fig. 2-8 Terminal voltage of WT1 in WF1. 40
Fig. 2-9 Active power output of WT1 in WF1. 41
Fig. 2-10 Reactive power output of WT1 in WF1..... 41
Fig. 2-11 Active power output of WF1. 42
Fig. 2-12 Reactive power output of WF1. 42
Fig. 2-13 Power losses of WF1 and WF2..... 43
Fig. 2-14 Power loss of whole system. 43
Fig. 2-15 Convergence performance of active power output of WF1. (t=20s) 44
Fig. 2-16 Convergence performance of active power output of WF2. (t=20s) 44
Fig. 2-17 Convergence performance of reactive power output of WF1 and WF2. (t=20s) 45
Fig. 3-1 System structure..... 50
Fig. 3-2 Strategy concept..... 51
Fig. 3-3 The structure of model predictive control..... 51
Fig. 3-4 AC-DC converter model. 52
Fig. 3-5 The feasible region of the AC-DC converter. 54

Fig. 3-6 The representative WT available wind power. 68
Fig. 3-7 The voltage of the boundary bus between the grid and OWFa. 69
Fig. 3-8 The active power output of OWFa. 69
Fig. 3-9 MV bus 1 voltage in OWFa. 70
Fig. 3-10 Voltage control performance of MV bus 1 in OWFa. 70
Fig. 3-11 WT96 terminal voltage in OWFa. 71
Fig. 3-12 WT96 output active power in OWFa. 72
Fig. 3-13 Voltage control performance of WT96 terminal bus in OWFa. 72
Fig. 3-14 Power loss of total system. 73
Fig. 3-15 Convergence performance of active power output of OWFs. (t=5s).... 73
Fig. 3-16 Convergence performance of reactive power output of OWFs. (t=5s). 74
Fig. 4-1 The configuration of system. 79
Fig. 4-2 Structure of the proposed DOVC scheme. 80
Fig. 4-3 The model of AC-DC converter. 83
Fig. 4-4 The communication topology. 87
Fig. 4-5 The control structure and topology of DC-DC converter. 88
Fig. 4-6 The DC-DC converter control loop. 89
Fig. 4-7 The representative wind speeds of WT1-WT8 in OWF1. 100
Fig. 4-8 The SOCs of representative ESSs. 101
Fig. 4-9 WT8 output active power in OWF1. 101
Fig. 4-10 The energy stored in ESS32 in OWF1. 101
Fig. 4-11 The boundary bus voltage in OWF1. 102
Fig. 4-12 The OWF1 active power output. 103
Fig. 4-13 The OWF1 reactive power output. 103
Fig. 4-14 The MV bus 1 voltage in OWF1. 104
Fig. 4-15 Voltage control performance of MV bus 1 in OWF1. 105
Fig. 4-16 WT32 terminal voltage in OWF1. 105
Fig. 4-17 WT32 output active power in OWF1. 105
Fig. 4-18 WT32 output reactive power in OWF1. 106
Fig. 4-19 Voltage control performance of WT32 terminal bus in OWF1. 107
Fig. 4-20 Convergence performance of active power output in OWFs (t=25s). 107
Fig. 4-21 Convergence performance of reactive power output in OWFs (t=25s).
..... 108

LIST OF ABBREVIATIONS

WF	wind farm
TS	transmission system
TSO	transmission system operator
OPF	optimal power flow
PI	proportional integral
WT	wind turbine
PD	proportional distribution
ESS	energy storage system
QP	quadratic programming
WFO	wind farm operator
PSO	particle swarm optimization
STATCOM	static synchronous compensators
SVC	static var compensators
DFIG	doubly fed induction generator
ECS	energy capacitor system
SDP	semidefinite programming
VSC	voltage source converter
OWF	offshore wind farm
OPC	optimal control method
ADMM	alternating direction method of multipliers
LVRT	low voltage ride through
DARPC	distributed active and reactive power control
MPC	model predictive control
MV	medium voltage
OARPD	optimal active and reactive power dispatch
TCL	thermostatically controller load
CARPC	centralized active and reactive power control

CHAPTER 1.

INTRODUCTION

1.1 Background

Global energy consumption may be increased by one-third in the next 25 years, especially the electricity demand [1]. In 2021, global electricity demand has been approaching the fastest increase in the last 10 years. Global electricity demand is due to increase by 4.5% in 2021, or over 1000 TWh [2]. Due to the significant increase of electricity demand, global energy-related carbon dioxide (CO2) emissions have been approaching the second-largest growth in one year [2]. Meaning, the global energy demand was met largely by the fossil fuel-based power plants in 2021. On the other hand, renewables are expected to provide more than 50% of the electricity supply growth all over the world in 2021. The share of wind in renewable generation is recording the largest growth, increasing by 275 TWh [2]. With the electricity demand and CO2 emissions increasing, a large number of energy policies have been released to decrease global carbon emission and realize the fossil fuel free vision of energy systems. For example, the Danish government has decided to eliminate dependence on fossil fuels in Denmark by 2050. The strategy of the Danish government introduces energy policy initiatives to transform Denmark into a fully sustainable country [1]. With significant increase of electricity demand and environmental policy constraints, the renewable energy including large-scale onshore and offshore wind power, photovoltaic solar, and wave power will be largely integrated into the modern power systems.

For example, the global wind installations maintain the steady and fast growth from 2001 to 2020, as Fig. 1-1 shown [1]-[3]. In Fig. 1-2, new installations of onshore wind power reached 86.9 GW, while the offshore wind power reached 6.1 GW in 2020 [3]. It is worth noting that 2020 is the year with the highest number of new wind installations for both onshore and offshore in history [3]. China, US, Brazil, Netherlands and Germany were the top five markets for new wind installations all over the world in 2020. A high proportion of wind power due to its large amount

of wind resources is seen in Denmark as well. The installed capacity of wind power in Denmark from 2001 to 2009 can be seen in Fig. 1-3 [3].

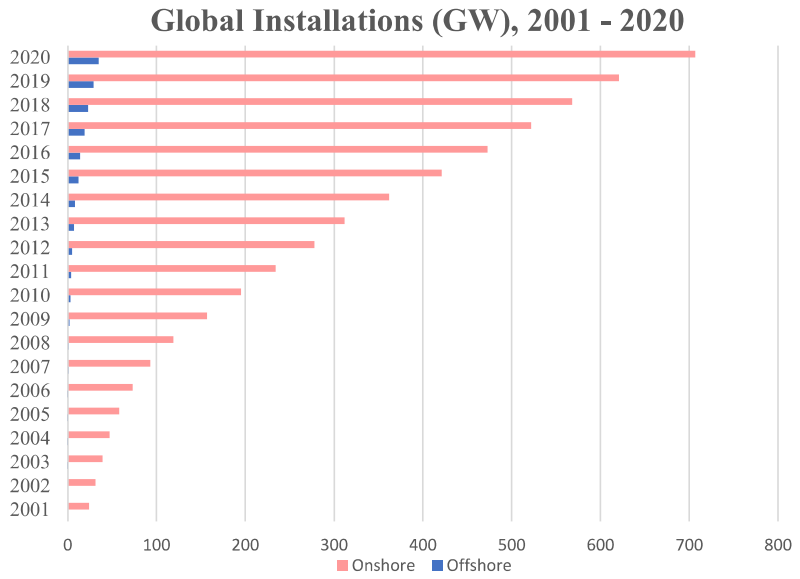

Fig. 1-1 Global installation for onshore and offshore wind power. Source: [1]-[3].

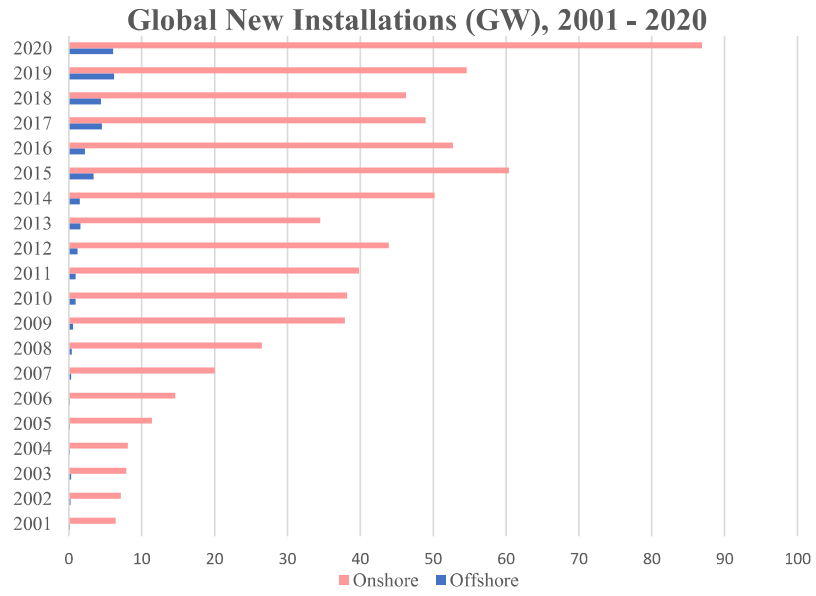

Fig. 1-2 Global new installation for onshore and offshore wind power. Source: [3].

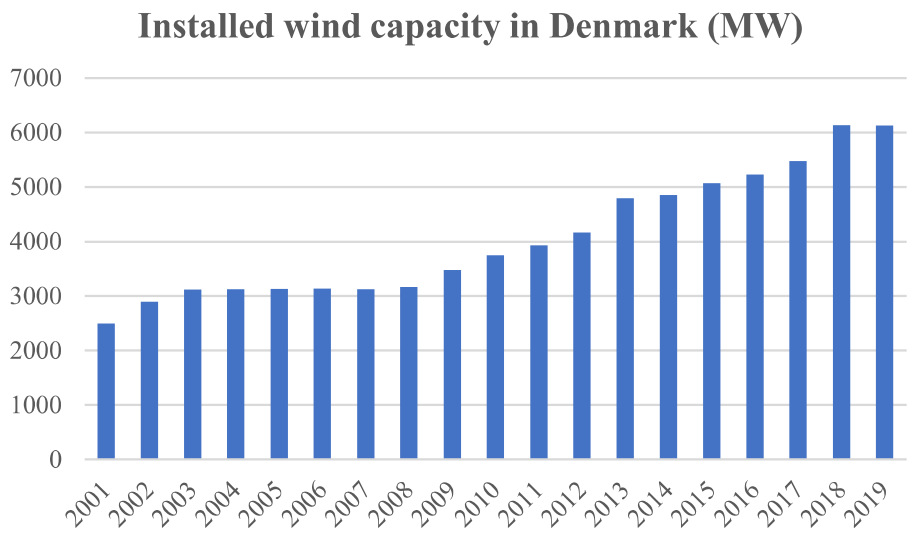

Fig. 1-3 The installed wind capacity in Denmark. Source:[3].

Due to the rapid development of large-scale onshore and offshore wind farms, the control and management methods for wind farms (WFs) have been proposed to reduce the influence of the inherent fluctuations and intermittency of wind power on the power system stability. The voltage control methods, in particular, have been studied to generate a suitable solution for a secure and economic operation of the wind farm.

Due to large-scale WFs connected to the grid, several challenges have been posed to the control and operation of the grid. With the penetration of renewable generation increasing, the voltage rise and a high level of power losses may occur in the operation of the grid. Thus, the effective control methods for the grid have been widely discussed to mitigate the operational challenges. The effective control methods can achieve the voltage regulation, mitigate the voltage deviation, and maintain a low level of power losses inside the grid.

The grid and WFs are physically connected and strongly coupled, however separately operated by two different operators: transmission system operator (TSO) and wind farm operator (WFO) [4]. Moreover, there is a limited amount of coordinated information exchange among TSO and WFOs during the operation process. For

example, the grid is managed by TSO and the information from WFO is not available to the TSO. Meanwhile, the offshore wind farm (OWF) is just simplified as a generator to provide power supply. Similarly, the OWF is operated by WFO with the dispatch command information from TSO, and the grid is only regarded as a voltage source. Therefore, the current limited coordination between TSO and WFOs introduces the challenges in the coordinated control of the coupled grid and wind farms.

In order to achieve an efficient coordinated control of the coupled grid and wind farms, this thesis studies the coordinated voltage control of AC-DC grid with large-scale wind farms. The following three subchapters present literature reviews on grid control, wind farm control, and coordinated voltage control for AC-DC grid with wind farms, followed by the contributions of the thesis.

1.2 Literature Review on Grid Control

Optimal power flow (OPF) is considered as one of the most important tools to achieve economical and stable operation for the bulk power system. OPF-based control methods allow to establish power system operating conditions that consider power loss management, generation cost, secure operation, voltage regulation, active and reactive power control, transmission line congestion and carbon emissions. The overview of OPF-based control methods is presented in Fig. 1-4. The literature review of each of the control methods is presented further on.

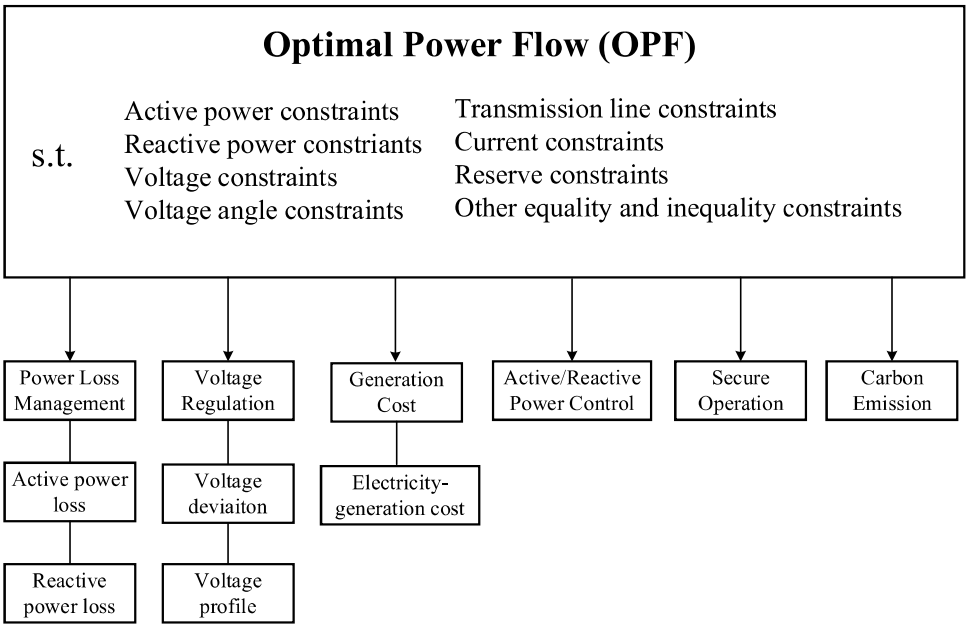

Fig. 1-4 Overview of OPF-based control methods. Source: [157].

- OPF-based Power Loss Management

Many studies have been focusing on the development of OPF-based methods related to power loss management in power system [5]-[10]. For example, the OPF-based method with improved coordinated descent algorithm was proposed to achieve a trade-off between power loss management and voltage regulation [5]. In [6], the OPF-based method with multi-time scale was proposed to reduce the power loss, power curtailment of distributed energy resource (DER), and satisfaction of loads in medium-voltage DC system with two different operation modes. An improved network model was adopted to calculate the OPF to minimize the power loss within the network [7]. In addition, a lot of optimization-based OPF methods were used to reduce the power loss, and other optimization objectives [8]-[10]. These optimization algorithms include among others sine-cosine algorithm [8], particle swarm optimization (PSO) [9], novel learning method [10]. In [8], a novel sine-cosine based-OPF method was conducted to minimize the power loss and achieve the voltage regulation in the transmission system (TS). A modified PSO-based OPF method was proposed to realize the hourly optimal load flow while considering the renewable energy in power system [9]. A novel learning-based OPF was used to optimize thermostatically controller load (TCL) to enhance operational flexibility [10].

- OPF-based Generation Cost Reduction

Several OPF-based methods have been generated to deal with the generation cost [11]-[12]. OPF with energy storage was modeled to minimize the generation cost and flatten the generation profiles while considering the dynamic process of the energy storage [11]. In [12], the multiperiod OPF model with the novel interior point technique was formulated to reduce the power loss with high efficiency.

- OPF-based Secure Operation

The secure operation of the grid has attracted the attention of many researchers due to the fast expansion of the grid. OPF focused on the secure operation was studied in [13]-[17]. A chance-constrained AC OPF model was formulated to handle the deviations of the renewable energy generation, and achieve a secure operation [13]. In [14], an OPF framework was proposed to generate the optimal generation schedule, maintain the voltage security, and reduce the power loss in hydro-thermal-wind system. In [15], a chance-constrained OPF framework was generated to achieve an economic and secure system operation with power balance consideration. In [16], a chance-constrained OPF model was formulated to ensure the economic and secure operation while taking the nonlinear AC power flow constraints and stochastic uncertainties into consideration. The robust OPF model was generated to maintain the secure operation for AC-DC TS while considering the uncertainties of the renewable generation and load [17].

- OPF-based Voltage Regulation

Regarding the voltage regulation, several control methods within OPF have been proposed [18]-[26]. A chance-constrained OPF model was formulated to optimize the setpoints of the RES and energy storage, and maintain the voltage within the feasible range under high probability [18]. A multi-stage robust OPF was modeled to schedule the power policies of several devices, and achieve the voltage management with the uncertainties of renewable energy [19], [20]. The OPF problem was formulated to reduce the voltage deviations, the cost of overestimation, and the penalty cost of underestimation of intermittent renewable energy in the grid [21]. A data-driven robust OPF model with the distributed framework was developed to protect the optimized solution against uncertainty in the probabilistic models, and dramatically reduce the empirical probability of voltage violations in distribution

systems [22]. Meanwhile, several studies used OPF-based methods with a decentralized scheme to solve the voltage regulation problem in the distribution systems with a large amount of DERs [23]-[26].

- OPF-based Optimal Active and Reactive Power Dispatch

As one of the most important branches of OPF problem, the optimal active and reactive power dispatch (OARPD) strategy has attracted a lot of attention [27]-[33]. The OARPD strategies based on OPF with different evolution algorithms were proposed to minimize the cost of renewable generators, and maintain the secure operation in power systems [27]-[30]. Several optimal reactive power dispatch strategies based on the optimization algorithms were proposed to minimize the transmission losses, voltage deviation, and maintain stability of the system [31]-[33].

- OPF-based Transmission Line Congestion Management

Regarding the transmission line congestion, a lot of OPF-based control methods were proposed to manage the transmission congestion [34]-[37]. The OPF-based multi-area congestion management framework was proposed to generate the switch-off the regional transmission line for each responding area, and successfully regulate the line congestion [34]. Considering the network reconfiguration, the stochastic OPF problem was modeled to reduce the transmission congestion, and avoid the renewable curtailment [35]. The congestion regulation scheme based on DC OPF was proposed to relieve the transmission congestion, and maximize the social welfare [36]. The OPF-based congestion management was proposed to generate the optimal capacity references of DERs to avoid the congestion across the transmission network [37].

- OPF-based Carbon Emission Reduction

With the development of the environment-friendly society, carbon emission reduction has also been discussed in OPF [38]-[44]. The OPF-based carbon footprint allocation method was modeled to reduce the emissions [38]. The distributed ADMM-based DC OPF model was formulated to address the carbon emission trading program, and calculation efficiency was obviously improved [39]. Furthermore, the power flow and carbon emission flow were modeled to obtain the carbon tax incidence in the TS in [40]. In [41], the OPF-based scheme was generated to minimize carbon emission, generation cost, and achieve power loss management in

power systems with wind farms. The modified imperialist competitive algorithm-based OPF was modeled to generate optimal power distribution in [42] to reduce carbon emissions and cost of generation in power systems. The regional carbon emission management based on probabilistic OPF was proposed to minimize regional and total carbon emission, and generation cost in AC grid [43],[44].

The above OPF-based control methods can effectively maintain the secure operation of the grid, and address the uncertainty of large-scale wind power. However, few studies have addressed the optimal power control of the grid with large-scale WFs and meanwhile achieved voltage management across the wind power collection systems.

1.3 Literature Review on Wind Farm Control

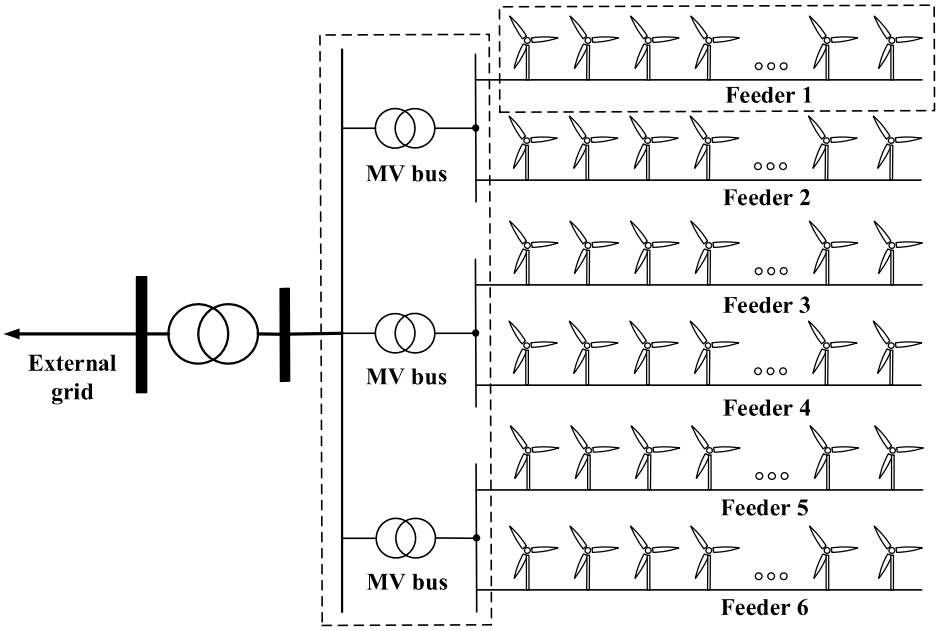

Fig. 1-5 The classical structure of offshore wind farm. Source: [74].

Due to the increasing number and size of the WFs, the voltage control for WF has attracted much attention. The classical structure of OWF is presented in Fig. 1-5. The effective voltage regulation inside WF is essential for secure and stable operation in large-scale WFs. According to the review on the voltage/reactive power control inside WF, the voltage/reactive power control methods include the applications of Static Synchronous Compensators (STATCOM), Static Var Compensators

(SVC), capacitor banks, energy storage systems (ESSs), and the voltage/reactive power control strategies with the effective control algorithms [45].

1.3.1 Voltage and Reactive Power Control with Devices

1.3.1.1 Voltage and Reactive Power Control with STATCOM

STATCOM applications were used in several voltage control methods to achieve efficient voltage management, due to the STATCOM's ability of providing the reactive power [46]-[53]. A centralized voltage control method with STATCOM was proposed to suppress the voltage fluctuations, and realize the voltage stability in the large-scale WF [46]. In [47], the STATCOM was applied to enhance the transient voltage stability, and improve the secure operation of WF. The application of STATCOM was studied to address the voltage stability problems for Doubly Fed Induction Generator (DFIG)-based WFs [48]. The control method with STATCOM/ESS topology can generate the reactive power reference to maintain the terminal bus voltage stable, and keep active power output of WF smoothy inside WFs [49]. The one-cycle-based voltage control strategy for STATCOMs was proposed to achieve the reactive power management, mainly to decrease the voltage variations inside WFs [50]. The reactive power management with STATCOM was proposed to maintain the optimal voltage profile, and reduce the active power losses inside WFs [51]. The STATCOM control scheme was generated to coordinate the positive and negative sequence of the voltage to minimize the torque oscillations in WFs [52].

1.3.1.2 Voltage and Reactive Power Control with SVC

Due to the quick response in providing reactive power, SVC has been widely applied in WFs to achieve the reactive power management and voltage regulation [53]-[56]. The new WF sizing method was developed to place SVCs to enhance the level of wind penetration, and improve the critical modes of voltage instability considering the high level of wind penetration [54]. The SVC control method based on fuzzy logic was generated to enhance the voltage stability, and the low voltage ride-through (LVRT) capability of the WF [55]. In [56], the convolutional neural network based reactive power control method was proposed to effectively reduce the voltage flicker by SVC in WF.

1.3.1.3 Voltage and Reactive Power Control with Capacitor Banks and Reactors

Capacitor banks and reactors have also been applied to reactive power management. In [57], the energy capacitor system (ECS) was developed to effectively reduce the fluctuations of terminal voltage and power output inside WFs while taking the fluctuating wind power into consideration. In [58], an online reactive power control strategy was proposed to achieve the optimal settings of transformers and reactors in WFs. In [59], a novel PSO-based reactive power control method was developed to optimally coordinate the switched reactors and tap positions of transformers in order to achieve the reactive power management in WFs. In [60], an effective voltage control method using stepped controllable shunt reactor was generated to maintain the voltage of terminal buses in large-scale WFs.

1.3.1.4 Voltage and Reactive Power Control with Synchronous Condensers

With the rapid increase of renewable energy source application, VSC-based energy resources have been used to supply electricity power on a large scale [61]-[64]. In [65], the impact of VSC control methods with synchronous condensers in VSC-based power system was studied. In [66], the optimal selection of control methods can be provided for a VSC-based energy source combined with a synchronous condenser at the point of common coupling. In [67], synchronous condenser was used to enhance the stability of voltage and frequency in the renewable-based systems. In [68], a power oscillation damping controller including synchronous condenser was developed to control the terminal voltage in order to provide damping services in VSC-based system.

1.3.1.5 Voltage and Reactive Power Control with Energy Storage Systems

Due to the fluctuating wind power, the ESSs including battery energy storage, fly-wheel, compressed air system, super capacitor have been used to maintain the stable and secure operation of WFs [45]. Regarding the energy storage systems, battery energy storage system can be seen as the most suitable solution for controlling the active and reactive power, and reduce the terminal voltage deviations in WF [45]. The proportional-integral (PI) based voltage controller was developed to regulate the terminal bus voltage, and smooth power output of wind turbine with ESSs [69]. A three-level hierarchical power control scheme was proposed to maintain the voltage of the point of common coupling bus, and regulate battery energy storage system within feasible range in wind-battery energy system [70]. The voltage control mode was generated to achieve voltage control and reactive power regulation by using distribution STATCOM and a fly-wheel energy storage system [71].

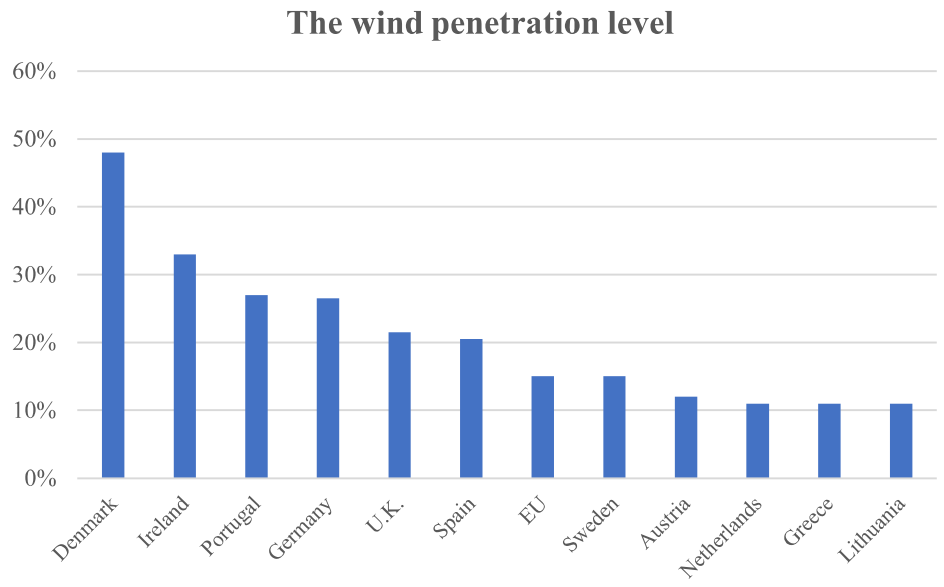

Fig. 1-6 The wind penetration level in top global wind markets. Source: [72].

1.3.2 Voltage and Reactive Power Control with Control Algorithms

Due to the high increase of wind penetration level in modern power system, several countries have published detailed grid codes to constrain the operation and construction of WFs. The wind penetration levels of some representative countries in top global wind markets are presented in Fig. 1-6 [72]. In order to fulfill the requirements from TSO and achieve the voltage regulation inside WF, the voltage/reactive power control methods have attracted much attention. For example, TSO requires that the voltage of the connection bus with voltage control method should be kept within the feasible range. Meanwhile, the voltage deviations of terminal buses inside wind power collection systems can also be reduced. Regarding the voltage/reactive power regulation, reactive power injection can be provided by different kinds of reactive power sources in WF, such as STATCOM, SVC, and capacitor [73]. Due to the large-scale WFs connecting to the transmission network, it is more convenient and economical to regard the wind turbines (WTs) as the reactive power supplier in WF. In addition, with the rapid development of the communication inside WF, it is possible to effectively control a large number of wind turbines. Meanwhile, the investment of the conventional reactive power sources in WF can be effectively reduced by the reactive power supply from wind turbine [73].

1.3.2.1 MPC-based Voltage Control

Several studies [73]-[89] proposed different optimization methods for voltage regulation and reactive power control in WFs such as, model predictive control (MPC), dynamic programming, multi agents, control cycle determination, and fuzzy logic analytic hierarchy process [45]. Regarding MPC method, several studies [74]-[80] have developed the voltage control model based on MPC in WF. In [74], the MPC-based voltage control method was proposed to maintain the voltages within the reasonable range, and minimize power losses in VSC-HVDC-connected OWFs. In [75], the MPC-based decentralized coordinated voltage management was developed to achieve the voltage regulation by coordinating the WTs and VSC inside WF. The autonomous voltage control scheme based on MPC was generated to optimally control four kinds of devices of reactive power generation, and maximize the reactive power reserve [76]. In [77], an enhanced voltage control method based on MPC was proposed to regulate the terminal bus voltage of VSC and wind turbines, and minimize the power losses across wind power collection system. The coordinated power control strategy based on MPC was developed to maintain the voltage within the feasible range, and generate the optimal references of active power output of WTs [78]. In [68], the MPC-based coordinated voltage control scheme was proposed to achieve voltage regulation, and prevent potential failures via optimizing Var capacity in WF. The two-tier combined power control scheme with MPC was proposed to minimize the voltage fluctuations in WF cluster. In the upper-tier control, the coordinated active and reactive power references were generated to improve the voltage regulation. In the lower-tier control, the hierarchical control method was proposed to reduce the voltage fluctuation of each wind turbine terminal bus [80].

1.3.2.2 Voltage Control based on Dynamic Programming

In order to achieve the voltage control, a number of studies [81]-[83] proposed dynamic programming in WF. In [81], a voltage control method based on heuristic dynamic programming and a novel neural network was proposed to coordinately control reactive power among DFIGs and STATCOM, and improve the fault ride-through capability inside a large-scale wind farm. The dynamic programming based reactive compensation strategy was proposed to coordinately control the actuations of all the capacitor banks in wind park [82]. The approximate dynamic programming based adaptive design strategy was proposed to optimize the reactive power control among DFIGs in order to enhance the transient stability of power systems [83].

1.3.2.3 Voltage Control based on Multi Agents

Another method for voltage regulation, multi agent system has been used to improve the voltage control performance in WF [84]-[85]. The multi-agent system-based voltage control scheme with a decentralized manner was proposed to coordinately control the voltages of each wind turbine bus and pilot bus in WF [84]. In [85], a multi agent clustering based distributed voltage control method was developed to achieve the goals of voltage improvement, total power losses, and cost of total investment for WTs and switched capacitor banks.

1.3.2.4 Voltage Control based on Fuzzy Logic Control

Many studies [86]-[89] have been proposed to realize the voltage regulation using fuzzy logic in wind power collection systems. The reactive power management based on fuzzy logic was proposed to enhance steady state voltage stability, and minimize the bus voltage deviation in AC grid with WFs [86]. An adaptive droop control strategy based on fuzzy logic was developed to coordinately manage the DC voltage deviation and power dispatch in multiterminal HVDC and WFs [87]. A supervisor with fuzzy logic was developed to control the voltage of DC bus and the operation of flywheel energy storage system in order to reduce the active power fluctuations [88]. A gain tuner based on fuzzy logic was developed to update PI controller in order to control the DC bus voltage, and obtain the quick dynamic response in DFIG-based WF [89].

1.3.3 Wind Farm Control Schemes

With the rapid development of wind power projects in the industrial area and wind power control methods in the academic area, several different control schemes for large-scale WFs have been proposed to improve the control performance of the secure and economical operation of WFs. The proposed control methods can be generally categorized into centralized, distributed and hierarchical control. A brief review of the advances in each of these areas will be provided in the following.

1.3.3.1 Centralized Control Scheme

Centralized control scheme treats the WF or the grid connected to WFs as a unique control area [90]. Thus, the central controller collects the global information of the WF. According to the global information, the central controller can solve the whole optimization problem, and provide references for the devices inside the WF. This kind of centralized control scheme represents a relatively simple control structure, and requires the less communication burden. An optimization method, where a central controller generates the power references of wind turbines, and manages the

torque and generator speed in WF, was developed in [91][91]. A centralized multi-input-multi-output robust controller was proposed to optimize the power references of the WTs and photovoltaic units in [92]. The central controller was generated to optimize the active and reactive power reference for the wind turbine, and delete the local reference considering a disturbance occurs [93]. In [76], the MPC-based centralized voltage controller was proposed to coordinately control the reactive power generation devices in order to achieve voltage regulation in the WF. However, this kind of centralized control scheme has the drawback, in which the huge information and data have to be processed, especially for the control of the power system combined with large-scale wind farms. Due to the massive information and data of the power system and the WFs, the optimization problem of the whole system may not be solved within an acceptable time.

1.3.3.2 Distributed Control Scheme

A distributed control scheme divides the whole system into several sub-systems, in which the control problem of each sub-system can be easily tackled. In a distributed control scheme, a large amount of information and data can be reduced evidently, and the global information can also be eliminated. Similarly, the communication burden of the whole system would be effectively reduced. In contrast to centralized control, the control of the whole system with distributed manner is not lost when a failure occurs [90]. For example, a distributed voltage control strategy was proposed to optimize the reactive power output among several WFs and WTs inside each WF, in order to achieve voltage management in a large-scale WF cluster [94]. A distributed control method was proposed to achieve the voltage and frequency regulation for wind power collection systems within two different operation modes [95]. A distributed and decentralized MPC method to maximize the active power generation of WFs with minimal control actions was described in [96]. A distributed secondary voltage control method with consensus protocol was proposed to control the voltage, and meanwhile achieve the optimal reactive power dispatch among the reactive power devices in WF [97]. A distributed power dispatch strategy with consensus protocol was proposed to realize the fair active and reactive power dispatch among several WFs, and optimize the active and reactive power references for each wind turbine in WF clusters [98]. An analytical target cascading based distributed voltage management was generated to reduce the voltage deviations of the terminal bus, and smooth the reactive power outputs of WTs in WF clusters [99]. The distributed control scheme shows promise in controlling large-scale WFs, especially in power system containing several large-scale WFs.

1.3.3.3 Hierarchical Control Scheme

The hierarchical control scheme relies on several control loops to achieve a good control performance. Several control loops can be used to simplify the complex voltage control program by spatial and temporal decomposition [90]. The hierarchical control scheme can also reduce the calculation burden of controllers. A hierarchical optimal voltage control method based on adaptive droop was proposed to reduce the voltage fluctuations of the terminal buses by coordinating the WTs and VSC in offshore WF [100]. A hierarchical active power control strategy was developed to optimize active power outputs of WTs and ESSs, and reduce fatigue loads in WFs in [101]. A hierarchical MPC-based method was proposed to enhance wind power scheduling and accommodation in large-scale wind power cluster in [102]. An MPC-based coordinated active and reactive power control strategy with consensus protocol was developed to generate the optimal reference of wind turbines, and control the terminal bus voltage in WFs [78]. In [103], a hierarchical distributed MPC scheme was proposed to achieve the coordinated dispatch of power generation and economic objectives within two different layers in renewable power system. A hierarchical inertial control strategy within two different levels was proposed to enhance the system frequency response, and minimize the WF operation cost in multiple WFs with ESSs [104]. The hierarchical model based on partial differential equation was proposed to ensure that the optimal active power generation trajectory can be tracked by the cumulative active power of the WF [105]. A hierarchical control scheme was developed to coordinate the reactive power generation among wind power plant clusters, and coordinately control the reactive power generation devices in WF clusters [106]. A hierarchical scheme based on nonlinear MPC was proposed to achieve the frequency support while reducing the calculation burden and increasing the efficiency in WF [107]. The Kriegers Flak Combined Grid Solution is the first hybrid asset project which uses HVAC/HVDC interconnector via massive offshore WTs between Danish and German sides [108]. The voltage control methods achieved by reactive power devices and OPF were applied in two different sides, respectively [108]. In [108], the coordinated control scheme was developed to use automatic voltage and reactive power control in order to achieve the voltage management in Danish side.

Wind farm control, especially for voltage or reactive power control, has been motivated for several kinds of objectives for WF: minimize the voltage deviation and fluctuation, voltage profile regulation, minimize the active and reactive power losses, reactive power management and support, secure operation of WF, etc. Fig.

1-7 shows the overview of the WF control concepts including the control schemes, the optimization-based control methods, control objectives.

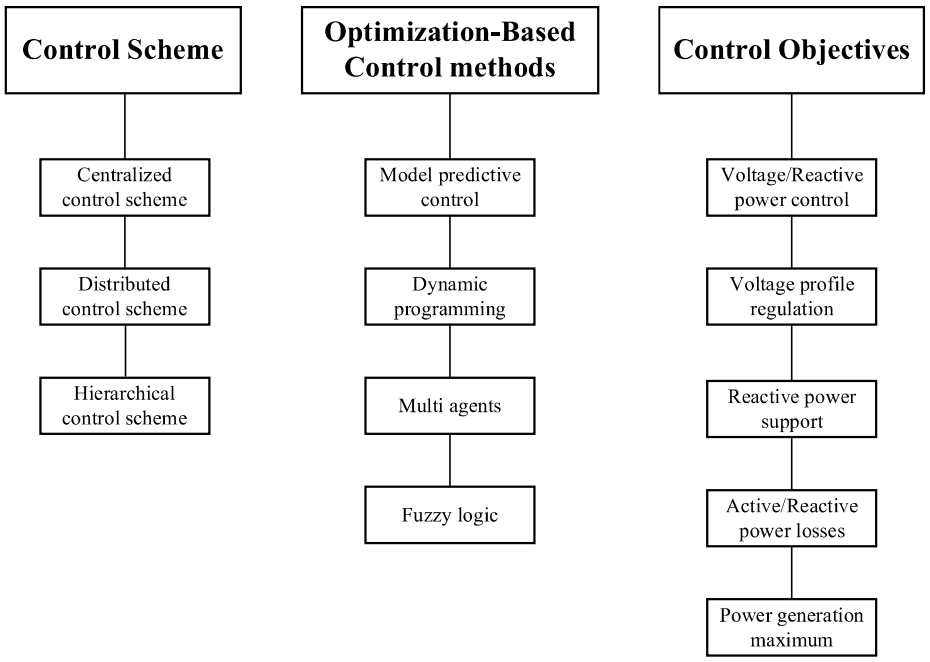

Fig. 1-7 The overview of WF control concepts.

1.4 Literature Review on Coordinated Voltage Control for AC-DC Grid with Wind Farms

The WF and TS are physically strongly coupled, however operated by two different operators: WFO, and TSO [4]. In addition, a limited amount of information is exchanged between several WFOs and TSO. Regarding the TS operation, the system has been managed by TSO with limited information from WFO side [4]. The reason behind this is that the WF is regarded as a power generation source, which only supplies the active and reactive power for the TS. Regarding the WF operation, the WF is operated by WFO just with the TSO command information from TSO side. Similarly, the TS is regarded as a voltage source [4].

The above operation scheme with a little coordination may bring some problems to the coordinated secure and economical operation of the TS and several large-scale WFs. Thus, the existing control methods would bring many operation challenges such as voltage deviation and fluctuation, power loss management, coordinate the secure and economical operation of the whole system, etc.

Regarding the coordinated voltage control for AC-DC grid with WFs, many studies [109]-[112] have been proposed to achieve the preliminary coordinated control for the whole system. As mentioned, in this kind of control scheme, the WF is regarded as a generation source only, from which the active and reactive power can be supplied. For example, in [109], a coordinated voltage management strategy was proposed to maintain the voltage stability of wind-penetrated power system while taking the dynamic process of DFIG-based wind turbine into consideration. The MPC-based voltage control method was developed to improve the voltage stability of the power system considering the volatile wind power penetration [110]. In [111], an active voltage control scheme was developed to generate the optimal reference of power generation of wind turbines, and suppress the grid voltage deviation influenced by wind power fluctuation. The effect-orientated method was proposed to improve the voltage stability within the short-term, and consider the system uncertainties in a power system with wind penetration [112]. In above control methods, the voltage regulation can be achieved in power system while the voltage control inside wind power system is not taken into consideration owing to the simplified representation of the WFs as a generation source. However, with the large-scale WF projects increasing, the voltage control or active/reactive power regulation inside the wind power system should also be addressed while voltage control for power system is solved.

In order to achieve the voltage control both in grid and WF, the two-stage control scheme has been proposed [113]-[115]. In [113], a two-stage voltage control scheme was proposed to improve the penetration level of wind power in sub-transmission system. For the first control stage, the voltage deviations can be suppressed by on-load tap changers [113]. For the second control stage, the slight voltage deviations can also be reduced by coordinating the reactive power outputs of virtual power plants in sub-transmission system [113]. A two-stage distributed reactive power control method was proposed to achieve optimal reactive power control for the distribution system with WFs [114]. In the upper control stage, the reactive power distribution was optimized in the distribution system while taking TSO command into consideration [114]. In the lower control stage, the optimal reactive power distribution can be realized while tracking reactive power command from the upper control stage [114]. In [115], a two-stage distributed optimization framework was used to model the power system with WFs and storage units in order to reduce operation cost of the system. In the first stage, the status of generators and storage units were optimized by day-ahead dispatching [115]. In the second stage, the references of power generation, storage unit output, and wind power curtailment were generated [115]. In the above two-stage control methods, the voltage

regulation can be realized both in grid and WFs. However, two-stage control methods cannot obtain the global optimal solution of the voltage control problem for grid and large-scale WFs.

1.5 Motivations and Contributions of the Thesis

Due to the rapidly increasing number and size of WFs, the wind power fluctuations and the interaction between large-scale WFs and grid have posed several technical challenges. These include voltage and reactive power control, optimal active and reactive power dispatch, power loss management, as well as huge computational and communicational burden of grid and WF controllers.

Moreover, the WFs and grid are physically connected and strongly coupled, which are operated by WFOs and TSO, respectively. In the process of operation, a limited coordinated information is exchanged between WFOs and TSO. In fact, the WF is managed by WFO only with the dispatch command information from TSO side, and meanwhile the grid is just regarded as a voltage source. Similarly, the grid is operated by TSO and the information from WFO side is not available to the TSO. The OWF is only simplified as a generator to provide power supply. Therefore, the existing limited coordination between WFOs and TSO introduces the challenges in the coordinated control and operation of the coupled grid and WFs.

Due to the large size of modern WFs, they can be seen as a wind power system including wind power generation, collection, transmission, and ESSs. Thus, the detailed dynamic behaviors of WT and ESS should be taken into consideration to enhance voltage control performance guaranteeing the global optimal solution in the coordinated voltage control strategy.

Considering the large-scale coupled voltage control problem, the computational burden of central controller is huge, and the problem may not be solved in an acceptable time. Therefore, it is necessary to develop a distributed calculation scheme to decompose the strongly coupled voltage control problem, and distribute the whole computational burden to several controllers.

Chapter 2: With WFs expanding both in size and number, the bulk wind power generated from the large-scale WFs needs to be transmitted through a meshed transmission grid. Coordinated power control of transmission system and WFs is a promising way to achieve optimal operation and improve control performance of the whole system. However, there is no study on the optimal power control for regional transmission system with WFs while considering the voltage regulation

and power loss management inside WFs. Therefore, this chapter proposes a distributed active and reactive power control strategy based on ADMM for regional AC transmission system with WFs. The proposed strategy optimizes the power distribution among the WFs in order to minimize the power losses of the transmission system while tracking the power command from the TSO, and minimize the voltage deviation of the terminal buses inside the WF from the rated value as well as power losses of the WF.

Chapter 3: The proposed active and reactive power control strategy in Chapter 2 provides efficient control performance for the transmission system combined with large-scale WFs, however, the details of the distributed optimal voltage control strategy are not studied. Therefore, the contribution of chapter 3 is the development of a distributed optimal voltage control scheme for the AC grid with voltage source converter (VSC) DC connection and offshore wind farms. In the proposed scheme, the optimal power flow of the AC grid with VSC DC connection within MPC is relaxed by using the semidefinite programming (SDP) relaxation technique. Meanwhile, the voltage control program based on MPC for the wind power collection system is modeled by taking the dynamics of wind turbines into consideration. Compared to conventional control schemes, the proposed scheme enhances the voltage control performance.

Chapter 4: The proposed optimal voltage control scheme can achieve the voltage regulation for the AC grid with DC connection and offshore wind farms. However, this kind of scheme may be ineffective in case of the cut-off wind speed of wind turbine. In addition, the large-scale distributed energy storage systems (DESSs) inside WF are not considered to achieve the better voltage control performance. Thus, the contribution of chapter 4 is to propose a distributed optimal voltage control scheme based on ADMM for AC grid with VSC-HVDC including offshore wind farms equipped with distributed ESSs. In the proposed scheme, the TSO command and cut-out wind speed are considered. In addition, the dynamic processes of wind turbines and ESSs are modeled to improve the voltage regulation. The OPF-based voltage control program inside AC grid with VSC-HVDC is relaxed. The voltage control and ESS management problem inside offshore wind power collection systems are formulated to minimize the voltage fluctuations as well as power losses, and achieve the fair utilization of ESS. The calculation and communication burden can be reduced with the proposed distributed calculation framework while the optimal control performance is guaranted.

1.6 Structure of the Thesis

Chapter 2 develops a distributed active and reactive power control strategy based on ADMM for regional AC transmission system with wind farms. Chapter 3 presents a distributed optimal voltage control scheme based on ADMM for AC grid with VSC DC connection and offshore wind farms. Chapter 4 provides a distributed optimal voltage control strategy based on ADMM for AC grid with VSC-HVDC including offshore wind farms equipped with distributed ESSs. The conclusions and future work are presented in Chapter 5.

1.7 List of Publications

The papers in relation to the Ph.D. study include:

1. **Pengda Wang**, Qiuwei Wu*, Sheng Huang, Canbing Li, and Bin Zhou, "ADMM-based Distributed Active and Reactive Power Control for Regional AC Grid with Wind Farms," *Journal of Modern Power Systems and Clean Energy*, Jun. 2021, Early Access.
2. **Pengda Wang**, Qiuwei Wu*, Sheng Huang, Bin Zhou, and Canbing Li, "Distributed Optimal Voltage Control Strategy for AC Grid with DC Connection and Offshore Wind Farms based on ADMM," *International Journal of Electrical Power and Energy System*, Submitting Response.
3. **Pengda Wang**, Qiuwei Wu*, Zhou Liu, Zhe Chen, Sheng Huang, Canbing Li, and Bin Zhou, "Distributed Optimal Voltage Control in AC Grid with VSC-HVDC including Offshore Wind Farms Equipped with Distributed ESSs," *IEEE Transactions on Power Systems*, In Process of Submitting.
4. **Pengda Wang**, Qiuwei Wu*, Sheng Huang, Canbing Li, and Bin Zhou, "Coordinated Voltage Control of Offshore Wind Farms Combined with AC Grid based on OPF-MPC Method," *12th IEEE PES Asia-Pacific Power and Energy Engineering Conference (APPEEC)*, 2020. DOI: 10.1109/APPEEC48164.2020.9220446.

The following work has been prepared during the course of the Ph.D. study, but has been omitted from the thesis because it can be partially covered by the above papers.

5. **Pengda Wang**, Qiuwei Wu*, Sheng Huang, Canbing Li, and Bin Zhou, "Coordinated Optimal Control of Offshore Wind Farms Combined with MTDC Network," Conference Paper, Unpublished.

The papers 1-4 are included in the Ph.D. thesis. In order to maintain the consistency, certain notations in the thesis may differ from the ones of the above papers.

CHAPTER 2.

DISTRIBUTED ACTIVE AND REACTIVE POWER CONTROL FOR REGIONAL AC POWER GRID WITH WIND FARMS

This chapter proposes a distributed active and reactive power control (DARPC) strategy based on the alternating direction method of multipliers (ADMM) for regional AC TS with wind farms. The chapter is based on the published papers 1 and 4 with minor changes to coherently fit into the framework of this Thesis[1].

2.1 Introduction

Wind power has been continuously developing due to the increasing demand of renewable energy and low-carbon energy policy [74]. With the wind power penetration increasing, the wind power fluctuations and the interaction between large-scale WFs and power systems have introduced several technical challenges, e.g., the optimal power allocation, voltage regulation, and coordination for the AC TS with WFs [116].

OPF has been widely used to solve the operation problem of the power system connected with WFs. There are a number of papers on OPF-based optimal operation of the power system with WFs [117]-[121]. In [117], a multi-period OPF model was formulated to minimize the operating cost in the power grid with offshore WFs. In [118], an OPF-based optimal generation schedule was proposed to minimize the total system cost and operate the system securely with wind power.

[1] This chapter is based on papers 1 and 4: 1) **Pengda Wang,** Qiuwei Wu*, Sheng Huang, Canbing Li, and Bin Zhou, "ADMM-based Distributed Active and Reactive Power Control for Regional AC Grid with Wind Farms," *Journal of Modern Power Systems and Clean Energy*, Jun. 2021, Early Access; and 4) **Pengda Wang**, Qiuwei Wu*, Sheng Huang, Canbing Li, and Bin Zhou, "Coordinated Voltage Control of Offshore Wind Farms Combined with AC Grid based on OPF-MPC Method," *12th IEEE PES Asia-Pacific Power and Energy Engineering Conference (APPEEC),* 2020.

In [119], an extended OPF model was used to minimize the generation cost of thermal units and wind units in the power system with WFs. In [120], a multi-objective stochastic OPF model was formulated to reduce the operating cost, emission and enhance the voltage stability in the power system with significant wind power penetration. In [121], an optimal reactive power dispatch strategy based on OPF was proposed to minimize the voltage stability index in a wind power integrated power system.

For the WF control, the conventional strategy is the proportional distribution (PD) control scheme. The active and reactive power references of WTs are proportionally distributed according to the available wind power, which is easy to implement [80]. However, the PD control scheme cannot achieve optimal power distribution inside the WF. Several optimization-based dispatch methods have been developed to overcome the disadvantage of the PD control scheme and achieve better control performance of the WF. In [122], an optimal power dispatch method was proposed to reduce the production cost and maximize the active power production of the WF. In [101], an optimal active power dispatch strategy was proposed to reduce fatigue loads in WFs with DESSs. In [123], an optimal reactive power dispatch method was developed to minimize the total losses in the WF.

With the WF expanding both in size and number, if the system operator tries to solve a global optimization problem of the WFs with the TS, it may be difficult to solve a large-scale OPF-based optimization problem with large-scale constraints in seconds. In order to meet the needs of fast calculation of WF dynamic control with strong fluctuations in wind speed, the ADMM has been applied to reduce the computation burden and communication burden of the controller [124], [125]. The ADMM-based optimization methods have been widely used in the WF optimal control [75], [80], [94], [126], [127]. In [80], an ADMM-based two-tier active and reactive power control scheme was proposed to achieve the optimal voltage regulation inside the WF cluster. In [94], an ADMM-based voltage control method was proposed for the large-scale WF cluster to coordinate the reactive power output among several WFs and WTs inside each WF. In [75], an MPC method based on ADMM was proposed to minimize voltage deviations and reactive power output fluctuations of WTs inside WFs. In [126], an ADMM-based optimal active power control method was proposed for synthetic inertial response of large-scale WFs. The aim is to minimize the differences in the rotor speed of the WTs and the wind energy loss.

In the existing studies, there is no study on the optimal power control for the regional TS with WFs while considering the voltage regulation and power loss management inside WFs. With the WF and TS expanding both in size and number, the large amount of wind power from the large-scale WF cluster has to be transported to the bulk power system through a meshed transmission grid. The coordination of the TS and WFs is necessary to achieve optimal operation of the whole system. Therefore, this chapter proposes a DARPC strategy based on ADMM for the regional TS with WFs. The proposed strategy aims to achieve the global optimal power control of the regional TS with WFs to minimize the total power losses while meeting the TSO requirements for active power demand, and regulate bus voltages inside each WF within a feasible range. The ADMM method is used to decompose the large-scale optimization problem. The non-convex OPF problem of the TS is relaxed by using SDP relaxation and Schur's complement [128]. Meanwhile, the branch flow model [116] is used to formulate the optimization problem of the WF. With the proposed DARPC strategy, the TS and WF controllers operate in parallel to solve the optimization problem in a distributed manner without loss of global optimality.

The main contribution of this chapter can be summarized as follows:

(1) A DARPC strategy is developed for the TS with WFs, which can achieve the global optimal power distribution and the voltage regulation for the coupled TS and WFs. The DARPC strategy can achieve a better control performance among the TS and WFs.

(2) The SDP relaxation and Schur's complement are adopted for the TS while the branch flow model is adopted for the WFs, which handle the inherent non-convexities of the OPF problem of the coupled TS and WFs. Thus, the original problem is transformed into a convex problem and can be solved using the ADMM framework while guaranteeing the global optimal solution.

(3) The ADMM-based DARPC strategy eliminates the requirement of the central controller and distributes the system computation task to several controllers to reduce the computation burden, implying the better scalability. The exchanged information between the TS controller and WF controllers only includes the global, local and dual variables of the boundary nodes, which improves the protection of the information privacy.

The rest of this chapter is organized as follows. Section 2.2 presents an overview of the proposed DARPC strategy. The TS optimization model and the WF optimization model are formulated in Sections 2.3 and 2.4, respectively. The distributed solution method based on the ADMM is described in Section 2.5. The simulation results and the discussion are presented in Section 2.6, followed by the conclusions.

2.2 Control Strategy Architecture

2.2.1 System Configuration

Fig. 2-1 shows the configuration of AC TS connected with WFs. Two WFs are connected to a modified IEEE 9-bus system. In the TS, Bus 1 is connected to the 345 kV external power system, and WF1 and WF2 with the nominal power rating of 160 MW are connected to Buses 2 and 3, respectively. Each WF is composed of two sections and each section has a medium voltage (MV) bus, which is located next to the 155 kV/33 kV substation transformer. Each 33 kV feeder consists of 8×5 MW WTs, which are arranged with 4 km away from each other.

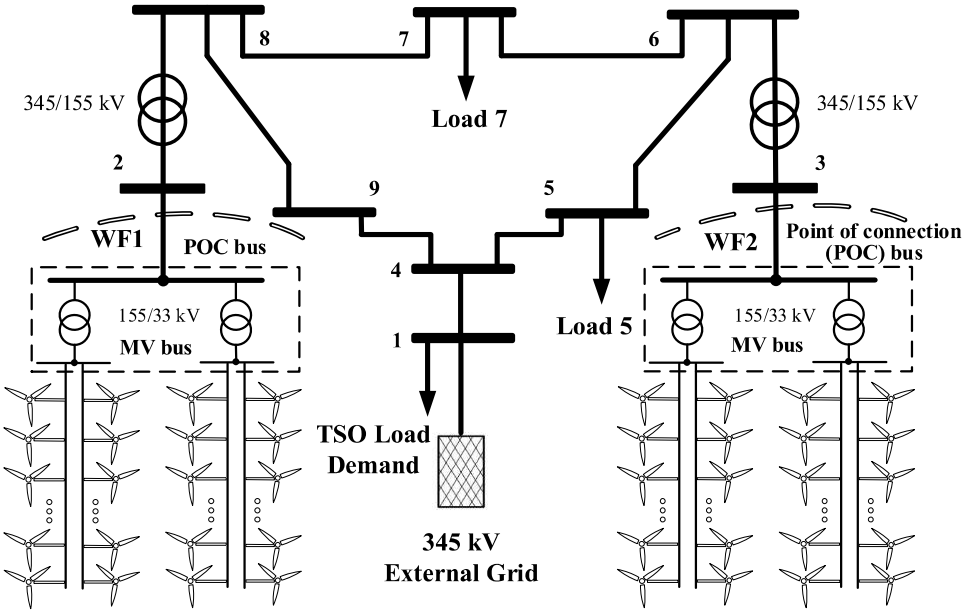

Fig. 2-1 Configuration of AC TS connected with WFs.

2.2.2 Concept of Proposed Strategy

Fig. 2-2 shows the structure of the proposed strategy. The TS and each WF are equipped with a controller. The whole system operates in a distributed manner by

using the ADMM to achieve the global optimal power distribution. The TSO sends the command $P_{\mathrm{d}}^{\mathrm{TSO}}$ to the TS controller. The TS controller also receives the information of available wind power $P_{\mathrm{WFs}}^{\mathrm{avi}}$ and admittance matrix of TS $\boldsymbol{Y}_{\mathrm{TS}}$. The TS controller solves the optimization problem of the TS to minimize the power losses of the TS and track the active power command from the TSO. Meanwhile, each WF controller generates WT power output references $P_{\mathrm{WT}}^{\mathrm{ref}}/Q_{\mathrm{WT}}^{\mathrm{ref}}$ to improve the voltage regulation performance and minimize power losses. The boundary information of optimal power references $P_{\mathrm{WF}}^{\mathrm{ref,TS}}/Q_{\mathrm{WF}}^{\mathrm{ref,TS}}$ and $P_{\mathrm{WF}}^{\mathrm{ref,WF}}/Q_{\mathrm{WF}}^{\mathrm{ref,WF}}$ is exchanged between the TS controller and WF controllers through the communication network. With part of calculation distributed to each WF controller, the large-scale constrained optimization problem is decomposed and the calculation burden can be significantly reduced without loss of the global optimality.

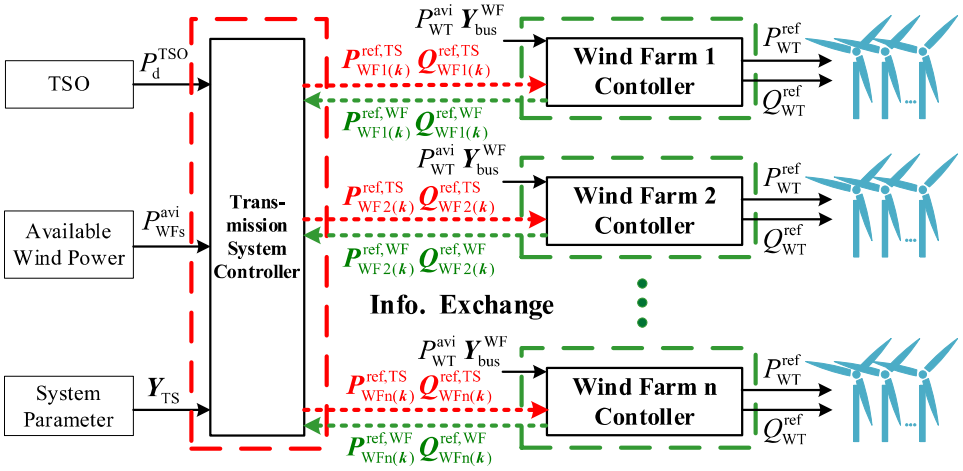

Fig. 2-2 Structure of proposed strategy.

2.3 TS Optimization Model

2.3.1 Objective Function and Constraints

2.3.1.1 Objective Function of TS

The objective function is to minimize the total power losses in the TS, which is equal to the total active power generation of WFs minus the total load of the TS. It can also be expressed as the summation of the injected active power into all the buses of the TS. Denote z^* as the conjugate of an arbitrary complex number z. Thus, the total power losses can be expressed as:

$$\begin{aligned} Obj_{\mathrm{TS}}^{\mathrm{Loss}} &= \sum_{i \in |\mathcal{N}_{\mathrm{TS}}|} (P_{\mathrm{WF}_i} - P_{\mathrm{D}_i}) \\ &= \sum_{i \in |\mathcal{N}_{\mathrm{TS}}|} \mathrm{Re}\{V_i I_i^*\} \end{aligned} \tag{2.1}$$

where P_{WF_i} is the power output of the i^{th} WF, which is connected to the terminal bus i in the TS directly, if the bus i is not associated with WF, then P_{WF_i}=0; P_{D_i} is the active load at bus i; V_i and I_i are the voltage and current associated with bus i, respectively; and $\mathcal{N}_{\mathrm{TS}}$ is the set of buses in the TS.

2.3.1.2 Constraints of TS

The OPF problem of the TS is subjected to a set of equality and inequality constraints. The equality constraints consist of the active/reactive power balance equations, as shown in (2.2) and (2.3), respectively.

$$P_{\mathrm{WF}_i} - P_{\mathrm{D}_i} = \mathrm{Re}\{V_i I_i^*\} \quad \forall i \in \mathcal{N}_{\mathrm{TS}} \tag{2.2}$$

$$Q_{\mathrm{WF}_i} - Q_{\mathrm{D}_i} = \mathrm{Im}\{V_i I_i^*\} \quad \forall i \in \mathcal{N}_{\mathrm{TS}} \tag{2.3}$$

where Q_{WF_i} is the reactive power output of the i^{th} WF, if the bus i is not associated with WF, then $Q_{\mathrm{WF}_i} = 0$.

The inequality constraints are expressed as:

$$P_{\mathrm{WF}_i}^{\min} \le P_{\mathrm{WF}_i} \le P_{\mathrm{WF}_i}^{\max} \tag{2.4}$$

$$Q_{\mathrm{WF}_i}^{\min} \le Q_{\mathrm{WF}_i} \le Q_{\mathrm{WF}_i}^{\max} \tag{2.5}$$

$$V_i^{\min} \le |V_i| \le V_i^{\max} \tag{2.6}$$

$$|S_{lm}| \le S_{lm}^{\max} \tag{2.7}$$

where $|V_i|$ is the voltage magnitude of the terminal bus i, S_{lm} is the apparent power flow through the transmission line from bus l to bus m; superscripts min and max are the lower and upper bounds of the corresponding values.

2.3.2 Convex Relaxation of OPF of TS

In this section, the SDP relaxation of the OPF problem of the TS is introduced. With the SDP relaxation applied, the non-convex OPF model of the TS can be transferred to a convex model and then solved under ADMM framework while guaranteeing the global optimal solution. Let matrix $\boldsymbol{Y}_{\mathrm{TS}}$ denotes the admittance matrix of TS. For $k \in \mathcal{N}_{\mathrm{TS}}$ and $(l, m) \in \boldsymbol{Line}$, $\boldsymbol{e}_k$ is the k^{th} basis vector in $\boldsymbol{R}^{|\mathcal{N}_{\mathrm{TS}}|}$, $\boldsymbol{e}_k^T$ is its transposed vector, and $\boldsymbol{Y}_k = \boldsymbol{e}_k \boldsymbol{e}_k^T \boldsymbol{Y}_{\mathrm{TS}}$. The π model of the transmission line (l, m) is applied; y_{lm} and $\bar{y}_{lm}$ are used to denote the value of the series and shunt sectors of the line (l, m), respectively [129]. Then $\boldsymbol{Y}_{lm} = (\bar{y}_{lm} + y_{lm})\boldsymbol{e}_l \boldsymbol{e}_l^T - y_{lm}\boldsymbol{e}_l \boldsymbol{e}_m^T$ is defined, which can be expressed as:

$$\boldsymbol{Y}_{lm} = \begin{bmatrix} 0 & \cdots & 0 & \cdots & 0 & \cdots & 0 \\ \vdots & & \vdots & & \vdots & & \vdots \\ 0 & \cdots & (\bar{y}_{lm} + y_{lm})_{ll} & \cdots & (-y_{lm})_{lm} & \cdots & 0 \\ \vdots & & \vdots & & \vdots & & \vdots \\ 0 & \cdots & 0 & \cdots & 0 & \cdots & 0 \end{bmatrix}_{|\mathcal{N}_{\mathrm{TS}}| \times |\mathcal{N}_{\mathrm{TS}}|} \tag{2.8}$$

In order to present the OPF of the TS in SDP form, the matrixes are defined as [129], [130]:

$$\boldsymbol{Y}_k^{\mathrm{TS}} = \frac{1}{2}\begin{bmatrix} \mathrm{Re}(\boldsymbol{Y}_k + \boldsymbol{Y}_k^T) & \mathrm{Im}(\boldsymbol{Y}_k^T - \boldsymbol{Y}_k) \\ \mathrm{Im}(\boldsymbol{Y}_k - \boldsymbol{Y}_k^T) & \mathrm{Re}(\boldsymbol{Y}_k + \boldsymbol{Y}_k^T) \end{bmatrix} \tag{2.9}$$

$$\bar{\boldsymbol{Y}}_k^{\mathrm{TS}} = -\frac{1}{2}\begin{bmatrix} \mathrm{Im}(\boldsymbol{Y}_k + \boldsymbol{Y}_k^T) & \mathrm{Re}(\boldsymbol{Y}_k - \boldsymbol{Y}_k^T) \\ \mathrm{Re}(\boldsymbol{Y}_k^T - \boldsymbol{Y}_k) & \mathrm{Im}(\boldsymbol{Y}_k + \boldsymbol{Y}_k^T) \end{bmatrix} \tag{2.10}$$

$$\boldsymbol{Y}_{lm}^{\mathrm{TS}} = \frac{1}{2}\begin{bmatrix} \mathrm{Re}(\boldsymbol{Y}_{lm} + \boldsymbol{Y}_{lm}^T) & \mathrm{Im}(\boldsymbol{Y}_{lm}^T - \boldsymbol{Y}_{lm}) \\ \mathrm{Im}(\boldsymbol{Y}_{lm} - \boldsymbol{Y}_{lm}^T) & \mathrm{Re}(\boldsymbol{Y}_{lm} + \boldsymbol{Y}_{lm}^T) \end{bmatrix} \tag{2.11}$$

$$\bar{\boldsymbol{Y}}_{lm}^{\mathrm{TS}} = -\frac{1}{2}\begin{bmatrix} \mathrm{Im}(\boldsymbol{Y}_{lm} + \boldsymbol{Y}_{lm}^T) & \mathrm{Re}(\boldsymbol{Y}_{lm} - \boldsymbol{Y}_{lm}^T) \\ \mathrm{Re}(\boldsymbol{Y}_{lm}^T - \boldsymbol{Y}_{lm}) & \mathrm{Im}(\boldsymbol{Y}_{lm} + \boldsymbol{Y}_{lm}^T) \end{bmatrix} \tag{2.12}$$

$$\boldsymbol{M}_k^{\mathrm{TS}} = \begin{bmatrix} \boldsymbol{e}_k \boldsymbol{e}_k^T & 0 \\ 0 & \boldsymbol{e}_k \boldsymbol{e}_k^T \end{bmatrix} \tag{2.13}$$

The real and imaginary sectors of the complex bus voltage vector $\boldsymbol{V}_{\mathrm{TS}} = [V_1, V_2, \cdots, V_{N_{\mathrm{TS}}}]_{1\times|\mathcal{N}_{\mathrm{TS}}|}$ is used to define $\boldsymbol{X}_{\mathrm{TS}}$, which is a $2|\mathcal{N}_{\mathrm{TS}}| \times 1$ variable vector.

$$\boldsymbol{X}_{\mathrm{TS}} = [\mathrm{Re}\{V_{\mathrm{TS}}\}^T \ \mathrm{Im}\{V_{\mathrm{TS}}\}^T]^T_{2|\mathcal{N}_{\mathrm{TS}}|\times 1}$$

Then, the V^*V^T can be substituted with a complex $2|\mathcal{N}_{\mathrm{TS}}| \times 2|\mathcal{N}_{\mathrm{TS}}|$ matrix $\boldsymbol{W}_{\mathrm{TS}}$, $\boldsymbol{W}_{\mathrm{TS}} = \boldsymbol{X}_{\mathrm{TS}}\boldsymbol{X}_{\mathrm{TS}}^T$.Then, the original complex formulation (2.1)-(2.7) can be split into the real and imaginary sectors [129].

$\mathrm{Tr}\{\boldsymbol{M}_a\}$ is used to represent the trace of an arbitrary square matrix $\boldsymbol{M}_a$. Then, the following (2.14)-(2.17) can be used to reformulate the objective function (2.1) and the constraints (2.2)-(2.7) with the new variable matrix $\boldsymbol{W}_{\mathrm{TS}}$.

$$\mathrm{Re}\{V_k I_k^*\} = \mathrm{Tr}\{\boldsymbol{Y}_k^{\mathrm{TS}}\boldsymbol{W}_{\mathrm{TS}}\} \tag{2.14}$$

$$\mathrm{Im}\{V_k I_k^*\} = \mathrm{Tr}\{\overline{\boldsymbol{Y}}_k^{\mathrm{TS}}\boldsymbol{W}_{\mathrm{TS}}\} \tag{2.15}$$

$$\left(V_k\right)^2 = \mathrm{Tr}\{\boldsymbol{M}_k^{\mathrm{TS}}\boldsymbol{W}_{\mathrm{TS}}\} \tag{2.16}$$

$$(\boldsymbol{S}_{lm})^2 = \mathrm{Tr}\{\boldsymbol{Y}_{lm}^{\mathrm{TS}}\boldsymbol{W}_{\mathrm{TS}}\}^2 + \mathrm{Tr}\{\overline{\boldsymbol{Y}}_{lm}^{\mathrm{TS}}\boldsymbol{W}_{\mathrm{TS}}\}^2 \tag{2.17}$$

2.3.2.1 Transformation of Objective Function

To transform the objective function (2.1) into the SDP form, (2.14) with the new variable matrix $\boldsymbol{W}_{\mathrm{TS}}$ is substituted into original function (2.1), and the SDP form of the objective function is:

$$Obj_{\mathrm{TS,Loss}}^{\mathrm{SDP}} = \sum_{k\in|\mathcal{N}_{\mathrm{TS}}|} \mathrm{Tr}\{\boldsymbol{Y}_k^{\mathrm{TS}}\boldsymbol{W}_{\mathrm{TS}}\} \tag{2.18}$$

2.3.2.2 Transformation of Constraints

The active/reactive power balance constraints in (2.2) and (2.3) can be combined with the WF active/reactive power output limits in (2.4) and (2.5). Then, the SDP form of the power balance constraints in terms of the power output limits can be obtained by substituting (2.14) and (2.15) into (2.2) and (2.3), which are expressed as:

$$P_{\mathrm{WF}_k}^{\min} - P_{\mathrm{D}_k} \le \mathrm{Tr}\{\boldsymbol{Y}_k^{\mathrm{TS}} \boldsymbol{W}_{\mathrm{TS}}\} \le P_{\mathrm{WF}_k}^{\max} - P_{\mathrm{D}_k} \tag{2.19}$$

$$Q_{\mathrm{WF}_k}^{\min} - Q_{\mathrm{D}_k} \le \mathrm{Tr}\{\overline{\boldsymbol{Y}}_k^{\mathrm{TS}} \boldsymbol{W}_{\mathrm{TS}}\} \le Q_{\mathrm{WF}_k}^{\max} - Q_{\mathrm{D}_k} \tag{2.20}$$

Similarly, substituting (2.16) into (2.6), the voltage constraint can be transformed into the SDP form:

$$(V_k^{\min})^2 \le \mathrm{Tr}\{\boldsymbol{M}_k^{\mathrm{TS}} \boldsymbol{W}_{\mathrm{TS}}\} \le (V_k^{\max})^2 \tag{2.21}$$

Substituting (2.17) into (2.7), the transmission line capacity constraint can be expressed as:

$$\mathrm{Tr}\{\boldsymbol{Y}_{lm}^{\mathrm{TS}} \boldsymbol{W}_{\mathrm{TS}}\}^2 + \mathrm{Tr}\{\overline{\boldsymbol{Y}}_{lm}^{\mathrm{TS}} \boldsymbol{W}_{\mathrm{TS}}\}^2 \le (\boldsymbol{S}_{lm}^{\max})^2 \tag{2.22}$$

In the SDP form, the constraints should be linear in $\boldsymbol{W}_{\mathrm{TS}}$. However, the constraint (2.22) is expressed as a quadratic constraint of $\boldsymbol{W}_{\mathrm{TS}}$. Thus, the Schur's complement is applied to transform the quadratic apparent line flow constraint (2.22) into a linear matrix inequality constraint as:

$$\begin{bmatrix} (\boldsymbol{S}_{lm}^{\max})^2 & \mathrm{Tr}\{\boldsymbol{Y}_{lm}^{\mathrm{TS}} \boldsymbol{W}_{\mathrm{TS}}\} & \mathrm{Tr}\{\overline{\boldsymbol{Y}}_{lm}^{\mathrm{TS}} \boldsymbol{W}_{\mathrm{TS}}\} \\ \mathrm{Tr}\{\boldsymbol{Y}_{lm}^{\mathrm{TS}} \boldsymbol{W}_{\mathrm{TS}}\} & 1 & 0 \\ \mathrm{Tr}\{\overline{\boldsymbol{Y}}_{lm}^{\mathrm{TS}} \boldsymbol{W}_{\mathrm{TS}}\} & 0 & 1 \end{bmatrix} \succeq 0 \tag{2.23}$$

At the same time, the non-convex constraint $\boldsymbol{W}_{\mathrm{TS}} = \boldsymbol{X}_{\mathrm{TS}} \boldsymbol{X}_{\mathrm{TS}}^T$ can be expressed as:

$$\boldsymbol{W}_{\mathrm{TS}} \succeq 0 \tag{2.24}$$

$$\mathrm{rank}(\boldsymbol{W}_{\mathrm{TS}}) = 1 \tag{2.25}$$

The convex relaxation is obtained by dropping the rank constraint (2.25), transforming the non-linear and non-convex OPF of the TS into a convex semidefinite program [128]. If the rank of $\boldsymbol{W}_{\mathrm{TS}}$ obtained from the SDP relaxation is 1, then $\boldsymbol{W}_{\mathrm{TS}}$ is the global optimum of the original non-linear and non-convex OPF of the TS [128]. Thus, the SDP relaxation of the OPF problem of the TS is expressed as:

$$\begin{cases} \min\ (18) \\ \text{s.t.}\ (19)-(24) \end{cases} \tag{2.26}$$

The optimization problem is implemented in MATLAB using the optimization toolbox YALMIP and the SDP solver MOSEK [130]. By solving the OPF problem of the TS in SDP form, the TS boundary variables of the optimal active/reactive power references of two WFs $\mathrm{Tr}\{\boldsymbol{Y}_{\mathrm{WF1}}^{\mathrm{TS}}\boldsymbol{W}_{\mathrm{TS}}\}/\mathrm{Tr}\{\overline{\boldsymbol{Y}}_{\mathrm{WF1}}^{\mathrm{TS}}\boldsymbol{W}_{\mathrm{TS}}\}$ and $\mathrm{Tr}\{\boldsymbol{Y}_{\mathrm{WF2}}^{\mathrm{TS}}\boldsymbol{W}_{\mathrm{TS}}\}/\mathrm{Tr}\{\overline{\boldsymbol{Y}}_{\mathrm{WF2}}^{\mathrm{TS}}\boldsymbol{W}_{\mathrm{TS}}\}$ are generated. These boundary variables can be exchanged between TS controller and WF controllers under the ADMM framework.

2.4 WF Optimization Model

Since a WF has a radial topology, the power flow in the WF can be expressed by the linearized branch flow model [131]-[134]. The power flow from the AC TS to the WF is defined as the positive direction in WF collection system.

$$-\mathrm{Tr}\{\boldsymbol{Y}_{\mathrm{WF}_k}^{\mathrm{TS}}\boldsymbol{W}_{\mathrm{TS}}\} = P_{\mathrm{WF}_k}^{\mathrm{ref,WF}},\ P_j + p_{j+1}^{\mathrm{WT}} = P_{j+1} \tag{2.27}$$

$$-\mathrm{Tr}\{\overline{\boldsymbol{Y}}_{\mathrm{WF}_k}^{\mathrm{TS}}\boldsymbol{W}_{\mathrm{TS}}\} = Q_{\mathrm{WF}_k}^{\mathrm{ref,WF}},\ Q_j + q_{j+1}^{\mathrm{WT}} = Q_{j+1} \tag{2.28}$$

$$V_{j+1} = V_j - \frac{R_j^{\mathrm{WF}}P_j + X_j^{\mathrm{WF}}Q_j}{V_0^{\mathrm{WF}}} \tag{2.29}$$

where $\mathrm{Tr}\{\boldsymbol{Y}_{\mathrm{WF}_k}^{\mathrm{TS}}\boldsymbol{W}_{\mathrm{TS}}\}/\mathrm{Tr}\{\overline{\boldsymbol{Y}}_{\mathrm{WF}_k}^{\mathrm{TS}}\boldsymbol{W}_{\mathrm{TS}}\}$ and $P_{\mathrm{WF}_k}^{\mathrm{ref,WF}}/Q_{\mathrm{WF}_k}^{\mathrm{ref,WF}}$ are the boundary optimization variables of the active/reactive power outputs for k^{th} WF processed in TS controller and WF controllers; $P_j + \mathrm{j}Q_j$ is the apparent power flowing from bus j to bus $j+1$, and $(j, j+1) \in \boldsymbol{Line}$; p_{j+1}^{WT} and q_{j+1}^{WT} are the active and reactive power generated by the WT associated with bus j+1; V_j is the voltage magnitude at bus j; $R_j^{\mathrm{WF}} + \mathrm{j}X_j^{\mathrm{WF}}$ is the complex impedance between bus j and bus $j+1$; V_0^{WF} is the voltage magnitude at the boundary bus associated with WF. Considering the capacity of each WF is much less than the TS, the bus 2 and bus 3 can be assumed as the slack buses for two WFs.

The per unit voltage variation should also be considered.

$$V_j^{\min} \le V_j \le V_j^{\max} \tag{2.30}$$

where $V_j^{\min}$ and $V_j^{\max}$ are generally set to be 0.95 p.u. and 1.05 p.u., respectively.

To minimize the power losses in each WF collection system, the power losses can be expressed as:

$$Obj_{\mathrm{WF}}^{\mathrm{Loss}} = \sum_{j=1}^{N_{\mathrm{WT}}} (p_j^{\mathrm{WT}}) - P_{\mathrm{WF}_k}^{\mathrm{ref,WF}} \tag{2.31}$$

where N_{WT} is the number of the WTs in WF.

The voltage variation for all buses inside WF should also be minimized.

$$Obj_{\mathrm{WF}}^{\mathrm{VD}} = \sum_{j=1}^{N_{\mathrm{WF}}} \left(V_j - V_{\mathrm{rated}}\right)^2 \tag{2.32}$$

where N_{WF} is the number of the buses in WF; and V_{rated} is the rated voltage in WF.

The active power output of each WT should be dispatched as close as possible to the PD-based reference [135].

$$Obj_{\mathrm{WF}}^{\mathrm{PD}} = \sum_{j=1}^{N_{\mathrm{WT}}} (p_j^{\mathrm{WT}} - p_{\mathrm{PD},j}^{\mathrm{ref}})^2 \tag{2.33}$$

The PD reference is defined as:

$$p_{\mathrm{PD},j}^{\mathrm{ref}} = \frac{P_{\mathrm{WT},j}^{\mathrm{avi}}}{\sum_j P_{\mathrm{WT},j}^{\mathrm{avi}}} P_{\mathrm{WF}}^{\mathrm{ref}} \tag{2.34}$$

where $P_{\mathrm{WT},j}^{\mathrm{avi}}$ is the available wind power of the j^{th} WT.

The WF optimization problem can be converted to a standard quadratic-programming (QP) problem and efficiently solved by QP solvers in milliseconds [74]. Thus, the WF optimization problem is as follows,

$$\begin{cases} \min\ (31) - (33) \\ \mathrm{s.t.}\ (27) - (30) \end{cases} \tag{2.35}$$

2.5 ADMM Formulation for Whole System

Considering the whole system consists of the TS and the several WFs with several hundreds or even thousands of WTs, the optimization problem of the whole system becomes a large-scale model with large-scale constraints. To reduce the computation burden, an ADMM-based DARPC strategy is proposed. The whole system can be partitioned into several areas: a TS area and two WF areas. With the ADMM algorithm implemented, the calculation of the TS and the WFs can be decoupled. Thus, the objective functions (2.18) and (2.31)-(2.33) can be distributed to the TS controller and WF controllers and processed in parallel while guaranteeing the global optimality. The optimization problem of the whole system is expressed as:

$$\begin{aligned}\min\ & \sum_{k=1}^{|\mathcal{N}_{\mathrm{TS}}|}\mathrm{Tr}\{\boldsymbol{Y}_k^{\mathrm{TS}}\boldsymbol{W}_{\mathrm{TS}}\}+\sum_{k=1}^{2}\left\{\sum_{j=1}^{N_{\mathrm{WT}}}(p_{j,k}^{\mathrm{WT}})-P_{\mathrm{WF}_k}^{\mathrm{ref,WF}}+\right.\\ & \left.\sum_{j=1}^{N_{\mathrm{WF}}}\left(V_{j,k}-V_{\mathrm{rated}}\right)^2+\sum_{j=1}^{N_{\mathrm{WT}}}(p_{j,k}^{\mathrm{WT}}-p_{\mathrm{PD},j,k}^{\mathrm{ref}})^2\right\}\end{aligned} \tag{2.36}$$

$$\begin{aligned}\text{s.t.}\quad & (2.19)-(2.24),\quad (2.27)-(2.30),\\ & \mathrm{Tr}\{\boldsymbol{Y}_{\mathrm{WF}_k}^{\mathrm{TS}}\boldsymbol{W}_{\mathrm{TS}}\}-P_{\mathrm{WF}_k}^{\mathrm{ref,WF}}=0,\ k=1,2.\\ & \mathrm{Tr}\{\overline{\boldsymbol{Y}}_{\mathrm{WF}_k}^{\mathrm{TS}}\boldsymbol{W}_{\mathrm{TS}}\}-Q_{\mathrm{WF}_k}^{\mathrm{ref,WF}}=0,\ k=1,2.\\ & \mathrm{Tr}\{\boldsymbol{M}_{\mathrm{WF}_k}^{\mathrm{TS}}\boldsymbol{W}_{\mathrm{TS}}\}-(V_k^{\mathrm{WF}})^2=0,\ k=1,2.\end{aligned} \tag{2.37}$$

where $\mathrm{Tr}\{\boldsymbol{M}_{\mathrm{WF}_k}^{\mathrm{TS}}\boldsymbol{W}_{\mathrm{TS}}\}$ and $(V_k^{\mathrm{WF}})^2$ are the square of the k^{th} boundary bus voltage processed in the TS controller and WF controllers, respectively. Thus, the augmented Lagrangian objective function of (2.36) can be expressed as:

$$\begin{aligned}\min\ & \sum_{k=1}^{|\mathcal{N}_{\mathrm{TS}}|}\mathrm{Tr}\{\boldsymbol{Y}_k^{\mathrm{TS}}\boldsymbol{W}_{\mathrm{TS}}\}+\sum_{k=1}^{2}\left\{\sum_{j=1}^{N_{\mathrm{WT}}}(p_{j,k}^{\mathrm{WT}})-P_{\mathrm{WF}_k}^{\mathrm{ref,WF}}+\right.\\ & \left.\sum_{j=1}^{N_{\mathrm{WF}}}\left(V_{j,k}-V_{\mathrm{rated}}\right)^2+\sum_{j=1}^{N_{\mathrm{WT}}}(p_{j,k}^{\mathrm{WT}}-p_{\mathrm{PD},j,k}^{\mathrm{ref}})^2\right\}\\ & +\sum_{k=1}^{2}\lambda_k^{\mathrm{P}}[\mathrm{Tr}\{\boldsymbol{Y}_{\mathrm{WF}_k}^{\mathrm{TS}}\boldsymbol{W}_{\mathrm{TS}}\}-P_{\mathrm{WF}_k}^{\mathrm{ref,WF}}]+\sum_{k=1}^{2}\frac{\rho}{2}\left\|\mathrm{Tr}\{\boldsymbol{Y}_{\mathrm{WF}_k}^{\mathrm{TS}}\boldsymbol{W}_{\mathrm{TS}}\}-P_{\mathrm{WF}_k}^{\mathrm{ref,WF}}\right\|^2\\ & +\sum_{k=1}^{2}\lambda_k^{\mathrm{Q}}[\mathrm{Tr}\{\overline{\boldsymbol{Y}}_{\mathrm{WF}_k}^{\mathrm{TS}}\boldsymbol{W}_{\mathrm{TS}}\}-Q_{\mathrm{WF}_k}^{\mathrm{ref,WF}}]+\sum_{k=1}^{2}\frac{\rho}{2}\left\|\mathrm{Tr}\{\overline{\boldsymbol{Y}}_{\mathrm{WF}_k}^{\mathrm{TS}}\boldsymbol{W}_{\mathrm{TS}}\}-Q_{\mathrm{WF}_k}^{\mathrm{ref,WF}}\right\|^2\end{aligned} \tag{2.38}$$

where the dual variables are defined as λ_k^P and λ_k^Q for the objective function; and the parameter ρ is considered as the penalty for the optimization variables in the TS that differ from the variables in the WFs.

The topology of system communication network is shown in Fig. 2-3.

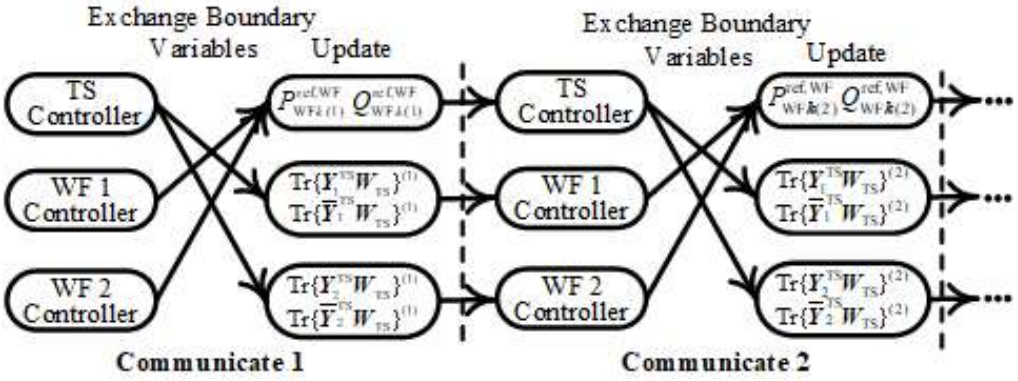

Fig. 2-3 Topology of system communication network.

The initial optimization variables and the dual variables are set to zero. r is defined as the step of iteration, and each iterative step includes the following steps:

1) The TS controller updates and solves the optimization variables in the TS by using the augmented Lagrangian objective function with the constraints of the TS,

$$\begin{cases} \left(\mathrm{Tr}\{\boldsymbol{Y}_{\mathrm{WF}_k}^{\mathrm{TS}}\boldsymbol{W}_{\mathrm{TS}}\},\mathrm{Tr}\{\overline{\boldsymbol{Y}}_{\mathrm{WF}_k}^{\mathrm{TS}}\boldsymbol{W}_{\mathrm{TS}}\}\right)(r+1)=\underset{\substack{\mathrm{Tr}\{\boldsymbol{Y}_{\mathrm{WF}_k}^{\mathrm{TS}}\boldsymbol{W}_{\mathrm{TS}}\}\\ \mathrm{Tr}\{\overline{\boldsymbol{Y}}_{\mathrm{WF}_k}^{\mathrm{TS}}\boldsymbol{W}_{\mathrm{TS}}\}}}{\arg\min}\sum_{k=1}^{|\mathcal{N}_{\mathrm{TS}}|}\mathrm{Tr}\{\boldsymbol{Y}_k^{\mathrm{TS}}\boldsymbol{W}_{\mathrm{TS}}\}+ \\ \sum_{k=1}^{2}\lambda_k^{\mathrm{P}}[\mathrm{Tr}\{\boldsymbol{Y}_{\mathrm{WF}_k}^{\mathrm{TS}}\boldsymbol{W}_{\mathrm{TS}}\}-P_{\mathrm{WF}_k}^{\mathrm{ref,WF}}(r)]+\sum_{k=1}^{2}\frac{\rho}{2}\left\|\mathrm{Tr}\{\boldsymbol{Y}_{\mathrm{WF}_k}^{\mathrm{TS}}\boldsymbol{W}_{\mathrm{TS}}\}-P_{\mathrm{WF}_k}^{\mathrm{ref,WF}}(r)\right\|^2+ \\ \sum_{k=1}^{2}\lambda_k^{\mathrm{Q}}[\mathrm{Tr}\{\overline{\boldsymbol{Y}}_{\mathrm{WF}_k}^{\mathrm{TS}}\boldsymbol{W}_{\mathrm{TS}}\}-Q_{\mathrm{WF}_k}^{\mathrm{ref,WF}}(r)]+\sum_{k=1}^{2}\frac{\rho}{2}\left\|\mathrm{Tr}\{\overline{\boldsymbol{Y}}_{\mathrm{WF}_k}^{\mathrm{TS}}\boldsymbol{W}_{\mathrm{TS}}\}-Q_{\mathrm{WF}_k}^{\mathrm{ref,WF}}(r)\right\|^2 \\ \mathrm{s.t.}(2.19)-(2.24),(2.37) \end{cases} \quad (2.39)$$

In (2.39), the augmented Lagrangian objective function is expressed as a quadratic function of matrix $\boldsymbol{W}_{\mathrm{TS}}$. However, in the SDP form, the objective function should be linear with $\boldsymbol{W}_{\mathrm{TS}}$. Thus, the objective function (2.40) and constraints (2.41)-(2.42)

are formulated to represent the original augmented Lagrangian objective (2.39) using the Schur's complement with auxiliary variables α_k^{P} and α_k^{Q}.

$$\begin{aligned}&\left(\mathrm{Tr}\{\boldsymbol{Y}_{\mathrm{WF}_k}^{\mathrm{TS}}\boldsymbol{W}_{\mathrm{TS}}\},\mathrm{Tr}\{\overline{\boldsymbol{Y}}_{\mathrm{WF}_k}^{\mathrm{TS}}\boldsymbol{W}_{\mathrm{TS}}\}\right)(r+1)=\\&\underset{\substack{\mathrm{Tr}\{\boldsymbol{Y}_{\mathrm{WF}_k}^{\mathrm{TS}}\boldsymbol{W}_{\mathrm{TS}}\}\\ \mathrm{Tr}\{\overline{\boldsymbol{Y}}_{\mathrm{WF}_k}^{\mathrm{TS}}\boldsymbol{W}_{\mathrm{TS}}\}}}{\arg\min}\sum_{k=1}^{|\mathcal{N}_{\mathrm{TS}}|}\mathrm{Tr}\{\boldsymbol{Y}_k^{\mathrm{TS}}\boldsymbol{W}_{\mathrm{TS}}\}+\sum_{k=1}^{2}(\alpha_k^{\mathrm{P}}+\alpha_k^{\mathrm{Q}})\end{aligned}\tag{2.40}$$

$$\begin{bmatrix}\lambda_k^{\mathrm{P}}\mathrm{Tr}\{\boldsymbol{Y}_{\mathrm{WF}_k}^{\mathrm{TS}}\boldsymbol{W}_{\mathrm{TS}}\}+a_k^{\mathrm{P}} & \sqrt{\frac{\rho}{2}}\mathrm{Tr}\{\boldsymbol{Y}_{\mathrm{WF}_k}^{\mathrm{TS}}\boldsymbol{W}_{\mathrm{TS}}\}+b_k^{\mathrm{P}}\\ \sqrt{\frac{\rho}{2}}\mathrm{Tr}\{\boldsymbol{Y}_{\mathrm{WF}_k}^{\mathrm{TS}}\boldsymbol{W}_{\mathrm{TS}}\}+b_k^{\mathrm{P}} & -1\end{bmatrix}\preceq 0,k=1,2.\tag{2.41}$$

$$\begin{bmatrix}\lambda_k^{\mathrm{Q}}\mathrm{Tr}\{\overline{\boldsymbol{Y}}_{\mathrm{WF}_k}^{\mathrm{TS}}\boldsymbol{W}_{\mathrm{TS}}\}+a_k^{\mathrm{Q}} & \sqrt{\frac{\rho}{2}}\mathrm{Tr}\{\overline{\boldsymbol{Y}}_{\mathrm{WF}_k}^{\mathrm{TS}}\boldsymbol{W}_{\mathrm{TS}}\}+b_k^{\mathrm{Q}}\\ \sqrt{\frac{\rho}{2}}\mathrm{Tr}\{\overline{\boldsymbol{Y}}_{\mathrm{WF}_k}^{\mathrm{TS}}\boldsymbol{W}_{\mathrm{TS}}\}+b_k^{\mathrm{Q}} & -1\end{bmatrix}\preceq 0,k=1,2.\tag{2.42}$$

$$\mathrm{s.t.}\,(2.19)-(2.24),(2.37)$$

where $a_k^{\mathrm{P}}=-\alpha_k^{\mathrm{P}}-\lambda_k^{\mathrm{P}}P_{\mathrm{WF}_k}^{\mathrm{ref,WF}}(r)$, $b_k^{\mathrm{P}}=-\sqrt{\frac{\rho}{2}}P_{\mathrm{WF}_k}^{\mathrm{ref,WF}}(r)$,

$a_k^{\mathrm{Q}}=-\alpha_k^{\mathrm{Q}}-\lambda_k^{\mathrm{Q}}Q_{\mathrm{WF}_k}^{\mathrm{ref,WF}}(r)$, $b_k^{\mathrm{Q}}=-\sqrt{\frac{\rho}{2}}Q_{\mathrm{WF}_k}^{\mathrm{ref,WF}}(r)$.

2) After updating the optimization variables in the TS, each WF controller solves its augmented Lagrangian problem with the constraints of the WF in parallel, and updates the optimization variables. For the kth WF controller, the objective function and constraint are expressed as:

$$
\begin{cases}
\left(P_{\mathrm{WF}_k}^{\mathrm{ref,WF}}, Q_{\mathrm{WF}_k}^{\mathrm{ref,WF}}\right)(r+1) = \underset{P_{\mathrm{WF}_k}^{\mathrm{ref,WF}}, Q_{\mathrm{WF}_k}^{\mathrm{ref,WF}}}{\arg\min} \\
\sum_{j=1}^{N_{\mathrm{WT}}} (p_{j,k}^{\mathrm{WT}}) - P_{\mathrm{WF}_k}^{\mathrm{ref,WF}} + \sum_{j=1}^{N_{\mathrm{WF}}} \left(V_{j,k} - V_{\mathrm{rated}}\right)^2 + \sum_{j=1}^{N_{\mathrm{WT}}} (p_{j,k}^{\mathrm{WT}} - p_{\mathrm{PD},j,k}^{\mathrm{ref}})^2 + \\
\lambda_k^{\mathrm{P}}[\mathrm{Tr}\{\boldsymbol{Y}_{\mathrm{WF}_k}^{\mathrm{TS}} \boldsymbol{W}_{\mathrm{TS}}\}(r+1) - P_{\mathrm{WF}_k}^{\mathrm{ref,WF}}] + \frac{\rho}{2}\left\|\mathrm{Tr}\{\boldsymbol{Y}_{\mathrm{WF}_k}^{\mathrm{TS}} \boldsymbol{W}_{\mathrm{TS}}\}(r+1) - P_{\mathrm{WF}_k}^{\mathrm{ref,WF}}\right\|^2 + \\
\lambda_k^{Q}[\mathrm{Tr}\{\overline{\boldsymbol{Y}}_{\mathrm{WF}_k}^{\mathrm{TS}} \boldsymbol{W}_{\mathrm{TS}}\}(r+1) - Q_{\mathrm{WF}_k}^{\mathrm{ref,WF}}] + \frac{\rho}{2}\left\|\mathrm{Tr}\{\overline{\boldsymbol{Y}}_{\mathrm{WF}_k}^{\mathrm{TS}} \boldsymbol{W}_{\mathrm{TS}}\}(r+1) - Q_{\mathrm{WF}_k}^{\mathrm{ref,WF}}\right\|^2 \\
k = 1, 2. \\
\mathrm{s.t.}(2.27) - (2.30), (2.37)
\end{cases}
\tag{2.43}
$$

These two sub-optimization problems can be solved quickly by using the commercial optimization solvers.

3) Update the dual variables in the WF controllers using (2.44)-(2.45).

$$
\lambda_k^{\mathrm{P}}(r+1) = \lambda_k^{\mathrm{P}}(r) + \rho[P_{\mathrm{WF}_k}^{\mathrm{ref,WF}}(r+1) - \mathrm{Tr}\{\boldsymbol{Y}_{\mathrm{WF}_k}^{\mathrm{TS}} \boldsymbol{W}_{\mathrm{TS}}\}(r+1)] \tag{2.44}
$$

$$
\lambda_k^{\mathrm{Q}}(r+1) = \lambda_k^{\mathrm{Q}}(r) + \rho[Q_{\mathrm{WF}_k}^{\mathrm{ref,WF}}(r+1) - \mathrm{Tr}\{\overline{\boldsymbol{Y}}_{\mathrm{WF}_k}^{\mathrm{TS}} \boldsymbol{W}_{\mathrm{TS}}\}(r+1)] \tag{2.45}
$$

With the part of the computation tasks distributed to each WF controller, the large-scale constrained optimization problem is decomposed. For the TS controller, the computation task is to deal with the objective function with the constraints inside the TS. Considering several WFs are connected to the TS, the computation task of the TS controller can be significantly reduced, and meanwhile the central controller and centralized communication can also be eliminated without loss of global optimality. For each WF controller, the computation task is an optimization problem with the constraints inside the WF and its computation burden is not heavy. Table A-1 presents the steps of the above solution method.

2.6 Case Study

2.6.1 Test System

The WFs with 64×5 MW WTs with a modified IEEE 9-bus system are used to demonstrate the performance of the proposed DARPC strategy. For the optimal control strategy, it is carried out every 5 s. In order to examine the performance of the proposed scheme, the simulation results are compared with the centralized active and reactive power control (CARPC) strategy and the ones with active and

reactive power PD control scheme [94]. In the CARPC strategy, the central controller can generate the active and reactive power references of each WT among WFs and achieve the optimal control performance [80]. Table B-1 presents the parameters of the system [80], [94].

2.6.2 Control Performance

The total simulation time is 600 s. Fig. 2-4 shows the available wind power for each WF. The available wind power fluctuates within [120,153] MW and [90,120] MW in WF1 and WF2, respectively. During t=200-400 s, the available wind power gradually rises. After t=400 s, the available wind power gradually decreases.

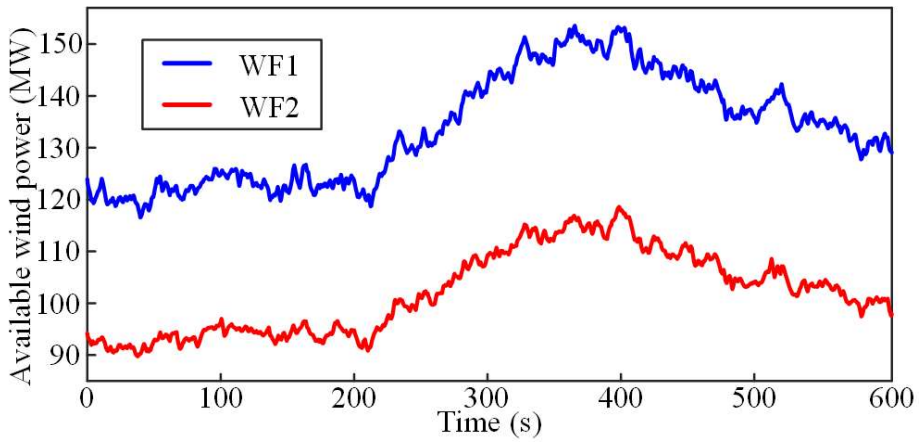

Fig. 2-4 Available wind power of each WF.

The MV bus voltage in WF1 is shown in Fig. 2-5. It can be seen that the ADMM-based DARPC strategy has the similar control performance as the CARPC strategy and they can both effectively control the MV bus voltage within the feasible range. The MV bus voltage is closer to the rated value using DARPC or CARPC strategy than using PD control scheme. The MV bus voltage with DARPC or CARPC strategy can be kept at 1.0019 p.u., and then gradually increases to 1.0250 p.u. with the active power output of WF1 increasing by 11.10 MW during t=200-400 s. After t=400 s, the MV bus voltage decreases slightly to 1.0140 p.u. with the active power output decreasing by 5.00 MW. Obviously, the voltage value difference between the DARPC and CARPC strategies is very small (less than 0.0005 p.u.). Meanwhile, the voltages with these two strategies also exhibit the similar variations.

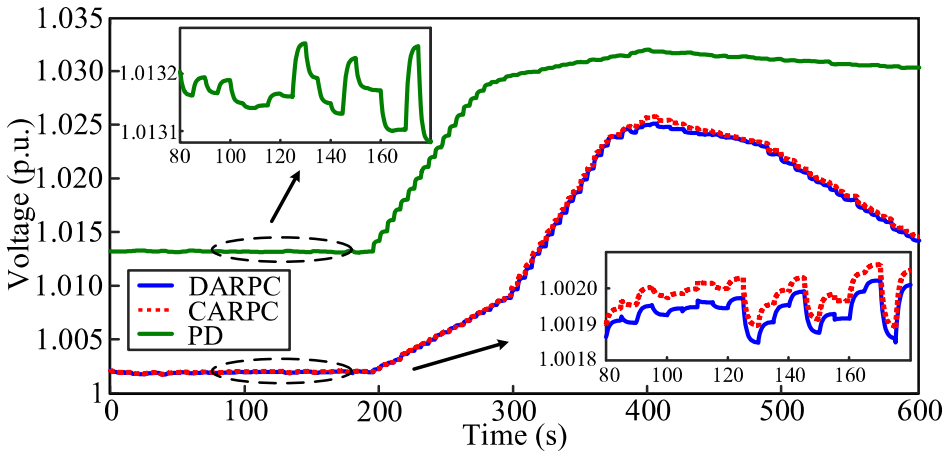

Fig. 2-5 MV bus voltage in WF1.

Fig. 2-6 shows the terminal voltage of WT32, which is located at the furthest position along the feeder in WF1. The performance with the DARPC and CARPC strategies is very similar and much better than PD control scheme. During the whole control period, the terminal voltage of WT32 can be kept within 1.024-1.048 p.u., while the voltage with PD control scheme is farther away from the rated value. The voltage deviation with the DARPC or CARPC strategy is also better than PD control scheme. The maximal voltage difference between the DARPC and CARPC strategies is 0.00008 p.u.

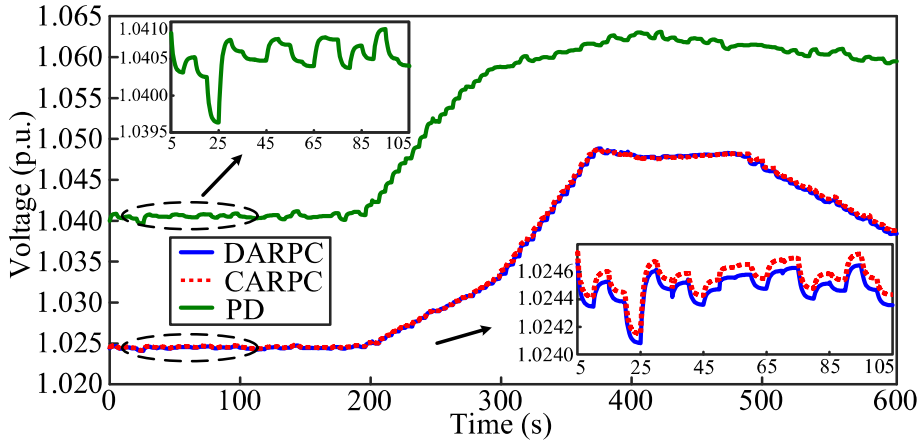

Fig. 2-6 Terminal voltage of WT32 in WF1.

WT1 is selected as the representative WT in WF1 to illustrate the performance of the WF control among three control strategies. In Fig. 2-7 - Fig. 2-10, during t=200-400 s, the terminal voltage of WT1 with DARPC or CARPC strategy gradually increases from 1.0123 p.u. to 1.0368 p.u. with the WT1 active and reactive power output increasing by 1.37 MW and 0.2025 Mvar, respectively. The WT1 terminal voltage is closer to the rated value, and the voltage fluctuation is also smaller using DARPC or CARPC strategy than using PD control scheme. Obviously, the voltage regulation, active and reactive power output of the DARPC and CARPC strategies are very similar, which show better control performance than PD control scheme.

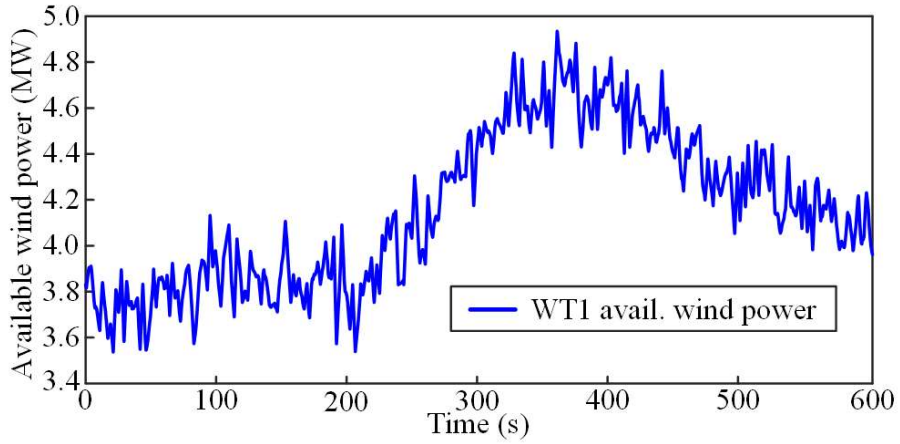

Fig. 2-7 Available wind power of WT1 in WF1.

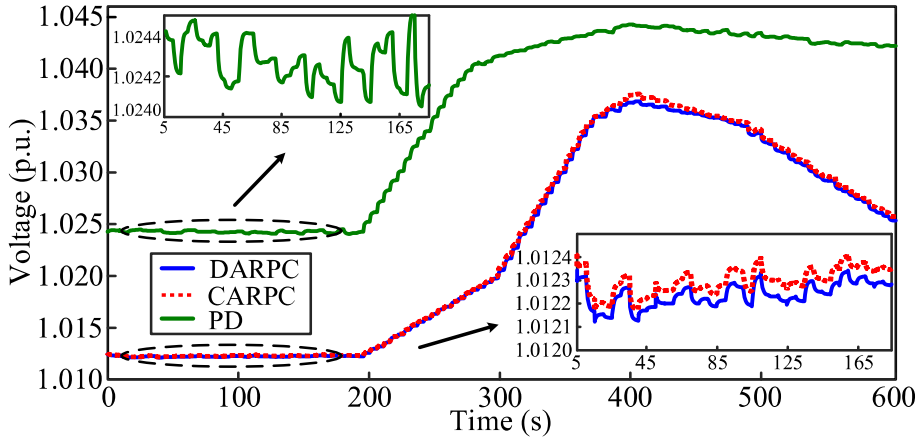

Fig. 2-8 Terminal voltage of WT1 in WF1.

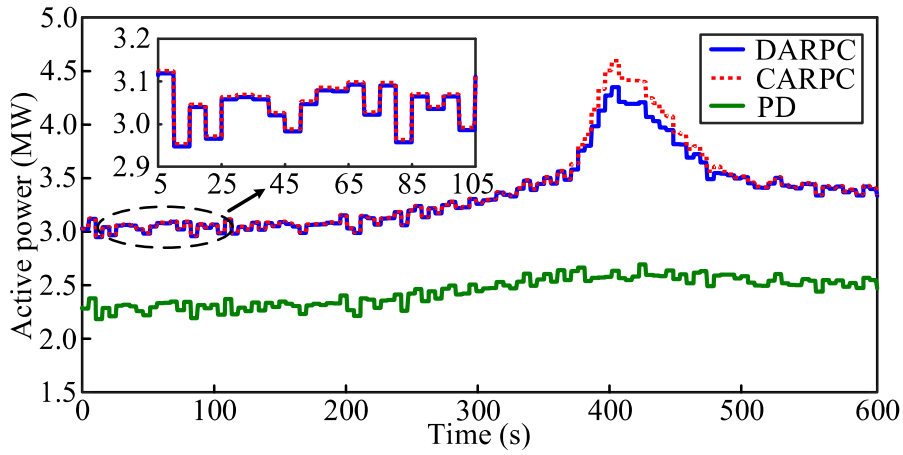

Fig. 2-9 Active power output of WT1 in WF1.

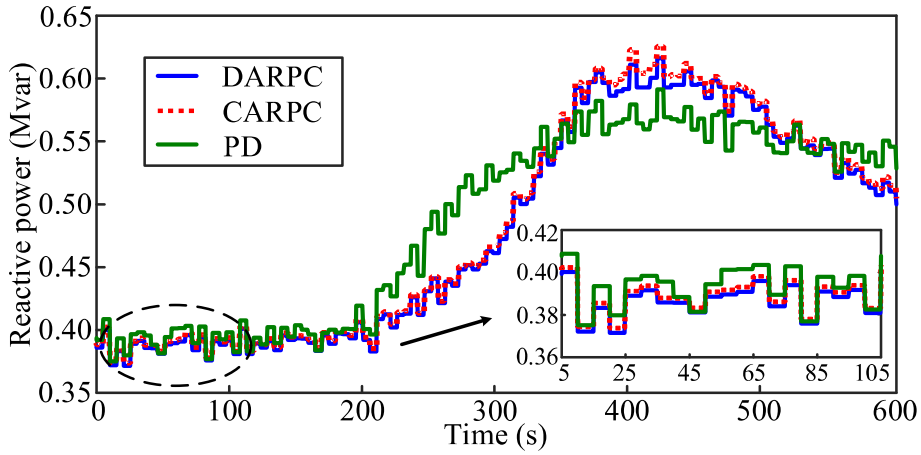

Fig. 2-10 Reactive power output of WT1 in WF1.

The active and reactive power outputs of WF1 are presented in Fig. 2-11-Fig. 2-12. The active and reactive power output of WF1 with DARPC is very similar with CARPC, and different from the PD method.

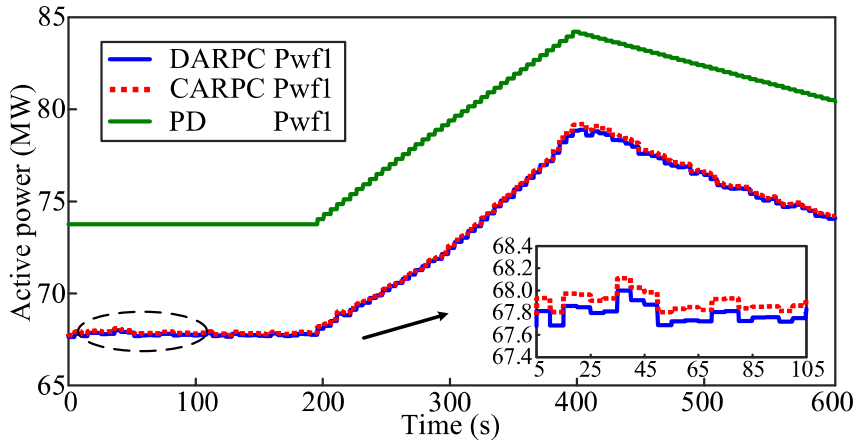

Fig. 2-11 Active power output of WF1.

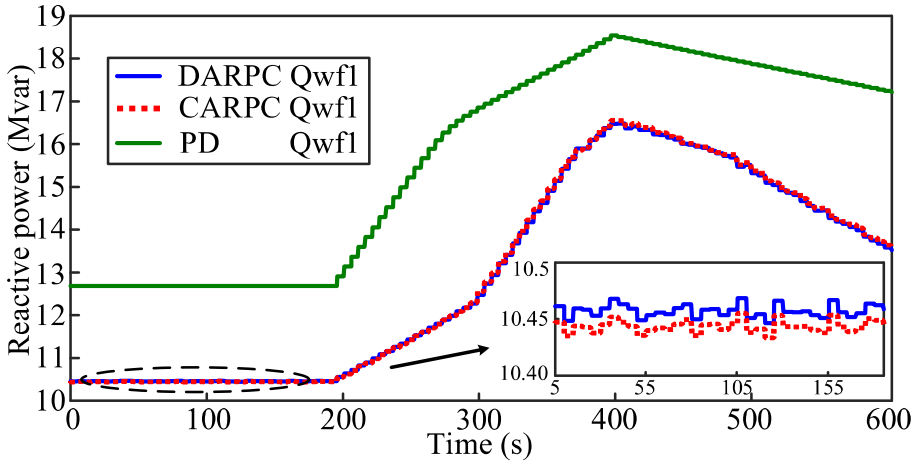

Fig. 2-12 Reactive power output of WF1.

The power losses of WF1 and WF2, and the whole system are shown in Fig. 2-13 and Fig. 2-14, respectively. It can be seen that the power losses with DARPC and CARPC strategies are very similar, the performance of which are much better than PD control scheme. Meanwhile, compared with the CARPC strategy, the DARPC strategy eliminates the central controller and largely reduces the computation burden and communication cost. Moreover, since each WF controller only exchanges the very little boundary information with the TS controller, the protection of information and data privacy is evidently improved.

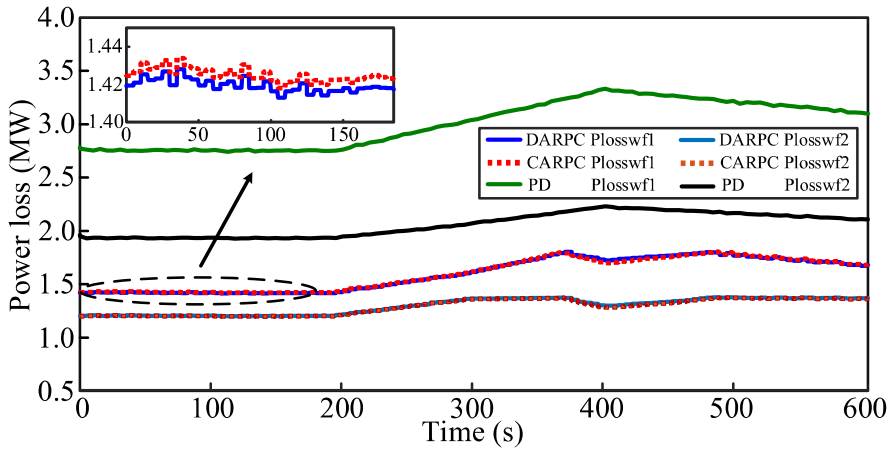

Fig. 2-13 Power losses of WF1 and WF2.

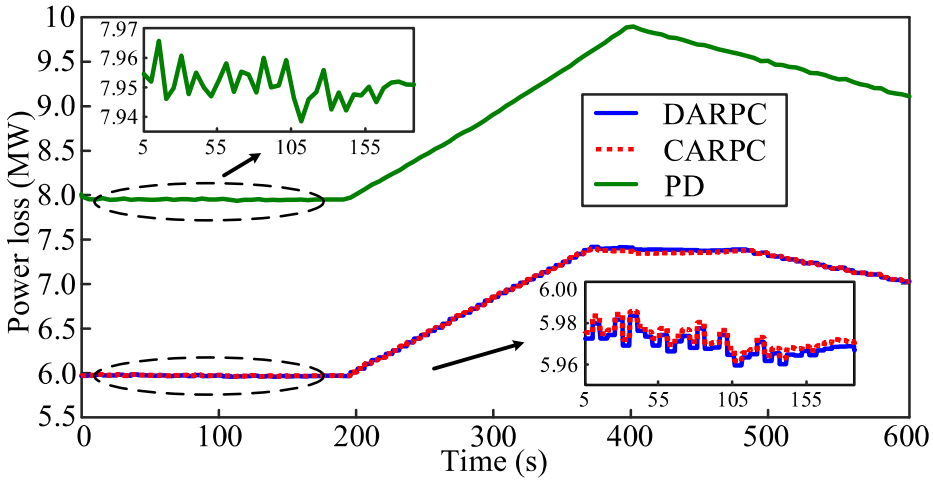

Fig. 2-14 Power loss of whole system.

Fig. 2-15-Fig. 2-17 show the convergence performance of the system. The boundary information of the active and reactive power outputs of WF1 and WF2 is selected to illustrate the results. The optimization variables in the TS and WF with the active power output for WF1 and WF2 converge to the same value and keep steady after 13 iterations. The convergence performance is acceptance. As shown in Fig. 2-17, the optimization variables in the TS and WF with the reactive power output for WF1 and WF2 converge to 10.46 Mvar and 14.08 Mvar in 13 iterations, respectively, which shows the excellent convergence performance.

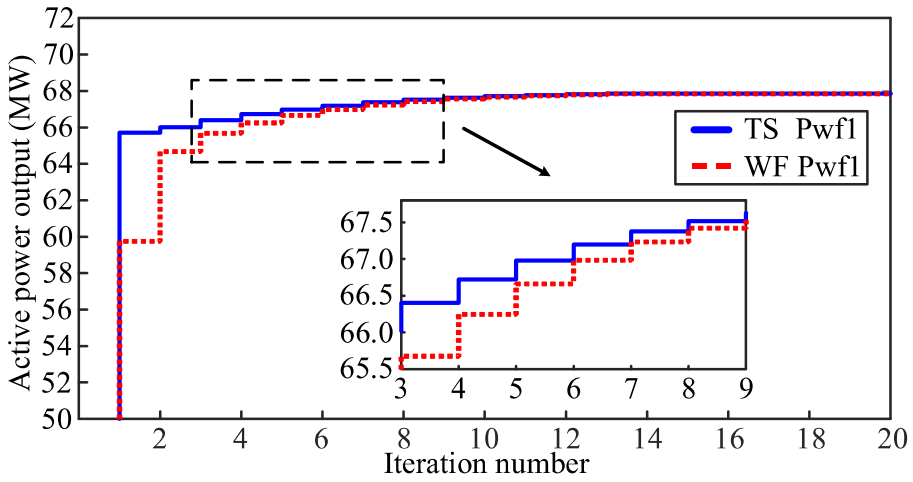

Fig. 2-15 Convergence performance of active power output of WF1. (t=20s)

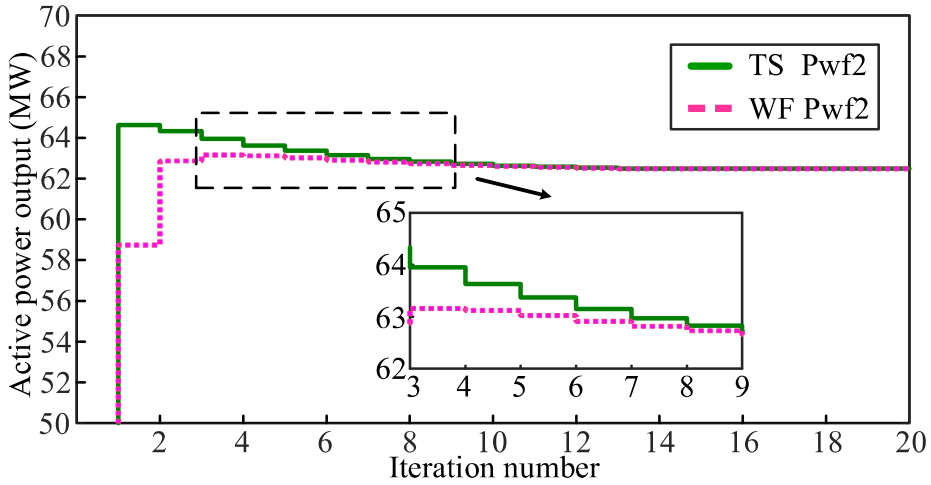

Fig. 2-16 Convergence performance of active power output of WF2. (t=20s)

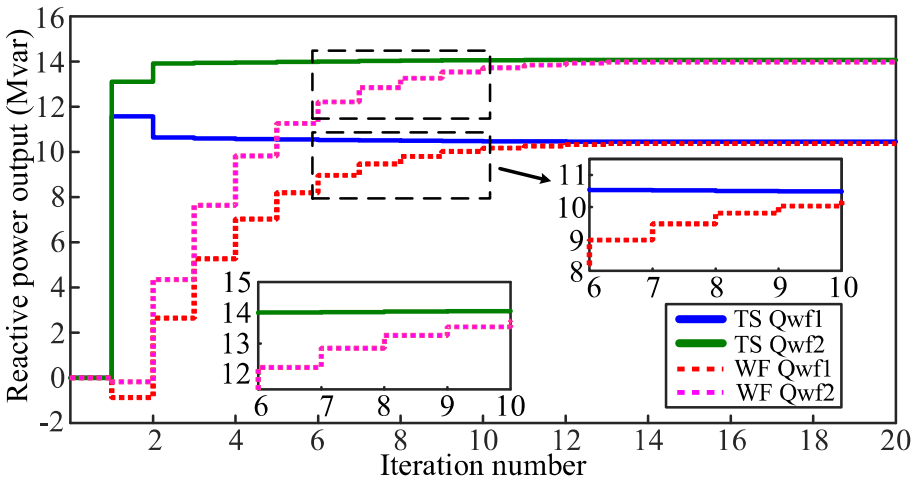

Fig. 2-17 Convergence performance of reactive power output of WF1 and WF2. (t=20s)

2.7 Summary

In this chapter, the ADMM-based DARPC strategy is proposed for the regional AC TS with WFs. The SDP relaxation with Schur's complement and branch flow model are adopted to address the nonconvexity and nonlinearity issues of the global optimal power distribution in the coupled TS and WFs. The ADMM is applied to decompose the large-scale strongly coupled optimization problem without loss of global optimality. The computation burden can be largely reduced with the DARPC strategy. Furthermore, the TS controller and WF controllers process in parallel only with the limited boundary information exchange, which improves information privacy of the whole system. As verified by the case studies, the proposed DARPC strategy can achieve the optimal power distribution among the WFs to minimize the power losses of the TS while minimizing the voltage deviation of the terminal buses as well as the power losses of the WF collection system.

CHAPTER 3.

DISTRIBUTED OPTIMAL VOLTAGE CONTROL STRATEGY FOR AC GRID WITH DC CONNECTION AND OFFSHORE WIND FARMS BASED ON ADMM

This chapter proposes a distributed optimal voltage control (DOVC) strategy based on ADMM for the AC grid with VSC DC connection and OWFs. The chapter is based on the paper 2 with minor changes to coherently fit into the framework of this Thesis[2]. The paper 2 is with submitting the response.

3.1 Introduction

Wind energy is rapidly growing due to the pressure of global carbon emission and fossil fuel free policy [135]-[136]. With the installed capacity of wind power increasing, the wind power intermittency and the interaction between the large-scale OWFs and AC-DC grid have posed several challenges, i.e., voltage control performance, optimal power distribution, communication burden, and coordinated operation strategy for power systems with wind power [116], [137], [138].

OPF is an effective tool to improve the operation performance of the AC grid with DC connection. The OPF-based control methods have received growing attention in recent years [17], [130], [139]-[141]. In [139], a hierarchical OPF model was formulated to minimize the generation and security control costs, and also achieve dynamic MTDC power dispatch regulation in AC-DC grid with WFs. Several OPF-based control methods have been proposed to achieve economic operation, minimize operational costs, and realize optimal reserve sharing in AC-DC grid [17],

[2] This chapter is based on paper 2: **Pengda Wang,** Qiuwei Wu*, Sheng Huang, Bin Zhou, and Canbing Li, "Distributed Optimal Voltage Control Strategy for AC Grid with DC Connection and Offshore Wind Farms based on ADMM," *International Journal of Electrical Power and Energy System*, Submitting Response.

[140], [141]. In [130], a chance constrained AC OPF model with convex relaxation was formulated to utilize HVDC control capabilities while considering the uncertainties of wind power generation in AC-DC grid. However, few studies exist regarding global optimal control strategies of the AC grid with DC connection and OWFs, and the voltage regulation inside OWFs is not taken into consideration.

With the number of WFs connected to the AC grid with DC connection increasing, the WF control strategies are necessary. Considering the simple implementation and effective use of wind power, the conventional PD and proportional integral (PI) control methods have been applied to WFs. Besides the PD or PI-based methods, a number of optimization-based dispatch schemes have been proposed to achieve better control performance inside WFs. In [80], [142], MPC-based power dispatch strategies were proposed to maintain the terminal bus voltages, reduce WT fatigue loads and achieve fair power sharing inside WFs. In [122], an optimal power dispatch method based on PSO was presented to achieve economic operation of both regular and irregular shaped OWFs. The distributed/decentralized control methods are also used in voltage control inside WFs. In [75], [143], the dual-based voltage control schemes were proposed to regulate the voltage profile across WF collection systems and adequate reactive power reserves.

With the huge OWF projects increasing, the central controller may fail to generate the optimal solution of large-scale optimization problem of power system with wind power in a fast way. Recently, the ADMM-based distributed optimization schemes have been used in power system to handle the computation burden [94], [104], [144]-[145]. In [144]-[145], the methods based on ADMM were proposed to solve the distributed OPF problem and multi-area optimal transmission switching problem. In [94], the ADMM-based voltage control methods were proposed to regulate terminal bus voltage and achieve economic operation by coordinating WT reactive power outputs inside OWFs. In [104], an ADMM-based hierarchical inertial control strategy was proposed to improve system frequency response by coordinating WT active power outputs. However, the distributed control has not been studied for the coordinated optimal control for the AC grid with DC connection incorporating OWFs as well as considering voltage regulation inside OWF collection systems.

Therefore, this chapter proposes a DOVC strategy for the AC grid with DC connection incorporating several OWFs. The aims are to achieve global optimal power distribution to minimize power losses of the AC grid with DC connection while regulating voltage profile inside the OWF within the feasible range and minimizing

power losses. The WT dynamic behavior is also considered. First, the non-convex OPF problem combined MPC of the AC grid with DC connection including VSC is transformed into a convex SDP program. Meanwhile, an MPC-based voltage control problem is formulated and transformed into a quadratic programming (QP) problem. Second, the ADMM-based calculation framework is used to decompose the large-scale optimization problem. With Schur complement [128] applied, the augment Lagrangian of AC-DC optimization subproblem can be reformulated as the semi-definite objective with semi-definite matrix constraints ensuring the convergence of ADMM. The main contribution of this chapter can be summarized as follows:

(1) A DOVC strategy is proposed to optimally control the coupled AC grid with DC connection and OWF collection systems. The voltage performance inside OWFs is also considered to achieve global optimal operation.

(2) The SDP relaxation is adopted for OPF in AC grid with DC connection while an MPC-based voltage control model inside OWF is formulated to obtain a global optimal solution, which handle the inherent non-convexities of the original problem. The Schur complement is used to ensure the convexity-preserving property of augment Lagrangian of the AC-DC optimization subproblem, which guarantees the convergence of ADMM.

(3) The distributed ADMM-based framework distributes the computation task to grid-side and OWF-side controllers, implying better optimization efficiency. The limited amount of boundary information is exchanged between two side controllers, significantly improving the protection of OWF information privacy.

This chapter is organized as follows. Section 3.2 presents the framework of the proposed DOVC strategy. The AC grid with DC connection and the OWF optimization models are formulated in section 3.3 and 3.4, respectively. The section 3.5 shows the distributed solution with the ADMM framework. The case study is presented in section 3.6, followed by the conclusions.

3.2 Control Strategy Architecture

3.2.1 System Configuration

The structure of the AC grid with DC connection incorporating three OWFs is shown in Fig. 3-1. Three OWFs are connected to a modified IEEE 30-bus system with a 345 kV DC link. In AC grid with DC connection, the bus 1 is connected to

the external power system, and OWFa, OWFb and OWFc with a rated power of 480 MW are placed at bus 2, 9 and 14, respectively. Each OWF is composed of two sections and each section has a MV bus. Every 24 WTs are collected through the 35 kV MV feeder in each section and arranged with the distance of 4 km.

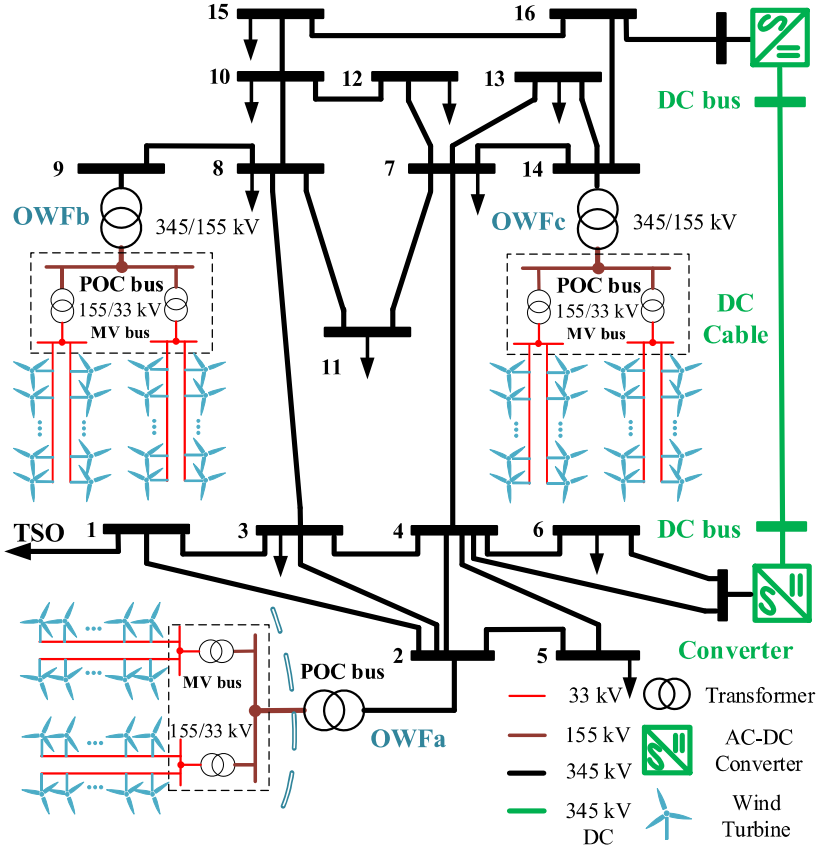

Fig. 3-1 System structure.

3.2.2 Strategy Concept

The structure of the proposed DOVC strategy is illustrated in Fig. 3-2. The DOVC strategy is designed in a distributed manner by using the ADMM. The AC grid with DC connection and each OWF are equipped with a controller. The AC-DC controller operates within MPC architecture to achieve the global optimal power distribution and minimize power losses inside the AC grid with DC connection while considering the TSO dispatch command and available wind power. In each OWF

controller, an MPC-based augmented Lagrangian optimization problem is formulated to achieve optimal voltage regulation and minimize power losses with local SCADA measurements inside OWFs. The DOVC strategy features the communication for very little boundary information instead of global information between two side controllers. The large-scale constrained optimization problem is decomposed and efficiently solved in parallel with the DOVC strategy while guaranteeing global optimality.

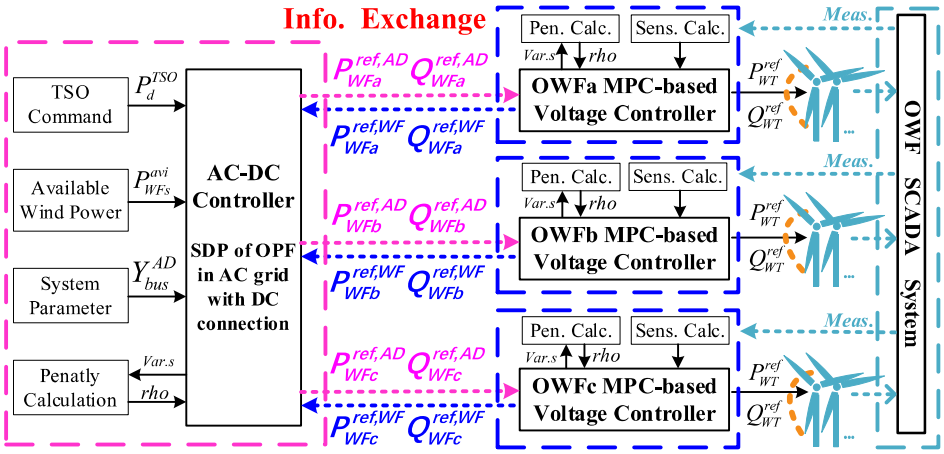

Fig. 3-2 Strategy concept.

3.3 AC Grid with DC Connection Optimization Model

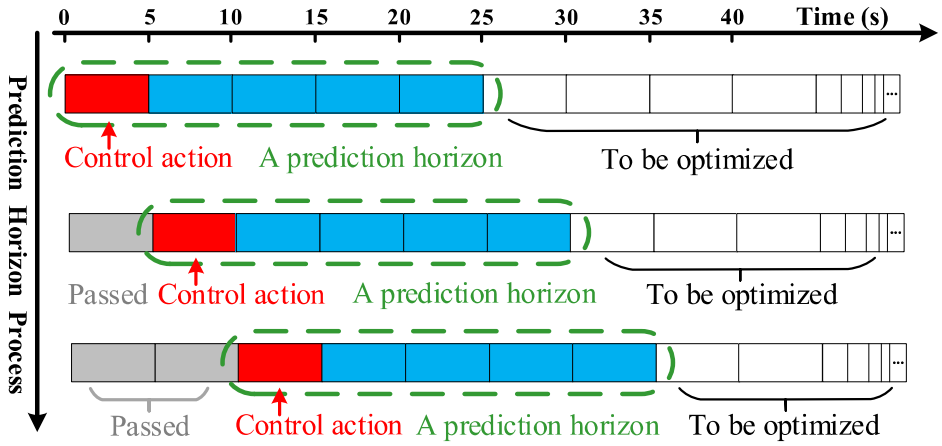

Fig. 3-3 The structure of model predictive control.

In this section, the MPC-based OPF of the AC grid with DC connection using the SDP relaxation is formulated. As Fig. 3-3 shown, the MPC output consists of a set of consecutive control actions, derived by minimizing the objectives over a prediction horizon window [146]-[147]. The MPC process has the capability of dealing with the constrained dynamic optimization problems, which includes dynamic parameters [148]-[149]. The OWF outputs are optimized for the whole horizon to minimize the power losses while tracking the TSO command.

3.3.1 MPC-based OPF of AC Grid with DC Connection Formulation

3.3.1.1 The Objective in AC Grid with DC Connection

The objective is to minimize the power losses in AC grid with DC connection, which is equal to the total active power generation including the OWFs and generators minus the total load. Denoting x^* as the conjugate of an arbitrary complex number x. Thus, the power loss objective in a control period is,

$$Obj_{\mathrm{AD}}^{\mathrm{Loss}} = \sum_{k}^{k+5}\sum_{i=1}^{N_{\mathrm{AD}}}(P_{\mathrm{OWF}_i}^{k} + P_{\mathrm{G}_i}^{k} - P_{\mathrm{D}_i}^{k}) = \sum_{k}^{k+5}\sum_{i=1}^{N_{\mathrm{AD}}}\mathrm{Re}\left\{V_i^k (I_i^k)^*\right\} \tag{3.1}$$

where $P_{\mathrm{OWF}_i}^{k}$ and $P_{\mathrm{G}_i}^{k}$ are the power output of the i-th OWF and generator at time step k which are connected to the i-th terminal bus in AC grid with DC connection directly; If the bus i is not associated with OWF or generator, then $P_{\mathrm{OWF}_i} = 0$ or $P_{\mathrm{G}_i} = 0$; $P_{D_i}^{k}$, V_i^k and I_i^k are the active load, voltage and current at time step k associated with bus i, respectively; N_{AD} is the number of buses in AC grid with DC connection.

3.3.1.2 The Constraints in VSC

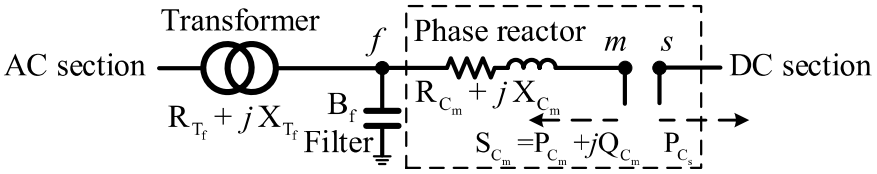

Fig. 3-4 AC-DC converter model.

Fig. 3-4 shows the model of the AC-DC converter with AC filter bus f, AC bus m and DC bus s. The AC-DC converter is modeled as VSC connecting AC section and DC section. The following assumptions are made in modeling the VSC: The

VSC can control the active/reactive power $P_{\mathrm{C}_m}/Q_{\mathrm{C}_m}$ and the AC terminal bus voltage. The resistance of the phase reactor is much smaller than its reactance. The difference of the phase angles $\delta_m - \delta_f$ for the AC bus m and the filter bus f in the VSC is small [130].

The voltage magnitude of the AC bus in the VSC at each time step k is upper bounded by,

$$\left|V_m^k\right| \le \gamma_a \left|V_s^k\right| \tag{3.2}$$

where V_m^k and V_s^k are the voltages of the AC bus m and the DC bus s at time step k, respectively; γ_a is the maximum modulation factor of the VSC.

The active power balance constraint of the VSC between the AC bus m and the DC bus s at time step k is,

$$P_{\mathrm{C}_m}^k + P_{\mathrm{C}_s}^k + P_{\mathrm{C}_{\mathrm{LOSS}}}^k = 0 \tag{3.3}$$

where $P_{\mathrm{C}_m}^k$ and $P_{\mathrm{C}_s}^k$ denote the active power injected into the AC bus m and the DC bus s at time step k, respectively; $P_{\mathrm{C}_{\mathrm{LOSS}}}^k$ denotes the power losses of the VSC at time step k. $P_{\mathrm{C}_{\mathrm{LOSS}}}^k$ is approximated by a quadratic function of the AC current magnitude $|I_m^k|$,

$$P_{\mathrm{C}_{\mathrm{LOSS}}}^k = a_m + b_m \left|I_m^k\right| + c_m \left|I_m^k\right|^2 \tag{3.4}$$

where a_m, b_m and c_m are the positive coefficients [130].

The transferable apparent power is upper bounded by its rated apparent power rating of the VSC. The apparent power constraint can be replaced with the maximum current limit of the VSC,

$$\left|S_{\mathrm{C}_m}^k\right|^2 = \left(P_{\mathrm{C}_m}^k\right)^2 + \left(Q_{\mathrm{C}_m}^k\right)^2 \le \left(\left|V_m^k\right| I_m^{\max}\right)^2 \tag{3.5}$$

where $S_{\mathrm{C}_m}^k$ and $Q_{\mathrm{C}_m}^k$ denote the transferable apparent and reactive power of the VSC associated with the AC bus m at time step k; $I_m^{\max}$ is the maximum current limit of the VSC.

In general, the maximum reactive power absorbed or injected by VSC is approximately proportional to its rated apparent power,

$$-\gamma_{\mathrm{b}} S_{\mathrm{C}_m}^{\mathrm{rated}} \le Q_{\mathrm{C}_m}^{k} \le \gamma_{\mathrm{c}} S_{\mathrm{C}_m}^{\mathrm{rated}} \tag{3.6}$$

where $S_{\mathrm{C}_m}^{\mathrm{rated}}$ is the rated apparent power of the VSC connected to the AC bus m; γ_{b} and γ_{c} are the positive constants associated with the lower and upper limits.

The VSC can operate in a feasible region as Fig. 3-5 shown. The apparent power of the VSC is bounded by a circle as the constraint (3.5) described. The reactive power capability of the VSC is limited by two dash lines as the constraint (3.6) implied.

3.3.1.3 The Constraints in AC Grid with DC Connection

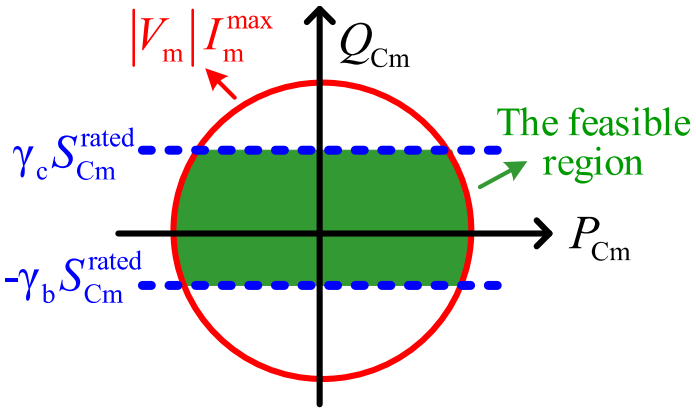

Fig. 3-5 The feasible region of the AC-DC converter.

The OPF problem of the AC grid with DC connection is subject to a set of equality and inequality constraints imposed by AC grid with DC connection including VSC. The equality constraints over each time step k consist of the active and reactive power balance equations,

$$P_{\mathrm{OWF}_i}^{k} + P_{\mathrm{G}_i}^{k} - P_{\mathrm{D}_i}^{k} = \mathrm{Re}\{V_i^{k} \left(I_i^{k}\right)^{*}\}, \quad \forall i \in \mathcal{N}_{\mathrm{AD}} \backslash \mathcal{N}^{\mathrm{VSC}} \tag{3.7a}$$

$$P_{\mathrm{C}_i}^{k} - P_{\mathrm{D}_i}^{k} = \mathrm{Re}\{V_i^{k} \left(I_i^{k}\right)^{*}\}, \quad \forall i \in \mathcal{N}^{\mathrm{VSC}} \tag{3.7b}$$

where $\mathcal{N}_{\mathrm{AD}}$ and $\mathcal{N}^{\mathrm{VSC}}$ are the sets of buses in the AC grid with DC connection and VSC, and $\mathcal{N}^{\mathrm{VSC}} \subseteq \mathcal{N}_{\mathrm{AD}}$. The DC section can be modeled as the AC section with purely resistive transmission lines and generators operating at unity power factor. Then, the constraints (3.7a) and (3.7b) can also be applied to describe the power balance formulas for the DC section by setting $I_i^k = (I_i^k)^*$ and $\mathrm{Re}\{V_i^k (I_i^k)^*\} = V_i^k I_i^k$.

The reactive power balance equations for the AC buses at each time step *k* are,

$$Q_{\mathrm{OWF}_i}^k + Q_{\mathrm{G}_i}^k - Q_{\mathrm{D}_i}^k = \mathrm{Im}\{V_i^k \left(I_i^k\right)^*\}, \ \forall i \in \mathcal{N}_{\mathrm{AC}} \tag{3.8a}$$

$$Q_{C_i}^k - Q_{\mathrm{D}_i}^k = \mathrm{Im}\{V_i^k \left(I_i^k\right)^*\}, \ \forall i \in \mathcal{N}_{\mathrm{AC}}^{\mathrm{VSC}} \tag{3.8b}$$

where $Q_{\mathrm{OWF}_i}^k$ and $Q_{\mathrm{G}_i}^k$ are the reactive power output of the *i*-th OWF and generator at time step *k* which are connected to the *i*-th terminal bus directly; If the bus *i* is not associated with OWF or generator, then $Q_{\mathrm{OWF}_i} = 0$ or $Q_{\mathrm{G}_i} = 0$; $Q_{\mathrm{D}_i}^k$ is the reactive load of bus *i* at time step *k*; $\mathcal{N}_{\mathrm{AC}} \subseteq \mathcal{N}_{\mathrm{AD}}$ is the set of AC buses that are not connected to VSC; $\mathcal{N}_{\mathrm{AC}}^{\mathrm{VSC}} \subseteq \mathcal{N}^{\mathrm{VSC}}$ is the set of AC side VSC buses.

As Fig. 3-4 shown, the VSC owns the AC side bus *m* and DC side bus *s* connecting AC section and DC section. The VSC power balance constraint (3.3) can be reformulated with constraint (3.7) substituted,

$$\mathrm{Re}\{V_m^k \left(I_m^k\right)^*\} + P_{\mathrm{D}_m}^k + \mathrm{Re}\{V_s^k \left(I_s^k\right)^*\} + P_{\mathrm{D}_s}^k + P_{\mathrm{C}_{\mathrm{LOSS}}}^k = 0 \tag{3.9}$$

In general, the fluctuation of the OWF power generation should be constrained according to the corresponding technical standards [150]. The ramping power limit of the OWF generation between two time steps is,

$$-\mathrm{RP}_{\mathrm{W}} \le P_{\mathrm{OWF}_i}^{k+1} - P_{\mathrm{OWF}_i}^k \le \mathrm{RP}_{\mathrm{W}} \tag{3.10}$$

where RP_{W} is the ramping power threshold of the OWF.

Other inequality constraints at each time step *k* are as,

$$P_{\mathrm{OWF}_i}^{\min} \le P_{\mathrm{OWF}_i}^k \le P_{\mathrm{OWF}_i}^{\max}, \ Q_{\mathrm{OWF}_i}^{\min} \le Q_{\mathrm{OWF}_i}^k \le Q_{\mathrm{OWF}_i}^{\max} \tag{3.11a}$$

$$V_i^{\min} \le \left|V_i^k\right| \le V_i^{\max} \tag{3.11b}$$

$$\left|S_{lm}^k\right| \le S_{lm}^{\max} \tag{3.11c}$$

where $P_{\mathrm{OWF}_i}^{\min}$, $P_{\mathrm{OWF}_i}^{\max}$, $Q_{\mathrm{OWF}_i}^{\min}$, $Q_{\mathrm{OWF}_i}^{\max}$, $V_i^{\min}$ and $V_i^{\max}$ are the lower and upper bounds on the *i*-th OWF active/reactive power outputs, and the *i*-th terminal bus voltage, respectively; $\left|V_i^k\right|$ is the voltage magnitude of the *i*-th terminal bus at time step *k*; S_{lm}^k is the apparent power flowing through the transmission line from bus *l* to bus *m* at time step *k*.

3.3.2 Convex Relaxation of AC-DC OPF within MPC

In this section, the semidefinite relaxation of the AC-DC OPF within MPC is introduced. With the SDP relaxation adopted, the non-linear non-convex AC-DC OPF including the VSC within MPC can be transformed into a convex model. This convex model formulates the OPF as a function of two positive semidefinite matrix variables $\boldsymbol{W}$ and $\boldsymbol{I}$ and the model can be solved under ADMM framework without loss of the global optimality.

Let matrix $\boldsymbol{Y}_{\mathrm{AD}}$ denotes admittance matrix of the AC grid with DC connection. For $i \in \mathcal{N}_{\mathrm{AD}}$ and $(l,m) \in Line$, e_i is the *i*-th basis vector in $R^{|N_{\mathrm{AD}}|}$, and $Y_i = e_i e_i^T \boldsymbol{Y}_{\mathrm{AD}}$. y_{lm} and $\bar{y}_{lm}$ are used to denote the value of series and shunt elements of line (l,m), respectively. Then $Y_{lm} = (\bar{y}_{lm} + y_{lm}) e_l e_l^T - y_{lm} e_l e_m^T$ is defined. In order to present the AC-DC OPF within MPC in SDP form, the auxiliary matrixes are introduced, and they are the same at each time step.

$$\mathbf{Y}_i^{\mathrm{AD}} = \frac{1}{2}\begin{bmatrix} \mathrm{Re}(Y_i + Y_i^T) & \mathrm{Im}(Y_i^T - Y_i) \\ \mathrm{Im}(Y_i - Y_i^T) & \mathrm{Re}(Y_i + Y_i^T) \end{bmatrix}$$

$$\overline{\mathbf{Y}}_i^{\mathrm{AD}} = \frac{-1}{2}\begin{bmatrix} \mathrm{Im}(Y_i + Y_i^T) & \mathrm{Re}(Y_i - Y_i^T) \\ \mathrm{Re}(Y_i^T - Y_i) & \mathrm{Im}(Y_i + Y_i^T) \end{bmatrix}$$

$$\mathbf{Y}_{lm}^{\mathrm{AD}} = \frac{1}{2}\begin{bmatrix} \mathrm{Re}(Y_{lm} + Y_{lm}^T) & \mathrm{Im}(Y_{lm}^T - Y_{lm}) \\ \mathrm{Im}(Y_{lm} - Y_{lm}^T) & \mathrm{Re}(Y_{lm} + Y_{lm}^T) \end{bmatrix}$$

$$\mathbf{M}_i^{\mathrm{AD}} = \begin{bmatrix} e_i e_i^T & 0 \\ 0 & e_i e_i^T \end{bmatrix}$$

$$\overline{\mathbf{Y}}_{lm}^{\mathrm{AD}} = \frac{-1}{2}\begin{bmatrix} \mathrm{Im}(Y_{lm} + Y_{lm}^T) & \mathrm{Re}(Y_{lm} - Y_{lm}^T) \\ \mathrm{Re}(Y_{lm}^T - Y_{lm}) & \mathrm{Im}(Y_{lm} + Y_{lm}^T) \end{bmatrix}$$

$$\mathbf{C}_i^{\mathrm{VSC}} = \begin{bmatrix} a_{mi} & b_{mi}/2 \\ b_{mi}/2 & c_{mi} \end{bmatrix}$$

$$\mathbf{M}_{lm}^{\mathrm{AD}} = \begin{bmatrix} (e_l - e_m)(e_l - e_m)^T & 0 \\ 0 & (e_l - e_m)(e_l - e_m)^T \end{bmatrix}$$

The real and imaginary values of the vector of the complex bus voltages $V_{\mathrm{AD}} = [V_1, V_2, \cdots, V_{N_{\mathrm{AD}}}]_{1\times N_{\mathrm{AD}}}$ can be used to define a variable column vector $\boldsymbol{X}_{\mathrm{AD}} = [\mathrm{Re}\{V_{\mathrm{AD}}\}\ \mathrm{Im}\{V_{\mathrm{AD}}\}]^T$. The variable column vector associated with $|I_i|$ for AC side VSC buses can be defined as $\boldsymbol{L}_i = [1\ |I_i|]^T, \forall i \in \mathcal{N}_{\mathrm{AC}}^{\mathrm{VSC}}$. Then, the formulation of AC-DC OPF within MPC (3.1)-(3.11) with complex variables where the V^*V^T and $\boldsymbol{L}_i\boldsymbol{L}_i^T$ can be substituted with the complex $2N_{\mathrm{AD}} \times 2N_{\mathrm{AD}}$-dimensional matrix $\boldsymbol{W}_{\mathrm{AD}}$ and 2×2-dimensional matrix $\boldsymbol{I}_i$,

$$\begin{aligned} &\boldsymbol{W}_{\mathrm{AD}} = \boldsymbol{X}_{\mathrm{AD}}\boldsymbol{X}_{\mathrm{AD}}^T \\ &\boldsymbol{I}_i = \boldsymbol{L}_i\boldsymbol{L}_i^T, \qquad \forall i \in \mathcal{N}_{\mathrm{AC}}^{\mathrm{VSC}} \end{aligned}$$

With the new variable matrixes $\boldsymbol{W}_{\mathrm{AD}}$ and $\boldsymbol{I}_i$ adopted, the original complex formulation can be split into the real and imaginary parts. $\mathrm{Tr}\{\boldsymbol{M}_i\}$ is used to represent the trace of a square matrix $\boldsymbol{M}_i$. Then the following (12a)-(12f) are used to reformulate the original model with the new variable matrixes $\boldsymbol{W}_{\mathrm{AD}}$ and $\boldsymbol{I}_i$ at each time step k,

$$\mathrm{Re}\{V_i^k \left(I_i^k\right)^*\} = \mathrm{Tr}\{\mathbf{Y}_i^{\mathrm{AD}}\boldsymbol{W}_{\mathrm{AD}}^k\}, \quad \forall i \in \mathcal{N}_{\mathrm{AD}} \tag{3.12a}$$

$$\mathrm{Im}\{V_i^k \left(I_i^k\right)^*\} = \mathrm{Tr}\{\overline{\mathbf{Y}}_i^{\mathrm{AD}}\boldsymbol{W}_{\mathrm{AD}}^k\}, \quad \forall i \in \mathcal{N}_{\mathrm{AD}} \tag{3.12b}$$

$$\left|V_i^k\right|^2 = \mathrm{Tr}\{\mathbf{M}_i^{\mathrm{AD}}\boldsymbol{W}_{\mathrm{AD}}^k\}, \quad \forall i \in \mathcal{N}_{\mathrm{AD}} \tag{3.12c}$$

$$\left|V_l^k - V_m^k\right|^2 = \mathrm{Tr}\{\mathbf{M}_{lm}^{\mathrm{AD}} \boldsymbol{W}_{\mathrm{AD}}^k\}, \quad \forall (l,m) \in Line \tag{3.12d}$$

$$\left|S_{lm}^k\right|^2 = \mathrm{Tr}\{\mathbf{Y}_{lm}^{\mathrm{AD}} \boldsymbol{W}_{\mathrm{AD}}^k\}^2 + \mathrm{Tr}\{\overline{\mathbf{Y}}_{lm}^{\mathrm{AD}} \boldsymbol{W}_{\mathrm{AD}}^k\}^2, \quad \forall (l,m) \in Line \tag{3.12e}$$

The power losses of the VSC (3.4) can be reformulated with $\boldsymbol{I}_i$,

$$P_{\mathrm{C_{LOSS}}}^k = \mathrm{Tr}\{\mathbf{C}_i^{\mathrm{VSC}} \boldsymbol{I}_i^k\}, \quad \forall i \in \mathcal{N}_{\mathrm{AC}}^{\mathrm{VSC}} \tag{3.12f}$$

3.3.2.1 Transformation of the AC-DC OPF within MPC

Substituting (3.12a) with $\boldsymbol{W}_{\mathrm{AD}}$ into the objective (3.1),

$$Obj_{\mathrm{AD}}^{\mathrm{Loss}} = \sum_{k}^{k+5} \sum_{i=1}^{N_{\mathrm{AD}}} \mathrm{Tr}\{\mathbf{Y}_i^{\mathrm{AD}} \boldsymbol{W}_{\mathrm{AD}}^k\} \tag{3.13}$$

The SDP form of the constraint (3.2) can be obtained by substituting (3.12c) into (3.2),

$$\mathrm{Tr}\{\mathbf{M}_m \boldsymbol{W}_{\mathrm{AD}}^k\} \le \gamma_a^2 \mathrm{Tr}\{\mathbf{M}_s \boldsymbol{W}_{\mathrm{AD}}^k\}, \quad \forall m \in \mathcal{N}_{\mathrm{AC}}^{\mathrm{VSC}}, \forall s \in \mathcal{N}_{\mathrm{DC}}^{\mathrm{VSC}} \tag{3.14}$$

Substituting (3.12a) and (3.12f) into (3.3), the SDP form of the active power balance constraint of the VSC at each time step k,

$$\mathrm{Tr}\{\mathbf{Y}_m^{\mathrm{AD}} \boldsymbol{W}_{\mathrm{AD}}^k\} + P_{\mathrm{D}_m}^k + \mathrm{Tr}\{\mathbf{Y}_s^{\mathrm{AD}} \boldsymbol{W}_{\mathrm{AD}}^k\} + P_{\mathrm{D}_s}^k + \mathrm{Tr}\{\mathbf{C}_i^{\mathrm{VSC}} \boldsymbol{I}_m^k\} = 0 \tag{3.15}$$

The element in the second row and the second column of $\boldsymbol{I}_i$ is defined as $\boldsymbol{I}_{i,a}$. According to Ohm's Law, the VSC current magnitude $\left|I_m^k\right|$ from filter bus f to AC bus m at time step k is,

$$\boldsymbol{I}_{m,a}^k = \left|I_m^k\right|^2 = (R_{\mathrm{C}m}^2 + X_{\mathrm{C}m}^2)^{-1} \mathrm{Tr}\{\mathbf{M}_{mf}^{\mathrm{AD}} \boldsymbol{W}_{\mathrm{AD}}^k\} \tag{3.16}$$

Similarly, the element in the second row and the first column of $\boldsymbol{I}_i$ is defined as $\boldsymbol{I}_{i,b}$,

$$\boldsymbol{I}_{m,b}^k \ge 0 \tag{3.17}$$

Substituting (3.12a) and (3.12b) into (3.5), the transferable apparent power constraint of the VSC is rewritten,

$$(\mathrm{Tr}\{\mathbf{Y}_m^{\mathrm{AD}}\boldsymbol{W}_{\mathrm{AD}}^k\}+P_{\mathrm{D}_m}^k)^2+(\mathrm{Tr}\{\overline{\mathbf{Y}}_m^{\mathrm{AD}}\boldsymbol{W}_{\mathrm{AD}}^k\}+Q_{\mathrm{D}_m}^k)^2\le(I_m^{\max})^2\mathrm{Tr}\{\mathbf{M}_m\boldsymbol{W}_{\mathrm{AD}}^k\} \tag{3.18}$$

Substituting (3.12b) into (3.6), the SDP form of the reactive power constraint of the VSC is,

$$-\gamma_b S_{\mathrm{C}_m}^{\mathrm{rated}}\le\mathrm{Tr}\{\overline{\mathbf{Y}}_m^{\mathrm{AD}}\boldsymbol{W}_{\mathrm{AD}}^k\}\le\gamma_c S_{\mathrm{C}_m}^{\mathrm{rated}} \tag{3.19}$$

The SDP form of the power balance constraints in terms of the power generation limits at time step k can be obtained by substituting (3.12a) and (3.12b) into (3.7a) and (3.8a),

$$P_{\mathrm{OWF}_i}^{\min}-P_{\mathrm{D}_i}^k\le\mathrm{Tr}\{\mathbf{Y}_i^{\mathrm{AD}}\boldsymbol{W}_{\mathrm{AD}}^k\}\le P_{\mathrm{OWF}_i}^{\max}-P_{\mathrm{D}_i}^k,\ \forall i\in\mathcal{N}_{\mathrm{AD}}^{\mathrm{OWF}} \tag{3.20}$$

$$Q_{\mathrm{OWF}_i}^{\min}-Q_{\mathrm{D}_i}^k\le\mathrm{Tr}\{\overline{\mathbf{Y}}_i^{\mathrm{AD}}\boldsymbol{W}_{\mathrm{AD}}^k\}\le Q_{\mathrm{OWF}_i}^{\max}-Q_{\mathrm{D}_i}^k,\ \forall i\in\mathcal{N}_{\mathrm{AD}}^{\mathrm{OWF}} \tag{3.21}$$

The ramping power limits of the OWFs at time step k (3.10) can be transformed into the SDP form,

$$-\mathrm{RP}_{\mathrm{W}}\le\mathrm{Tr}\{\mathbf{Y}_i^{\mathrm{AD}}\boldsymbol{W}_{\mathrm{AD}}^{k+1}\}-\mathrm{Tr}\{\mathbf{Y}_i^{\mathrm{AD}}\boldsymbol{W}_{\mathrm{AD}}^k\}+P_{\mathrm{D}_i}^{k+1}-P_{\mathrm{D}_i}^k\le\mathrm{RP}_{\mathrm{W}} \tag{3.22}$$

Similarly, the voltage constraint (3.11b) at time step k can be transformed into the SDP form,

$$\left|V_i^{\min}\right|^2\le\mathrm{Tr}\{\mathbf{M}_i^{\mathrm{AD}}\boldsymbol{W}_{\mathrm{AD}}^k\}\le\left|V_i^{\max}\right|^2 \tag{3.23}$$

The transmission line capacity constraint at time step k can be obtained by substituting (3.12e) into (3.11c),

$$\mathrm{Tr}\{\mathbf{Y}_{lm}^{\mathrm{AD}}\boldsymbol{W}_{\mathrm{AD}}^k\}^2+\mathrm{Tr}\{\overline{\mathbf{Y}}_{lm}^{\mathrm{AD}}\boldsymbol{W}_{\mathrm{AD}}^k\}^2\le\left|S_{lm}^{\max}\right|^2 \tag{3.24}$$

The constraints (3.18) and (3.24) are expressed as the quadratic formulas of matrix $\boldsymbol{W}_{\mathrm{AD}}$. To obtain the MPC-based AC-DC OPF optimization problem linear in $\boldsymbol{W}_{\mathrm{AD}}$ at each time step k, the Schur complement is applied to transform the quadratic

transferable apparent power constraint of the VSC (3.18) into a linear matrix inequality constraint as,

$$\begin{bmatrix} \left(I_m^{\max}\right)^2 \mathrm{Tr}\{\mathbf{M}_m^{\mathrm{AD}} \boldsymbol{W}_{\mathrm{AD}}^k\} & \mathrm{Tr}\{\mathbf{Y}_m^{\mathrm{AD}} \boldsymbol{W}_{\mathrm{AD}}^k\} + P_{D_m}^k & \mathrm{Tr}\{\overline{\mathbf{Y}}_m^{\mathrm{AD}} \boldsymbol{W}_{\mathrm{AD}}^k\} + Q_{D_m}^k \\ \mathrm{Tr}\{\mathbf{Y}_m^{\mathrm{AD}} \boldsymbol{W}_{\mathrm{AD}}^k\} + P_{D_m}^k & 1 & 0 \\ \mathrm{Tr}\{\overline{\mathbf{Y}}_m^{\mathrm{AD}} \boldsymbol{W}_{\mathrm{AD}}^k\} + Q_{D_m}^k & 0 & 1 \end{bmatrix} \succeq 0 \quad (3.25)$$

Similarly, the constraint (3.24) can be transformed as,

$$\begin{bmatrix} \left|S_{lm}^{\max}\right|^2 & \mathrm{Tr}\{\mathbf{Y}_{lm}^{\mathrm{AD}} \boldsymbol{W}_{\mathrm{AD}}^k\} & \mathrm{Tr}\{\overline{\mathbf{Y}}_{lm}^{\mathrm{AD}} \boldsymbol{W}_{\mathrm{AD}}^k\} \\ \mathrm{Tr}\{\mathbf{Y}_{lm}^{\mathrm{AD}} \boldsymbol{W}_{\mathrm{AD}}^k\} & 1 & 0 \\ \mathrm{Tr}\{\overline{\mathbf{Y}}_{lm}^{\mathrm{AD}} \boldsymbol{W}_{\mathrm{AD}}^k\} & 0 & 1 \end{bmatrix} \succeq 0 \quad (3.26)$$

Meanwhile, the non-convex constraints $\boldsymbol{W}_{\mathrm{AD}}^k = \boldsymbol{X}_{\mathrm{AD}}^k (\boldsymbol{X}_{\mathrm{AD}}^k)^T$ and $\boldsymbol{I}_m^k = \boldsymbol{L}_m^k (\boldsymbol{L}_m^k)^T, \forall m \in \mathcal{N}_{\mathrm{AC}}^{\mathrm{VSC}}$ can be expressed as,

$$\boldsymbol{W}_{\mathrm{AD}}^k \succeq 0, \ \boldsymbol{I}_{\mathrm{m}}^k \succeq 0 \quad (3.27)$$

$$\mathrm{rank}\left(\boldsymbol{W}_{\mathrm{AD}}^k\right) = 1, \ \mathrm{rank}\left(\boldsymbol{I}_{\mathrm{m}}^k\right) = 1 \quad (3.28)$$

The convex relaxation is obtained by dropping the rank constraint (3.28), relaxing the non-linear, non-convex AC-DC OPF within MPC to a convex semidefinite program at each time step *k*. If the rank of $\boldsymbol{W}_{\mathrm{AD}}^k$ is 1, and the rank of $\boldsymbol{I}_m^k$ is 1, then the global optimum of the original optimization problem is obtained [130]. Thus, the SDP relaxation of the AC-DC OPF within MPC is,

Minimize Objective function (3.13)

Subject to Constraints (3.14)-(3.17), (3.19)-(3.23), (3.25)-(3.27)

The optimization problem can be solved by using the toolbox YALMIP with MOSEK solver in MATLAB [151]. By solving the MPC-based AC-DC OPF problem, the boundary variables of the optimal active/reactive power references at each time step *k* for three OWFs $\mathrm{Tr}\{\mathbf{Y}_2^{\mathrm{AD}} \boldsymbol{W}_{\mathrm{AD}}^k\}$/$\mathrm{Tr}\{\overline{\mathbf{Y}}_2^{\mathrm{AD}} \boldsymbol{W}_{\mathrm{AD}}^k\}$, $\mathrm{Tr}\{\mathbf{Y}_9^{\mathrm{AD}} \boldsymbol{W}_{\mathrm{AD}}^k\}$/$\mathrm{Tr}\{\overline{\mathbf{Y}}_9^{\mathrm{AD}} \boldsymbol{W}_{\mathrm{AD}}^k\}$,

and $\mathrm{Tr}\{\mathbf{Y}_{14}^{\mathrm{AD}}\boldsymbol{W}_{\mathrm{AD}}^{k}\}/\mathrm{Tr}\{\overline{\mathbf{Y}}_{14}^{\mathrm{AD}}\boldsymbol{W}_{\mathrm{AD}}^{k}\}$ are generated. For each time step, the boundary variables can be exchanged between two side controllers under ADMM framework.

3.4 Offshore Wind Farm Control

The OWF controllers can optimize the active and reactive power generation of all WTs to achieve the voltage regulation and reduce the power losses inside OWFs. Meanwhile, the AC-DC and OWF boundary variables converge to the common values under ADMM framework. In this section, the MPC method is used [142].

3.4.1 Modeling of Offshore Wind Farm

Suppose the current measurements and active/reactive power references are $P_{\mathrm{WT}}(t_0)$ / $Q_{\mathrm{WT}}(t_0)$ and $P_{\mathrm{WT}}^{\mathrm{ref}}$ / $Q_{\mathrm{WT}}^{\mathrm{ref}}$. The dynamic response of WT control system can be modeled [135],

$$\begin{aligned}\Delta P_{\mathrm{WT}} &= \frac{1}{1+s\mathrm{T}_{\mathrm{WT}}^{\mathrm{P}}}\Delta P_{\mathrm{WT}}^{\mathrm{ref}}\\ \Delta Q_{\mathrm{WT}} &= \frac{1}{1+s\mathrm{T}_{\mathrm{WT}}^{\mathrm{Q}}}\Delta Q_{\mathrm{WT}}^{\mathrm{ref}}\end{aligned} \tag{3.29}$$

where $T_{\mathrm{WT}}^{\mathrm{P}}$ and $T_{\mathrm{WT}}^{\mathrm{Q}}$ are the time constants [74].

Thus, the continuous state space of the OWF with N_{WT} WTs can be modeled as,

$$\Delta\dot{x} = \boldsymbol{A}_{\mathrm{C}}\Delta x + \boldsymbol{B}_{\mathrm{C}}\Delta u \tag{3.30}$$

where $\Delta x = [\Delta P_{\mathrm{WT_1}},\cdots,\Delta P_{\mathrm{WT}_{N_{\mathrm{WT}}}},\Delta Q_{\mathrm{WT_1}},\cdots,\Delta Q_{\mathrm{WT}_{N_{\mathrm{WT}}}}]^{\mathrm{T}}$,

$\Delta u = [\Delta P_{\mathrm{WT_1}}^{\mathrm{ref}},\cdots,\Delta P_{\mathrm{WT}_{N_{\mathrm{WT}}}}^{\mathrm{ref}},\Delta Q_{\mathrm{WT_1}}^{\mathrm{ref}},\cdots,\Delta Q_{\mathrm{WT}_{N_{\mathrm{WT}}}}^{\mathrm{ref}}]^{\mathrm{T}}$,

$\boldsymbol{A}_{\mathrm{C}} = \mathrm{diag}[-1/\mathrm{T}_{\mathrm{WT_1}}^{\mathrm{P}},\cdots,-1/\mathrm{T}_{\mathrm{WT}_{N_{\mathrm{WT}}}}^{\mathrm{P}},-1/\mathrm{T}_{\mathrm{WT_1}}^{\mathrm{Q}},\cdots,-1/\mathrm{T}_{\mathrm{WT}_{N_{\mathrm{WT}}}}^{\mathrm{Q}}]$,

$\boldsymbol{B}_{\mathrm{C}} = \mathrm{diag}[1/\mathrm{T}_{\mathrm{WT_1}}^{\mathrm{P}},\cdots,1/\mathrm{T}_{\mathrm{WT}_{N_{\mathrm{WT}}}}^{\mathrm{P}},1/\mathrm{T}_{\mathrm{WT_1}}^{\mathrm{Q}},\cdots,1/\mathrm{T}_{\mathrm{WT}_{N_{\mathrm{WT}}}}^{\mathrm{Q}}]$.

Accordingly, the continuous model (3.30) can be transformed into the discrete model with the sampling time $\triangle\,\mathrm{T_P}$,

$$\Delta x(k+1) = \boldsymbol{A}_{\mathrm{d}}\Delta x(k) + \boldsymbol{B}_{\mathrm{d}}\Delta u(k) \tag{3.31}$$

where $\mathbf{A}_{\mathrm{d}} = e^{\mathbf{A}_{\mathrm{c}}\triangle \mathrm{T_P}}, \mathbf{B}_{\mathrm{d}} = \int_0^{\triangle \mathrm{T_P}} e^{\mathbf{A}_{\mathrm{c}}t}\,\mathbf{B}_{\mathrm{c}}\mathrm{d}t.$

The voltage sensitivity coefficients can be efficiently calculated based on SCADA measurements including the terminal bus voltages and phase angles during OWF dynamic control process [74].

3.4.2 MPC-based Offshore Wind Farm Control

3.4.2.1 The Objective Function in OWF

The objective function can be described as,

$$\min \sum_{k}^{k+5}\left(\left\|\Delta \boldsymbol{V}_{\mathrm{MV}}^{\mathrm{pre}}(k)\right\|_{\mathrm{w_{MV}}}^2 + \left\|\Delta \boldsymbol{V}_{\mathrm{WT}}^{\mathrm{pre}}(k)\right\|_{\mathrm{w_{WT}}}^2 + \left\|\boldsymbol{P}_{\mathrm{Loss}}^{\mathrm{pre}}(k)\right\|_{\mathrm{w_{LO}}}^2 + \left\|\Delta \boldsymbol{P}_{\mathrm{WT}}^{\mathrm{pd}}(k)\right\|_{\mathrm{w_{PD}}}^2\right) \tag{3.32}$$

where $\mathrm{w_{MV}}, \mathrm{w_{WT}}, \mathrm{w_{LO}}$ and $\mathrm{w_{PD}}$ are the weighting factors for four objectives;

$\triangle \boldsymbol{V}_{\mathrm{MV}}^{\mathrm{pre}} = \left[\triangle V_{\mathrm{MV}_1}^{\mathrm{pre}},..,\triangle V_{\mathrm{MV}_{N_{\mathrm{MV}}}}^{\mathrm{pre}}\right]^{\mathrm{T}}$;

$\triangle \boldsymbol{V}_{\mathrm{WT}}^{\mathrm{pre}} = \left[\triangle V_{\mathrm{WT}_1}^{\mathrm{pre}},..,\triangle V_{\mathrm{WT}_{N_{\mathrm{WT}}}}^{\mathrm{pre}}\right]^{\mathrm{T}}$;

$\triangle \boldsymbol{P}_{\mathrm{WT}}^{\mathrm{pd}} = \left[\triangle P_{\mathrm{WT}_1}^{\mathrm{pd}},..,\triangle P_{\mathrm{WT}_{N_{\mathrm{WT}}}}^{\mathrm{pd}}\right]^{\mathrm{T}}$.

The first and second objectives are for voltage regulation. The MV bus can regulate the voltage deviation of the subzone including its two radial feeders. The terminal voltages of MV/WT buses can be limited in a feasible range. The predictive values $\triangle V_{\mathrm{MV}_i}^{\mathrm{pre}}$ and $\triangle V_{\mathrm{WT}_i}^{\mathrm{pre}}$ are,

$$\Delta V_{\mathrm{MV}_i}^{\mathrm{pre}}(k) = V_{\mathrm{MV}_i}(t_0) + \frac{\partial V_{\mathrm{MV}_i}}{\partial P_{\mathrm{WT}}}\Delta P_{\mathrm{WT}}(k) + \frac{\partial V_{\mathrm{MV}_i}}{\partial Q_{\mathrm{WT}}}\Delta Q_{\mathrm{WT}}(k) - V_{\mathrm{MV}_i}^{\mathrm{rated}} \tag{3.33}$$

$$\Delta V_{\mathrm{WT}_i}^{\mathrm{pre}}(k) = V_{\mathrm{WT}_i}(t_0) + \frac{\partial V_{\mathrm{WT}_i}}{\partial P_{\mathrm{WT}}}\Delta P_{\mathrm{WT}}(k) + \frac{\partial V_{\mathrm{WT}_i}}{\partial Q_{\mathrm{WT}}}\Delta Q_{\mathrm{WT}}(k) - V_{\mathrm{WT}_i}^{\mathrm{rated}} \tag{3.34}$$

where $V_{\mathrm{MV}_i}(t_0)/V_{\mathrm{WT}_i}(t_0)$ are the voltage measurements of the *i*-th MV/WT terminal bus at the current time t_0; $V_{\mathrm{MV}_i}^{\mathrm{rated}}/V_{\mathrm{WT}_i}^{\mathrm{rated}}$ are the rated values of the *i*-th MV/WT terminal bus voltages; $\partial V/\partial P$ and $\partial V/\partial Q$ are the voltage sensitivity coefficients with respect to the active and reactive power injections.

The third objective is to minimize the power losses inside OWF. The predictive values $P_{\mathrm{Loss}}^{\mathrm{pre}}$ are,

$$P_{\mathrm{Loss}}^{\mathrm{pre}}(k) = P_{\mathrm{Loss}}^{\mathrm{OWF}}(t_0) + \frac{\partial P_{\mathrm{Loss}}^{\mathrm{OWF}}}{\partial P_{\mathrm{WT}}}\Delta P_{\mathrm{WT}}(k) + \frac{\partial P_{\mathrm{Loss}}^{\mathrm{OWF}}}{\partial Q_{\mathrm{WT}}}\Delta Q_{\mathrm{WT}}(k) \tag{3.35}$$

where $\partial P_{\mathrm{Loss}}^{\mathrm{OWF}}/\partial P_{\mathrm{WT}}$ and $\partial P_{\mathrm{Loss}}^{\mathrm{OWF}}/\partial Q_{\mathrm{WT}}$ are partial derivatives of power losses with respect to WT active/reactive power outputs.

The fourth objective is to minimize the deviation of power reference to the PD-based power value $P_{\mathrm{WT}}^{\mathrm{pd\_ref}}$. The predictive value $\Delta P_{\mathrm{WT}}^{\mathrm{pd}}$ and $P_{\mathrm{WT}}^{\mathrm{pd\_ref}}$ is,

$$\Delta P_{\mathrm{WT}_i}^{\mathrm{pd}}(k) = P_{\mathrm{WT}_i}(t_0) + \Delta P_{\mathrm{WT}_i}(k) - P_{\mathrm{WT}_i}^{\mathrm{pd\_ref}} \tag{3.36}$$

$$P_{\mathrm{WT}_i}^{\mathrm{pd\_ref}} = (P_{\mathrm{WT}_i}^{\mathrm{avi}} / \sum_i P_{\mathrm{WT}_i}^{\mathrm{avi}}) P_{\mathrm{OWF}}^{\mathrm{ref}} \tag{3.37}$$

3.4.2.2 The Constraints in OWF

The fluctuation of OWF power generation between two time steps should be limited in an acceptable range with the technical standards,

$$-\mathrm{RP_W} \le \sum_{i=1}^{N_{\mathrm{WT}}}[P_{\mathrm{WT}_i}(k+1) - P_{\mathrm{WT}_i}(k)] \le \mathrm{RP_W} \tag{3.38}$$

The available active and reactive power of WT is limited by,

$$0 \le P_{\mathrm{WT}_i}(k) \le P_{\mathrm{WT}_i}^{\mathrm{avi}} \tag{3.39}$$

$$Q_{\mathrm{WT}_i}^{\min}(k) \le Q_{\mathrm{WT}_i}(k) \le Q_{\mathrm{WT}_i}^{\max}(k) \tag{3.40}$$

The MPC-based optimization problem of the OWF can be reformulated as a standard QP problem and efficiently solved by commercial QP solver [74].

3.5 ADMM Formulation for the Whole System

Considering the whole system consists of the AC grid with DC connection including VSC and several OWFs with several hundreds of WTs, the optimization problem is a large-scale model with the large-scale constraints. To reduce the huge computation burden, an ADMM-based DOVC strategy is proposed. The ADMM decomposes the convex optimization problem into the AC-DC subproblem and several OWF subproblems, which are small and efficiently solved. Thus, the objectives (3.13) and (3.32) can be distributed to the AC-DC controller and OWF controllers and solved in parallel without loss of global optimality. The optimization problem can be formulated as an ADMM problem,

$$\begin{aligned}
&\min \sum_{k}^{k+5}[\sum_{i=1}^{N_{\mathrm{AD}}} \mathrm{Tr}\{\mathbf{Y}_i^{\mathrm{AD}} \boldsymbol{W}_{\mathrm{AD}}^{k}\} + \left\|\Delta \boldsymbol{V}_{\mathrm{MV}}^{\mathrm{pre}}(k)\right\|_{\mathrm{w_{MV}}}^{2} + \\
&\quad \left\|\Delta \boldsymbol{V}_{\mathrm{WT}}^{\mathrm{pre}}(k)\right\|_{\mathrm{w_{WT}}}^{2} + \left\|\boldsymbol{P}_{\mathrm{Loss}}^{\mathrm{pre}}(k)\right\|_{\mathrm{w_{LO}}}^{2} + \left\|\Delta \boldsymbol{P}_{\mathrm{WT}}^{\mathrm{pd}}(k)\right\|_{\mathrm{w_{PD}}}^{2}] \\
&\text{s.t.} \quad (3.14)-(3.17),(3.19)-(3.23),(3.25)-(3.27),(3.40)-(3.42) \qquad (3.41) \\
&\quad \mathrm{Tr}\{\mathbf{Y}_i^{\mathrm{AD}} \boldsymbol{W}_{\mathrm{AD}}^{k}\} - P_{\mathrm{OWF}_i}^{\mathrm{ref},k} = 0, i = 1,2,3. \\
&\quad \mathrm{Tr}\{\overline{\mathbf{Y}}_i^{\mathrm{AD}} \boldsymbol{W}_{\mathrm{AD}}^{k}\} - Q_{\mathrm{OWF}_i}^{\mathrm{ref},k} = 0, i = 1,2,3. \\
&\quad \mathrm{Tr}\{\mathbf{M}_i^{\mathrm{AD}} \boldsymbol{W}_{\mathrm{AD}}^{k}\} - (V_{\mathrm{OWF}_i}^{k})^2 = 0, i = 1,2,3. \qquad (3.42)
\end{aligned}$$

The above constraints guarantee the boundary variable values of AC-DC and OWF controllers are the same. In order to eliminate the need of a central controller, an ADMM-based computational framework is proposed.

The initial optimization variables and the dual variables $\lambda_i^{\mathrm{P},k}$ and $\lambda_i^{\mathrm{Q},k}$ are set to zero. r and ρ are defined as the step of iteration and the penalty for the optimization variables in AC-DC being different from the ones in OWFs. Each iterative step includes the following steps:

1) The AC-DC controller solves the AC-DC optimization variables by using the augmented Lagrangian with the constraints of the AC grid with DC connection, and it updates the optimization variables,

$$
\begin{aligned}
&(\mathrm{Tr}\{\mathbf{Y}_i^{\mathrm{AD}}\boldsymbol{W}_{\mathrm{AD}}^k\},\mathrm{Tr}\{\overline{\mathbf{Y}}_i^{\mathrm{AD}}\boldsymbol{W}_{\mathrm{AD}}^k\})(r+1)=\arg\min\sum_{k}^{k+5}[\sum_{i=1}^{N_{\mathrm{AD}}}\mathrm{Tr}\{\mathbf{Y}_i^{\mathrm{AD}}\boldsymbol{W}_{\mathrm{AD}}^k\}\\
&+\sum_{i=1}^{3}\lambda_i^{\mathrm{P},k}[\mathrm{Tr}\{\mathbf{Y}_i^{\mathrm{AD}}\boldsymbol{W}_{\mathrm{AD}}^k\}-P_{\mathrm{OWF}_i}^{\mathrm{ref},k}(r)]+\sum_{i=1}^{3}\frac{\rho}{2}\left\|\mathrm{Tr}\{\mathbf{Y}_i^{\mathrm{AD}}\boldsymbol{W}_{\mathrm{AD}}^k\}-P_{\mathrm{OWF}_i}^{\mathrm{ref},k}(r)\right\|^2\\
&+\sum_{i=1}^{3}\lambda_i^{\mathrm{Q},k}[\mathrm{Tr}\{\overline{\mathbf{Y}}_i^{\mathrm{AD}}\boldsymbol{W}_{\mathrm{AD}}^k\}-Q_{\mathrm{OWF}_i}^{\mathrm{ref},k}(r)]+\sum_{i=1}^{3}\frac{\rho}{2}\left\|\mathrm{Tr}\{\overline{\mathbf{Y}}_i^{\mathrm{AD}}\boldsymbol{W}_{\mathrm{AD}}^k\}-Q_{\mathrm{OWF}_i}^{\mathrm{ref},k}(r)\right\|^2]
\end{aligned}
\tag{3.43}
$$

s.t. (3.14)-(3.17), (3.19)-(3.23), (3.25)-(3.27), (3.42).

The augment Lagrangian (3.43) is expressed as a quadratic of matrix $\boldsymbol{W}_{\mathrm{AD}}^k$. However, in the SDP form, the formula should be linear with $\boldsymbol{W}_{\mathrm{AD}}^k$. Thus, (3.44)-(3.46) can be used to replace with (3.43) using the Schur complement with auxiliary variables $\beta_i^{\mathrm{P,k}}$ and $\beta_i^{\mathrm{Q,k}}$ at each time step k,

$$
\begin{aligned}
(\mathrm{Tr}\{\mathbf{Y}_i^{\mathrm{AD}}\boldsymbol{W}_{\mathrm{AD}}^k\},\mathrm{Tr}\{\overline{\mathbf{Y}}_i^{\mathrm{AD}}\boldsymbol{W}_{\mathrm{AD}}^k\})(r+1)=\arg\min\sum_{k}^{k+5}[\sum_{i=1}^{N_{\mathrm{AD}}}\mathrm{Tr}\{\mathbf{Y}_i^{\mathrm{AD}}\boldsymbol{W}_{\mathrm{AD}}^k\}\\
+\sum_{i=1}^{3}(\beta_i^{\mathrm{P},k}+\beta_i^{\mathrm{Q},k})]
\end{aligned}
\tag{3.44}
$$

$$
\begin{bmatrix}
\lambda_i^{\mathrm{P},k}\mathrm{Tr}\{\mathbf{Y}_i^{\mathrm{AD}}\boldsymbol{W}_{\mathrm{AD}}^k\}+a_i^{\mathrm{P},k} & \sqrt{\rho/2}\mathrm{Tr}\{\mathbf{Y}_i^{\mathrm{AD}}\boldsymbol{W}_{\mathrm{AD}}^k\}+b_i^{\mathrm{P},k}\\
\sqrt{\rho/2}\mathrm{Tr}\{\mathbf{Y}_i^{\mathrm{AD}}\boldsymbol{W}_{\mathrm{AD}}^k\}+b_i^{\mathrm{P},k} & -1
\end{bmatrix}\preceq 0.\ i=1,2,3. \tag{3.45}
$$

$$
\begin{bmatrix}
\lambda_i^{\mathrm{Q},k}\mathrm{Tr}\{\overline{\mathbf{Y}}_i^{\mathrm{AD}}\boldsymbol{W}_{\mathrm{AD}}^k\}+a_i^{Q,k} & \sqrt{\rho/2}\mathrm{Tr}\{\overline{\mathbf{Y}}_i^{\mathrm{AD}}\boldsymbol{W}_{\mathrm{AD}}^k\}+b_i^{Q,k}\\
\sqrt{\rho/2}\mathrm{Tr}\{\overline{\mathbf{Y}}_i^{\mathrm{AD}}\boldsymbol{W}_{\mathrm{AD}}^k\}+b_i^{\mathrm{Q},k} & -1
\end{bmatrix}\preceq 0.\ i=1,2,3. \tag{3.46}
$$

s.t. (3.14)-(3.17), (3.19)-(3.23), (3.25)-(3.27), (3.42).

where $a_i^{\mathrm{P},k}=-\beta_i^{\mathrm{P,k}}-\lambda_i^{\mathrm{P},k}P_{\mathrm{OWF}_i}^{\mathrm{ref},k}(r)$,

$b_i^{\mathrm{P},k}=-\sqrt{\rho/2}P_{\mathrm{OWF}_i}^{\mathrm{ref},k}(r)$,

$a_i^{\mathrm{Q},k}=-\beta_i^{\mathrm{Q,k}}-\lambda_i^{\mathrm{Q},k}Q_{\mathrm{OWF}_i}^{\mathrm{ref},k}(r)$,

$b_i^{\mathrm{Q},k}=-\sqrt{\rho/2}Q_{\mathrm{OWF}_i}^{\mathrm{ref},k}(r)$.

2) After updating the AC-DC optimization variables, each OWF controller solves its augmented Lagrangian with the constraints inside the OWF in parallel, and updates the OWF optimization variables. For *i*-th OWF controller,

$$
\begin{aligned}
&(P_{\mathrm{OWF}_i}^{\mathrm{ref},k}, Q_{\mathrm{OWF}_i}^{\mathrm{ref},k})(r+1) = \arg\min \sum_{k}^{k+5} [\left\|\Delta \boldsymbol{V}_{\mathrm{MV}}^{\mathrm{pre}}(k)\right\|_{\mathrm{w_{MV}}}^2 + \left\|\Delta \boldsymbol{V}_{\mathrm{WT}}^{\mathrm{pre}}(k)\right\|_{\mathrm{w_{WT}}}^2 + \left\|\boldsymbol{P}_{\mathrm{Loss}}^{\mathrm{pre}}(k)\right\|_{\mathrm{w_{LO}}}^2 + \\
&\left\|\Delta \boldsymbol{P}_{\mathrm{WT}}^{\mathrm{pd}}(k)\right\|_{\mathrm{w_{PD}}}^2 + \lambda_i^{\mathrm{P},k}[\mathrm{Tr}\{\mathbf{Y}_i^{\mathrm{AD}} \boldsymbol{W}_{\mathrm{AD}}^k\}(\mathrm{r+1}) - P_{\mathrm{OWF}_i}^{\mathrm{ref},k}] + \frac{\rho}{2}\left\|\mathrm{Tr}\{\mathbf{Y}_i^{\mathrm{AD}} \boldsymbol{W}_{\mathrm{AD}}^k\}(\mathrm{r+1}) - P_{\mathrm{OWF}_i}^{\mathrm{ref},k}\right\|^2 \\
&+\lambda_i^{\mathrm{Q},k}[\mathrm{Tr}\{\overline{\mathbf{Y}}_i^{\mathrm{AD}} \boldsymbol{W}_{\mathrm{AD}}^k\}(\mathrm{r+1}) - Q_{\mathrm{OWF}_i}^{\mathrm{ref},k}] + \frac{\rho}{2}\left\|\mathrm{Tr}\{\overline{\mathbf{Y}}_i^{\mathrm{AD}} \boldsymbol{W}_{\mathrm{AD}}^k\}(\mathrm{r+1}) - Q_{\mathrm{OWF}_i}^{\mathrm{ref},k}\right\|^2]
\end{aligned}
\tag{3.47}
$$

s.t. (3.38)-(3.40), (3.42).

3) Update the dual variables in the OWF controllers,

$$
\lambda_i^{\mathrm{P},k}(r+1) = \lambda_i^{\mathrm{P},k}(r) + \rho[P_{\mathrm{OWF}_i}^{\mathrm{ref},k}(r+1) - \mathrm{Tr}\{\mathbf{Y}_i^{\mathrm{AD}} \boldsymbol{W}_{\mathrm{AD}}^k\}(r+1)] \tag{3.48}
$$

$$
\lambda_i^{\mathrm{Q},k}(r+1) = \lambda_i^{\mathrm{Q},k}(r) + \rho[Q_{\mathrm{OWF}_i}^{\mathrm{ref},k}(r+1) - \mathrm{Tr}\{\overline{\mathbf{Y}}_i^{\mathrm{AD}} \boldsymbol{W}_{\mathrm{AD}}^k\}(r+1)] \tag{3.49}
$$

The solution procedure of DOVC strategy based on ADMM is illustrated in Algorithm. Considering the several OWFs are connected to the AC grid with DC connection, the computation burden of the AC-DC controller can be significantly reduced, and meanwhile the need of the central controller is eliminated while guaranteeing the global optimality of control performance. For each OWF controller, the task is a small-scale optimization problem with the constraints only inside OWF and its burden is also not heavy.

Algorithm Steps of DOVC strategy based on ADMM

1: Input the data of TSO command, available wind power, system parameters, measurements of OWF SCADA system, etc.
2: Set step of iteration r=0, primal and dual tolerances $\in$.
3: Initialize optimization variables, and dual variables $\lambda_i^{P,k}$, $\lambda_i^{Q,k}$.
4: The AC-DC controller solves augmented Lagrangian (3.44)-(3.46) with constraints (3.14)-(3.17), (3.19)-(3.23), (3.25)-(3.27), (3.42) of AC grid with DC connection, and updates AC-DC optimization variables.
5: After updating AC-DC optimization variables, each OWF controller solves its augmented Lagrangian (3.47) with constraints (3.38)-(3.40), (3.42) inside OWF, and updates the OWF optimization variables.
6: Update dual variables $\lambda_i^{P,k}$, $\lambda_i^{Q,k}$.
7: Check if primal and dual residuals are less than the tolerances, then iteration will be stopped. Otherwise, the iteration will continue.

3.6 Case Study

3.6.1 Test System

The modified system shown in Fig. 3-1 is used to demonstrate the control performance of the proposed DOVC strategy. For the control of the AC grid with DC connection, each time step and the horizon of OPF calculation within MPC is 5 and 25 s, respectively. For the OWF control, the sampling time ΔT_{p}, the control period T_{c} and the prediction horizon T_{p} are set as 5, 5 and 25 s, respectively. In order to examine the control performance of the DOVC strategy, several control methods are applied to make comparisons: 1) Centralized optimal active and reactive power control (COARPC) strategy (with the same optimization model) [80]; 2) Optimal control (OPC) method [74]; 3) Conventional centralized PD method [74]; 4) A two-stage optimal control (TS) scheme [80]. Table B-2 presents the parameters of the system [74], [98], [99].

3.6.2 Control Performance

The total simulation time is 200s. During t = 0 ~ 45 s, the dispatch command is set as 368 MW. During t = 45 ~ 130 s, the command gradually increases to 518 MW. After t = 130 s, the command gradually decreases to 418 MW. Each of the 6 WTs shares the same wind condition in each OWF. Considering the huge amount of data, only the wind condition of the first four representative groups for WT1 ~ 24 in OWFa is shown in Fig. 3-6.

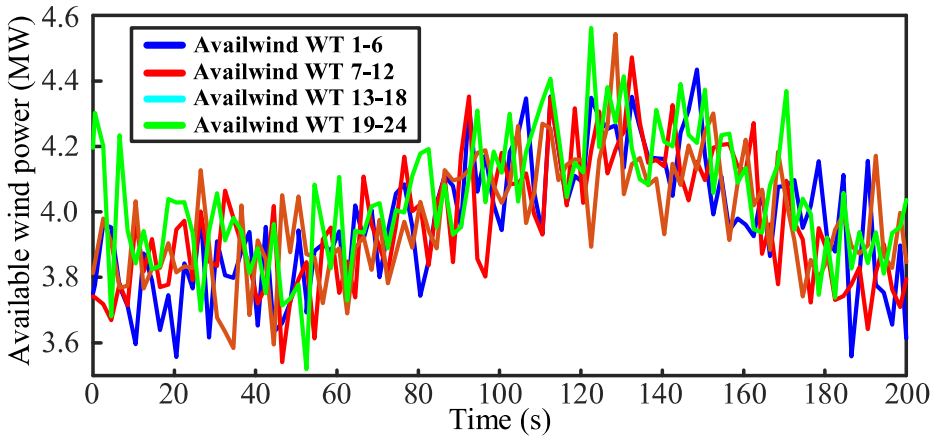

Fig. 3-6 The representative WT available wind power.

The voltage of the boundary bus between the gird and OWFa (the slack bus of OWFa) is shown in Fig. 3-7. It can be seen that the distributed control strategy DOVC with ADMM owns the similar control performance as the centralized control strategy COARPC. The slack bus voltage can be kept at 1.0075 p.u., and then gradually increases to 1.018 p.u. with the active power output of OWFa increased by 131 MW during t = 45 ~ 130 s as Fig. 3-8 shown. After 130s, the slack bus voltage decreases to 1.0101 p.u. with the active power output decreased by 81 MW. The voltage value difference between DOVC and COARPC is very small. Meanwhile, the other three control methods can also maintain the slack bus voltage within the feasible range. However, compared with the DOVC or COARPC, the slack bus voltage with the other three methods is farther away from the rated value. The performance with the TS is quite different from other methods during the active power output rising and decreasing process of OWFa (t = 45 ~ 200 s). It is because that, in the TS method, the objective of the first stage is minimizing the power loss of the AC grid with DC connection without consideration of voltage regulation inside OWFa.

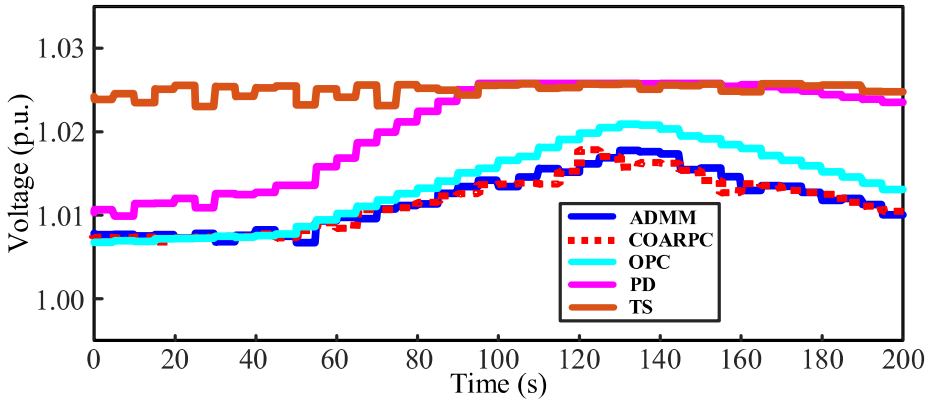

Fig. 3-7 The voltage of the boundary bus between the grid and OWFa.

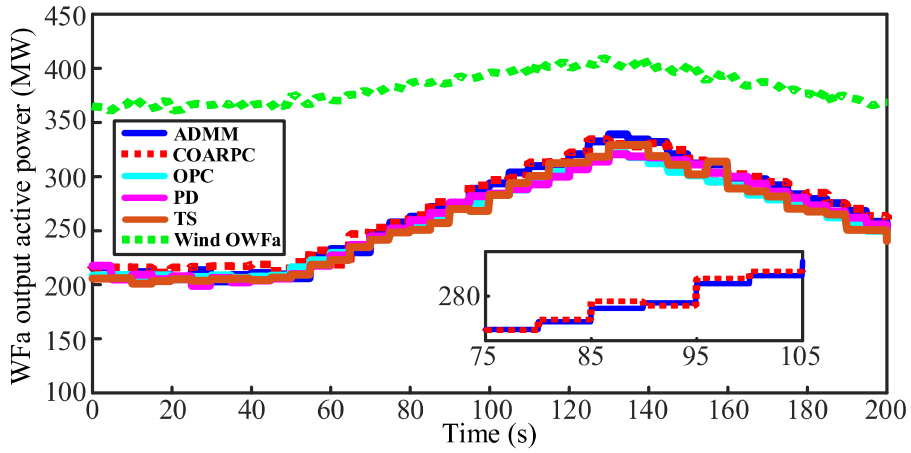

Fig. 3-8 The active power output of OWFa.

The voltage of MV bus 1 in OWFa is shown in Fig. 3-9. It can be seen that the DOVC with ADMM has the very similar voltage control performance with the COARPC (less than 0.0018 p.u.) and much better than the other three control methods. With the active power output of OWFa increased by 131 MW, the MV bus voltage with DOVC or COARPC just increased by 0.003 p.u., which is much smaller voltage rise than 0.014 p.u. with OPC method and 0.021 p.u. with PD method. Fig. 3-10 illustrates the MV bus voltage is much closer to the rated value using DOVC or COARPC than using the other three methods.

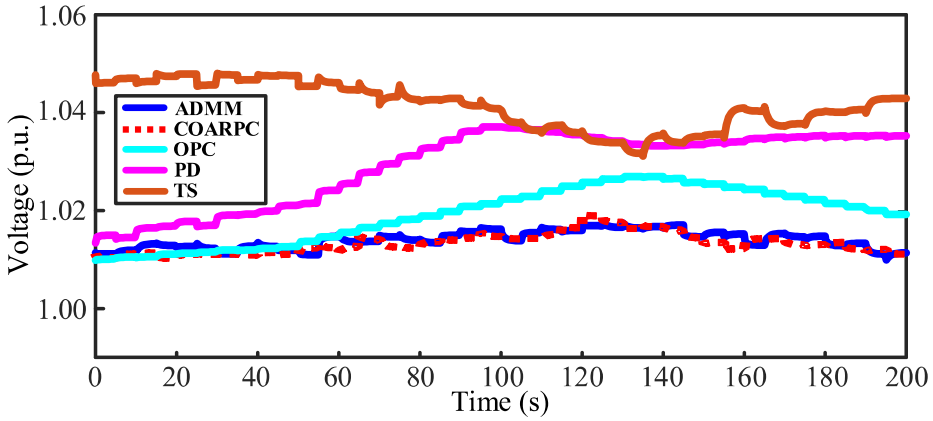

Fig. 3-9 MV bus 1 voltage in OWFa.

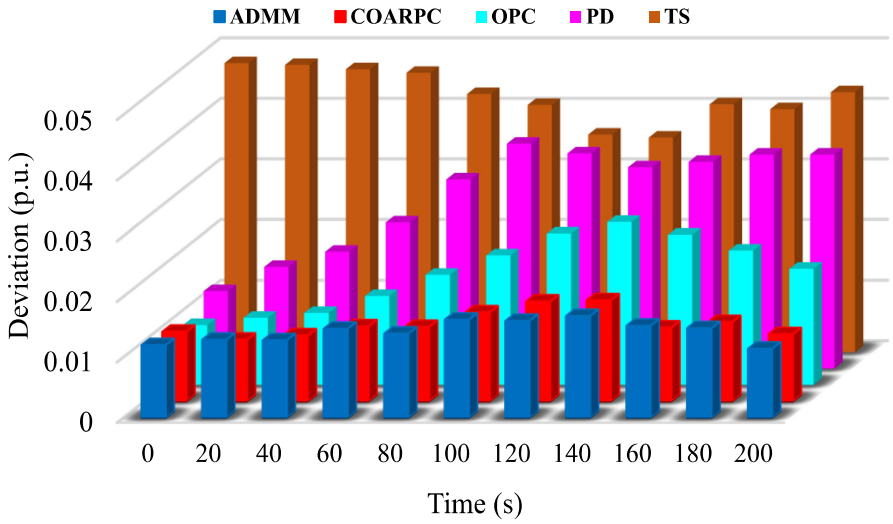

Fig. 3-10 Voltage control performance of MV bus 1 in OWFa.

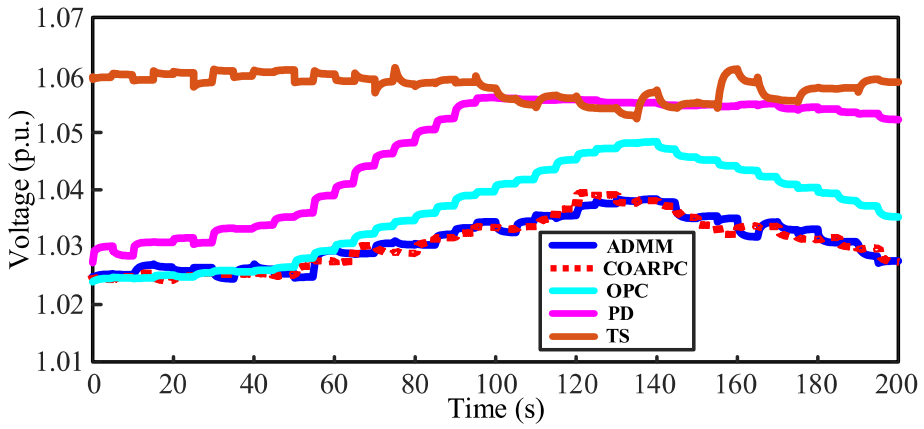

Fig. 3-11 WT96 terminal voltage in OWFa.

WT96 is located at the furthest position along the last feeder in OWFa. WT96 is selected as the representative WT to illustrate the control performance among 5 different methods. In Fig. 3-11 - Fig. 3-12, with the active power output of WT96 increased by approximately 1.0 MW (during t = 45 ~ 130 s), the WT96 terminal bus voltage with DOVC or COARPC only increased by 0.013 p.u., and the voltage rise values with OPC and PD are 1.62 times and 1.69 times of 0.013 p.u., respectively. During the whole control period, the WT96 terminal bus voltage can be kept within 1.025 ~ 1.038 p.u., while the voltages with other three methods are farther away from the rated value as Fig. 3-13 shown. Obviously, the DOVC and COARPC have the similar control performance and the maximal voltage difference is less than 0.002 p.u.

The power losses of total system with all control methods are similar. However, compared with the centralized control methods, the DOVC with the distributed manner eliminates the central controller and evidently reduces communication cost. Moreover, since the very little boundary variables are exchanged between grid-side and OWF-side controllers, the protection of data privacy is hugely improved.

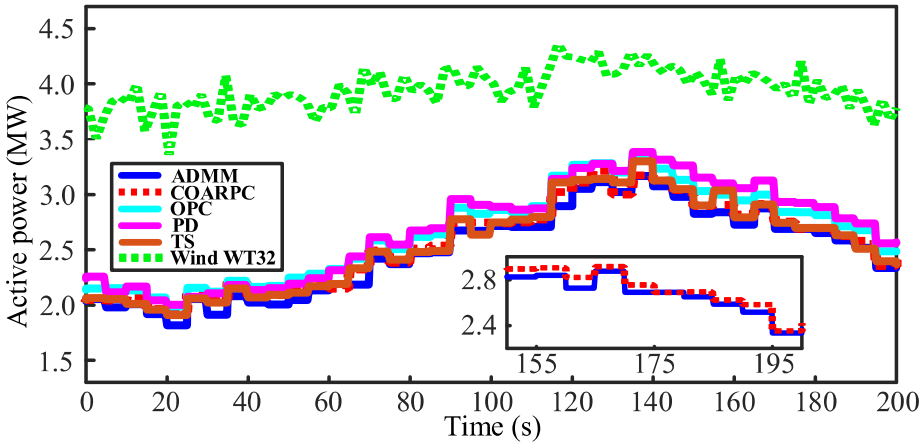

Fig. 3-12 WT96 output active power in OWFa.

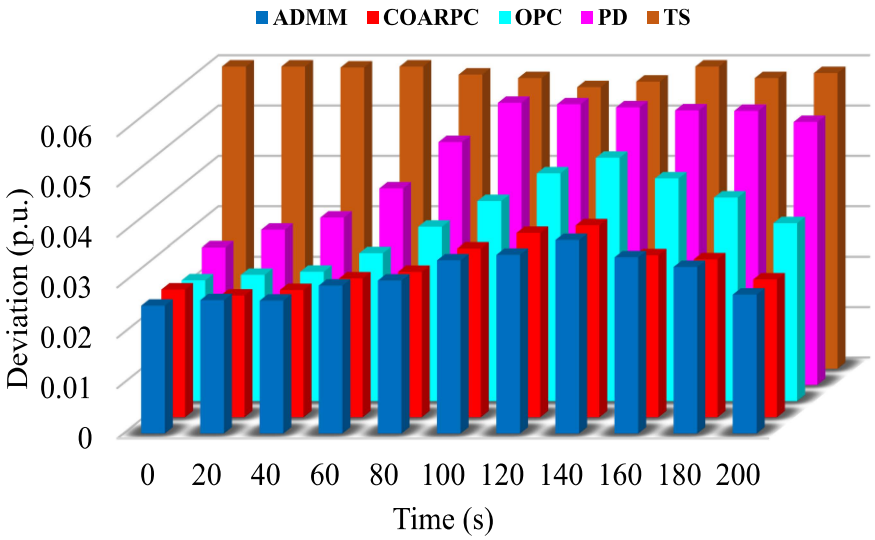

Fig. 3-13 Voltage control performance of WT96 terminal bus in OWFa.

The system convergence performance is shown in Fig. 3-15 - Fig. 3-16. The OWF active and reactive power output boundary variables in grid-side and OWF-side controllers are selected to illustrate the convergence results. After 20 iterations, the AC-DC and OWF boundary variables with the active power output for three OWFs converge to the common values and keep steady. As Fig. 3-16 shown, the AC-DC

and OWF boundary variables with the reactive power output for three OWFs converge to -5.8, 21.5, and 34.5 Mvar in 18 iterations. The above convergence performance is acceptable.

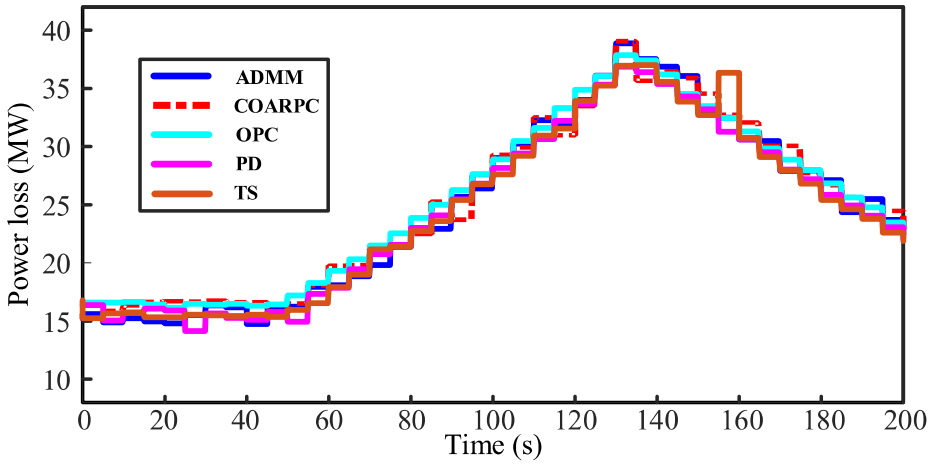

Fig. 3-14 Power loss of total system.

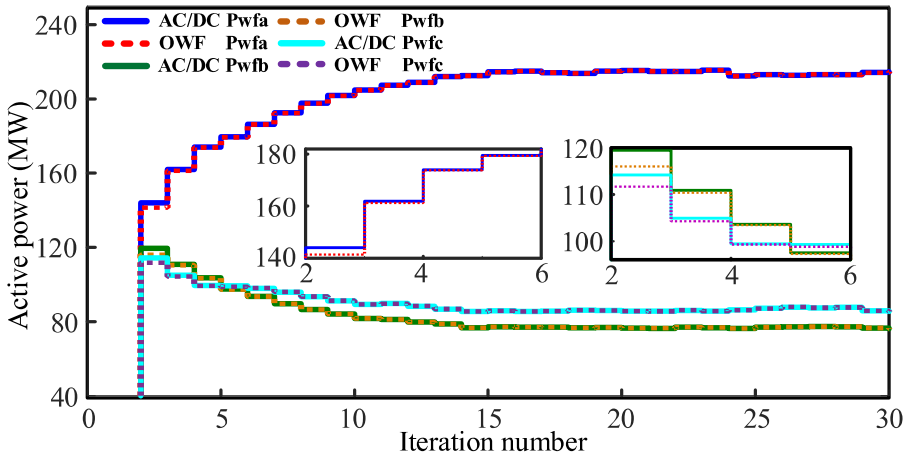

Fig. 3-15 Convergence performance of active power output of OWFs. (t=5s)

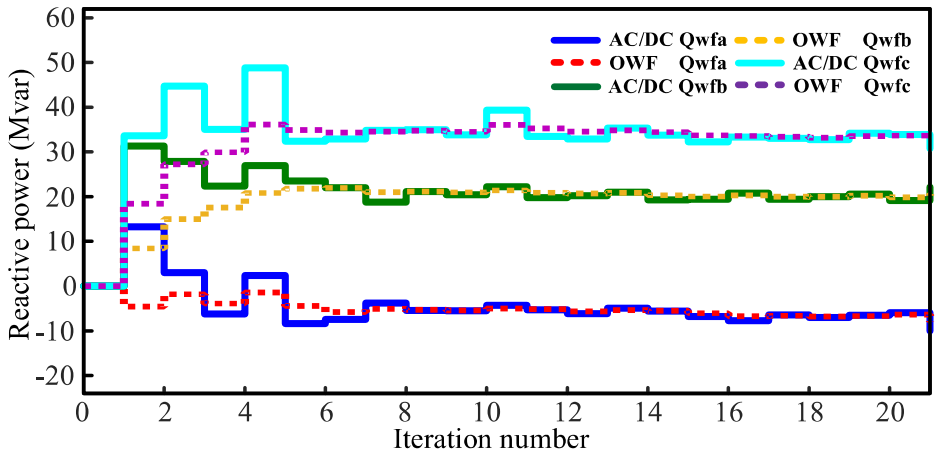

Fig. 3-16 Convergence performance of reactive power output of OWFs. (t=5s)

3.7 Summary

In this chapter, the ADMM-based DOVC strategy with MPC is proposed for the AC grid with DC connection and OWFs. The SDP relaxation technique is adopted to the AC grid with DC connection, which efficiently solves the nonconvexity and nonlinearity issues of the optimal power distribution and voltage regulation in the coupled grid and OWFs. Then, the large-scale strongly coupled optimization problem is decomposed and solved by using the ADMM without loss of global optimality. Moreover, AC-DC and OWF controllers operate in parallel only with a limited amount of boundary information exchanged, implying better OWF information privacy. The case studies show that the DOVC strategy achieves the same voltage control performance as the centralized method. Compared to other control methods such as OPC, PD and TS, the proposed DOVC strategy has the better control performance, which can be implemented for the future AC grid with DC connection incorporating several OWFs.

CHAPTER 4.

DISTRIBUTED OPTIMAL VOLTAGE CONTROL IN AC GRID WITH VSC-HVDC INCLUDING OFFSHORE WIND FARMS EQUIPPED WITH DISTRIBUTED ESSS

This chapter proposes a DOVC scheme based on the ADMM for AC grid with VSC-HVDC including OWFs. The OWFs are equipped with distributed energy storage systems. The chapter is based on the paper 3 with minor changes to coherently fit into the framework of the thesis[3]. The paper 3 is in process of submitting.

4.1 Introduction

The integration of large-scale offshore wind power into power systems is encouraged by government policies to decrease global carbon emission and realize fossil fuel free vision [94], [101]. The grid and WFs are physically connected and coupled, but separately managed by TSO and WFO, respectively [4]. The limited coordination of system operation exists among TSO and WFOs. The grid is operated by TSO without any WFO information. The OWF is simplified as a generator. Similarly, the OWF is managed by WFO only with TSO dispatch command, and the grid can be simplified as the voltage source. Therefore, the current limited coordination among TSO and WFOs creates the difficulty for the control and operation of the power systems. As the installed capacity of modern OWFs is hugely increasing, the control and operation of grid and OWFs without simultaneous consideration may face significant challenges, i.e., feeder voltage profile regulation, optimal active and reactive power distribution, coordinated control scheme for grid with

[3] This chapter is based on paper 3: **Pengda Wang,** Qiuwei Wu*, Zhou Liu, Zhe Chen, Sheng Huang, Canbing Li, and Bin Zhou, "Distributed Optimal Voltage Control in AC Grid with VSC-HVDC including Offshore Wind Farms Equipped with Distributed ESSs," The manuscript is completed, and in process of submitting.

OWFs [137], [143].

OPF-based control methods are known as the fundamental tools to achieve power system optimization and control including the voltage regulation issue [152]. In [4], [153], a coordinated transmission and distribution AC OPF was proposed to mitigate voltage rises and resolve the over-voltage issue with DER penetration increasing. In [151], [130], the OPF with SDP relaxation was used to achieve optimal power distribution and minimize the power losses of regional AC TS. In [154]-[155], the reactive power optimization with the interval uncertainties was modelled to optimize the voltage profile, and improve the voltage quality, as well for maintaining a low level of real power losses of the grid. However, few studies exist regarding coordinated optimal voltage control schemes for power systems connected to large-scale WFs while taking into account feeder voltage regulation across wind power collection systems.

Due to the fluctuation and intermittency of wind power, the negative voltage fluctuation problems have been occurred in WFs. In order to improve the operation performance, the WFs need to maintain the feeder voltage profile within the feasible range. With the simple implementation advantage, the conventional PD and PI have been effectively used in WF control. To overcome the disadvantages of the conventional control methods on voltage performance inside WFs, several optimization-based voltage control strategies have been motivated. In [74], [94], [100], MPC-based voltage control methods were proposed to minimize voltage deviation, and coordinate reactive power outputs of WTs, as well for improving economic operation inside each WF. With the increasing of WFs in number and size, the ESS has been considered as an effective tool to improve the flexible and controllable operation in WFs. Several MPC-based optimal active power control schemes were proposed to optimize the active power references of WTs and ESSs inside WFs, aiming to achieve a low level of fatigue load of doubly-fed induction generator (DFIG)-based WTs [101], [142].

Due to the fast development of huge WF projects, the central controller may not be able to generate the optimal control action of large-scale optimization problems for power systems with large-scale WFs including ESSs in a fast way. Therefore, the ADMM-based distributed control methods have been proposed for power systems [94], [100], [101]. In [94], [100], the proposed distributed voltage control strategy based on ADMM provides a coordinated reactive power solution for maintaining the terminal bus voltage, realizing economic operation inside WFs. The ADMM-based active power control methods were proposed to generate optimal active

power references for WTs and ESSs with computation burden efficiently reduced [101]. However, the distributed control scheme has not been used for optimal voltage control for power systems with large-scale OWFs including distributed ESSs, as well for regulating the feeder voltage profile inside wind power collection systems.

In this chapter, the DOVC scheme is designed for AC grid with VSC-HVDC including large-scale OWFs equipped with distributed ESSs. The global optimal power distribution of AC-HVDC is achieved while the WTs and distributed ESSs are optimally coordinated to regulate feeder voltage profile, minimize power losses, and achieve fair utilization among all ESSs inside OWFs. The TSO command, the state-of-charge (SOC) of ESSs within a specified range, and cut-out wind speed of WT are also considered. In addition, the dynamic processes of WTs and ESSs are modelled to improve the voltage regulation. With Schur complement applied [151], the augment Lagrangian of AC grid with VSC-HVDC optimization program can be reformulated as the semi-definite objectives with semi-definite constraints guaranteeing the convergence of ADMM. In order to reduce the calculation and communicate burden of grid controller, part of the computation task is distributed to each OWF controller. With the distributed framework applied, the grid controller only solves the optimization problem with grid side constraints, and OWF controllers solve the small-scale optimization problems with local OWF constraints. The main contribution of the paper is summarized as follows:

(1) A DOVC scheme is designed for achieving optimal voltage regulation in AC grid with VSC-HVDC including the strongly coupled large-scale OWFs equipped with distributed ESSs. In addition, the feeder voltage profile inside OWFs is optimally regulated without loss of global optimality.

(2) The non-linear non-convex OPF program of AC grid with VSC-HVDC is transformed into convex semidefinite one with SDP relaxation adopted, while the OPC-based voltage control model in wind power collection systems with distributed ESSs is formulated to generate the global optimal solution. The convexity-preserving property of augment Lagrangian of AC grid with VSC-HVDC optimization subproblem is guaranteed by the Schur complement, in which the inherent non-convexities of the original program are tackled.

(3) The ADMM-based distributed framework distributes the computation and monitoring tasks of the grid controller to several OWF controllers, implying better robustness and optimization efficiency. In addition, only the limited amount of

boundary information is exchanged between two side controllers, enhancing the protection of OWF information privacy.

The rest of this chapter is organized as follows. Section 4.2 presents the framework of the proposed DOVC scheme. The AC-HVDC grid optimization model and OWF control model are formulated in section 4.3 and 4.4, respectively. The section 4.5 gives the distributed solution with ADMM framework. The simulation results are presented in section 4.6, followed by the summary.

4.2 Optimal Voltage Control Architecture

4.2.1 System Configuration

The structure of the AC grid with VSC-HVDC including two OWFs equipped with distributed ESSs is shown in Fig. 4-1. OWF1 and OWF2 are connected to the modified IEEE 30-bus system incorporating HVDC network. Each OWF consists of 32×5 MW WTs. Each WT is equipped with an ESS including a DC-DC converter and an energy storage unit. Every 8 WTs are collected through the 35 kV MV feeder, and placed at the distance of 4 km.

4.2.2 Strategy Concept

Fig. 4-2 shows the structure of the proposed DOVC scheme. The DOVC scheme is designed in a distributed fashion with the ADMM. The control scheme is divided into several parts: a) AC grid with HVDC control part, and b) OPC-based voltage control method inside each OWF. In the first part, the available wind power for each OWF $P_{\mathrm{WF}}^{\mathrm{avi}}$ and TSO dispatch command P_{TSO} are synchronized. The synchronized information can be used in the OPF. Moreover, the rank-relaxed OPF-based AC-HVDC controller with SDP relaxation can achieve the global optimal power distribution, and minimize the power losses. In OWF-side part, the SCADA and sensor system of OWF can collect the operating information of WTs and ESSs inside OWF. Each OWF controller formulates voltage control problem as an OPC-based augmented Lagrangian optimization problem, and then solves it to obtain active/reactive power references of each WT $P_{\mathrm{WT}}^{\mathrm{ref}}/Q_{\mathrm{WT}}^{\mathrm{ref}}$ and power reference of total ESSs $P_{\mathrm{ESS,WF}}^{\mathrm{sum}}$. The ESS control block is used to achieve fair utilization among all ESSs, and generate power reference of each ESS $P_{\mathrm{ESS}}^{\mathrm{ref}}$ while tracking $P_{\mathrm{ESS,WF}}^{\mathrm{sum}}$. The DOVC scheme only exchanges the limited amount of local, global and dual variables between grid and OWF controllers. The large-scale voltage control problem is decomposed, and solved in parallel with the DOVC scheme while guaranteeing global optimality of control performance.

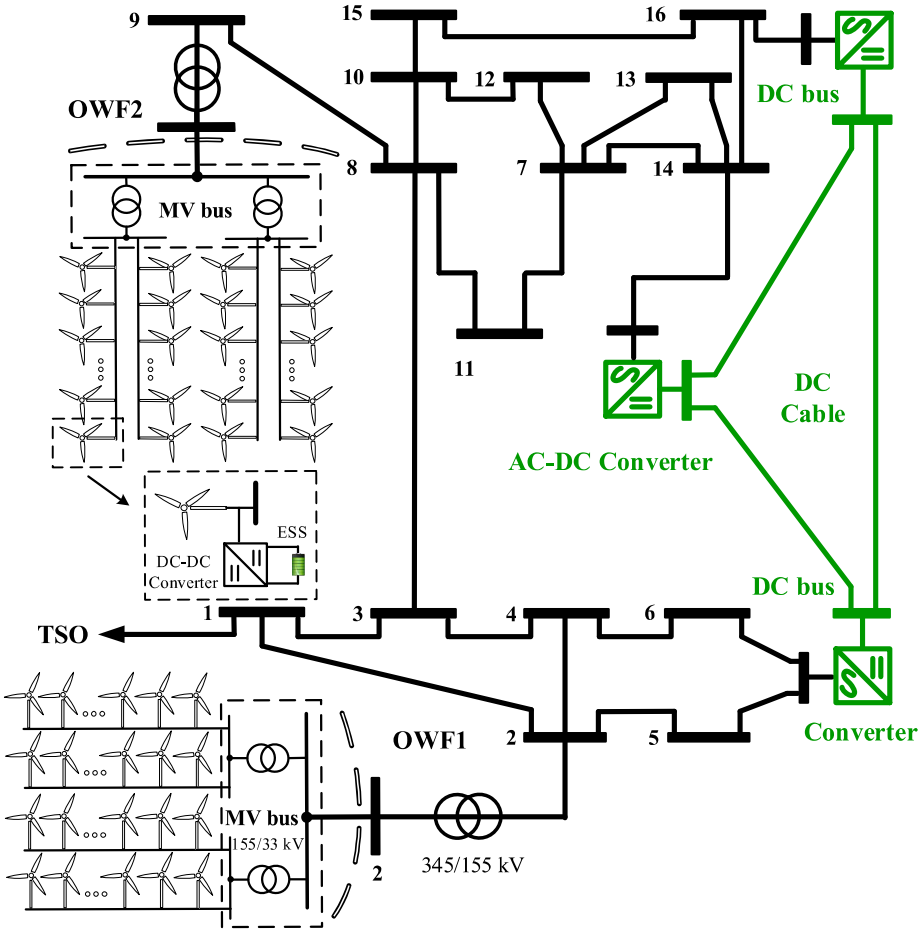

Fig. 4-1 The configuration of system.

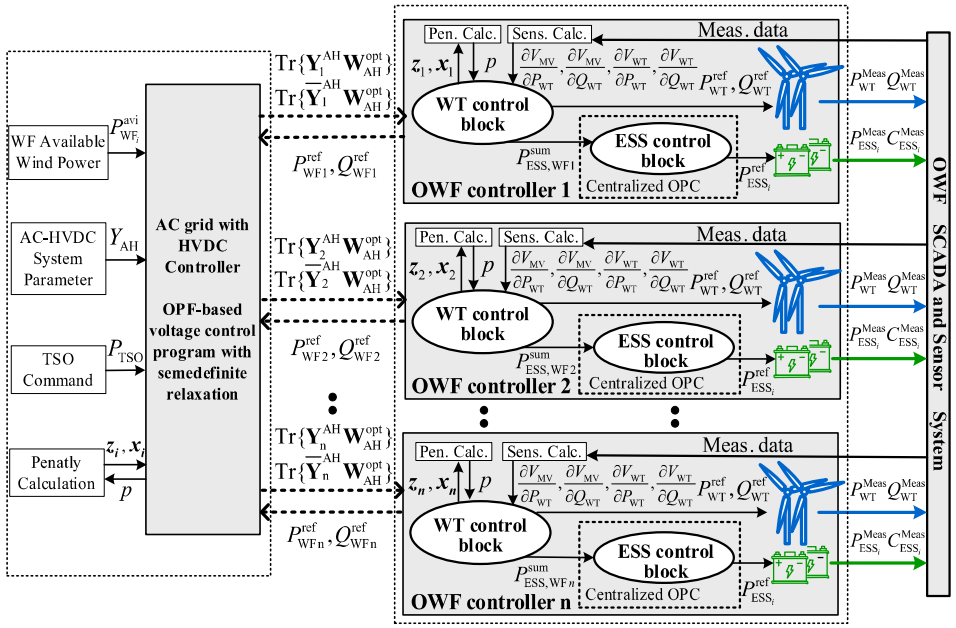

Fig. 4-2 Structure of the proposed DOVC scheme.

4.3 AC Grid with VSC-HVDC Optimization Model

In this section, the semidefinite relaxation of the voltage control program of the AC grid with VSC-HVDC is formulated. The non-linear non-convex OPF-based voltage control program can be relaxed by using the SDP relaxation, and then transformed into a semidefinite model. The convex model formulates the voltage control program as a function of two positive semidefinite matrix variables $\boldsymbol{W}_{\mathrm{AH}}$ and $\boldsymbol{I}$. The model can be solved in the distributed manner while guaranteeing the global optimality of the control performance.

4.3.1 Semidefinite Relaxation of Voltage Control Program of AC Grid with VSC-HVDC

Let matrix Y_{AH} denotes admittance matrix of the system. For $i \in \mathcal{N}_{\mathrm{AH}}$ and $(l,m) \in \boldsymbol{\Omega}_{\mathrm{Line}}$, e_i is the i-th basis vector in $\boldsymbol{R}^{|\mathcal{N}_{\mathrm{AH}}|}$, and y_{lm} and $\bar{y}_{lm}$ are the values of series and shunt elements of line (l,m). The system consists of interconnected AC grid and HVDC network which are connected by several AC-DC converters. The HVDC network can be modeled as the AC grid with purely resistive transmission lines, and generators operating at unity power factor [129]. In order to model the voltage control program in SDP form, the following matrixes are defined [153],

$$Y_i := e_i e_i^{\mathrm{T}} Y_{\mathrm{AH}}$$

$$Y_{lm} := \left(\bar{y}_{lm} + y_{lm}\right) e_l e_l^{\mathrm{T}} - y_{lm} e_l e_m^{\mathrm{T}}$$

$$\mathbf{M}_{lm}^{\mathrm{AH}} := \mathrm{diag}\left[(e_l - e_m)(e_l - e_m)^{\mathrm{T}},\ (e_l - e_m)(e_l - e_m)^{\mathrm{T}} \right]$$

$$\mathbf{Y}_i^{\mathrm{AH}} := \frac{1}{2}\begin{bmatrix} \mathrm{Re}(Y_i + Y_i^{\mathrm{T}}) & \mathrm{Im}(Y_i^{\mathrm{T}} - Y_i) \\ \mathrm{Im}(Y_i - Y_i^{\mathrm{T}}) & \mathrm{Re}(Y_i + Y_i^{\mathrm{T}}) \end{bmatrix}$$

$$\overline{\mathbf{Y}}_i^{\mathrm{AH}} := \frac{-1}{2}\begin{bmatrix} \mathrm{Im}(Y_i + Y_i^{\mathrm{T}}) & \mathrm{Re}(Y_i - Y_i^{\mathrm{T}}) \\ \mathrm{Re}(Y_i^{\mathrm{T}} - Y_i) & \mathrm{Im}(Y_i + Y_i^{\mathrm{T}}) \end{bmatrix}$$

$$\mathbf{Y}_{lm}^{\mathrm{AH}} := \frac{1}{2}\begin{bmatrix} \mathrm{Re}(Y_{lm} + Y_{lm}^{\mathrm{T}}) & \mathrm{Im}(Y_{lm}^{\mathrm{T}} - Y_{lm}) \\ \mathrm{Im}(Y_{lm} - Y_{lm}^{\mathrm{T}}) & \mathrm{Re}(Y_{lm} + Y_{lm}^{\mathrm{T}}) \end{bmatrix}$$

$$\mathbf{M}_i^{\mathrm{AH}} := \mathrm{diag}\left[e_i e_i^{\mathrm{T}},\ e_i e_i^{\mathrm{T}} \right]$$

$$\overline{\mathbf{Y}}_{lm}^{\mathrm{AH}} := \frac{-1}{2}\begin{bmatrix} \mathrm{Im}(Y_{lm} + Y_{lm}^{\mathrm{T}}) & \mathrm{Re}(Y_{lm} - Y_{lm}^{\mathrm{T}}) \\ \mathrm{Re}(Y_{lm}^{\mathrm{T}} - Y_{lm}) & \mathrm{Im}(Y_{lm} + Y_{lm}^{\mathrm{T}}) \end{bmatrix}$$

$$\mathbf{C}_i^{\mathrm{Conv}} := \begin{bmatrix} a_{mi} & b_{mi}/2 \\ b_{mi}/2 & c_{mi} \end{bmatrix}$$

The formulation of the OPF-based voltage control program with complex variables can be rewritten with the two semidefinite matrixes $2N_{\mathrm{AH}} \times 2N_{\mathrm{AH}}$-dimensional matrix $\boldsymbol{W}_{\mathrm{AH}}$ and 2×2-dimensional matrix $\boldsymbol{I}_i$,

$$\boldsymbol{W}_{\mathrm{AH}} := \boldsymbol{X}_{\mathrm{AH}} \boldsymbol{X}_{\mathrm{AH}}^{\mathrm{T}}$$

$$\boldsymbol{I}_i := \boldsymbol{T}_i \boldsymbol{T}_i^{\mathrm{T}},\ \forall i \in \mathcal{N}_{\mathrm{AC}}^{\mathrm{Conv}}$$

where the variable column vector and complex bus voltage of the system are

$\boldsymbol{X}_{\mathrm{AH}} \coloneqq [\mathrm{Re}\{V_{\mathrm{AH}}\}^{\mathrm{T}}\ \mathrm{Im}\{V_{\mathrm{AH}}\}^{\mathrm{T}}]^{\mathrm{T}}$ and $V_{\mathrm{AH}} \coloneqq [V_1, V_2, \cdots, V_{N_{\mathrm{AH}}}]_{1\times|\mathcal{N}_{\mathrm{AH}}|}$; The variable column vector associated with $|I_i|$ for AC side converter buses is $\boldsymbol{T}_i \coloneqq [1\ |I_i|]^{\mathrm{T}}, \forall i \in \mathcal{N}_{\mathrm{AC}}^{\mathrm{Conv}}$; $\mathcal{N}_{\mathrm{AH}}$ is the set of buses in AC grid with VSC-HVDC.

4.3.1.1 The Objectives of Voltage Control Program in Grid

The objectives in AC grid with VSC-HVDC are,

$$\min_{\boldsymbol{W}_{\mathrm{AH}}, \lambda_{\mathrm{c}}, Q_{\mathrm{C}_i}} \sum_{i=1}^{|\mathcal{N}_{\mathrm{AH}}|} \mathrm{Tr}\{\mathbf{Y}_i^{\mathrm{AH}} \boldsymbol{W}_{\mathrm{AH}}\}_{\mathrm{w_{PL}}} - \left(\lambda_{\mathrm{c}} - \lambda_{\mathrm{rated}}\right)_{\mathrm{w_{VO}}} + \sum_{i=1}^{|\mathcal{N}_{\mathrm{AH}}|} \left(\mathrm{C} * Q_{\mathrm{C}_i}\right)_{\mathrm{W_{QS}}} \quad (4.1)$$

where $\mathrm{w_{PL}}$, $\mathrm{w_{VO}}$, and $\mathrm{w_{QS}}$ are weighting factors of three sub-objectives.

The first sub-objective is to minimize the power losses of the system. It is also the semidefinite expression of the total active power generation of OWFs minus the total load. The second sub-objective is to maximize the voltage stability margin. λ_{c} and λ_{rated} stand for critical loading point and the loading point decided by TSO command, respectively. In order to model the critical point, the variable column vector $\boldsymbol{X}_{\mathrm{AH}}^{\mathrm{C}} \coloneqq [\mathrm{Re}\{V_{\mathrm{AH}}^{\mathrm{C}}\}^{\mathrm{T}}\ \mathrm{Im}\{V_{\mathrm{AH}}^{\mathrm{C}}\}^{\mathrm{T}}]^{\mathrm{T}}$ and $\boldsymbol{T}_i^{\mathrm{C}} \coloneqq [1\ |I_i^{\mathrm{C}}|]^{\mathrm{T}}$ are created to represent the maximum loading point. $[\mathrm{Re}\{V_{\mathrm{AH}}^{\mathrm{C}}\}^{\mathrm{T}}\ \mathrm{Im}\{V_{\mathrm{AH}}^{\mathrm{C}}\}^{\mathrm{T}}]^{\mathrm{T}}$ and $\boldsymbol{T}_i^{\mathrm{C}} \coloneqq [1\ |I_i^{\mathrm{C}}|]^{\mathrm{T}}$ are created to represent the maximum loading point. The third sub-objective is to minimize the cost of reactive power support. Q_{C_i} and C are the reactive power support at bus i and cost of reactive power support per Mvar.

4.3.1.2 The Constraints of Voltage Control Program in Grid

The active/reactive power balance constraints in terms of the reactive power support Q_{C_i} and power generation limits of OWFs are,

$$\underline{P}_{\mathrm{WF}_i} - P_{\mathrm{D}_i} \le \mathrm{Tr}\{\mathbf{Y}_i^{\mathrm{AH}} \boldsymbol{W}_{\mathrm{AH}}\} \le \overline{P}_{\mathrm{WF}_i} - P_{\mathrm{D}_i}, \forall i \in \mathcal{N}_{\mathrm{AH}} \quad (4.2)$$

$$\underline{P}_{\mathrm{WF}_i} - \lambda_{\mathrm{c}} P_{\mathrm{D}_i} \le \mathrm{Tr}\{\mathbf{Y}_i^{\mathrm{AH}} \boldsymbol{W}_{\mathrm{AH}}^{\mathrm{C}}\} \le \overline{P}_{\mathrm{WF}_i} - \lambda_{\mathrm{c}} P_{\mathrm{D}_i}, \forall i \in \mathcal{N}_{\mathrm{AH}} \quad (4.3)$$

$$\underline{Q}_{\mathrm{WF}_i} - Q_{\mathrm{D}_i} \le \mathrm{Tr}\{\overline{\mathbf{Y}}_i^{\mathrm{AH}} \boldsymbol{W}_{\mathrm{AH}}\} - Q_{\mathrm{C}_i} \le \overline{Q}_{\mathrm{WF}_i} - Q_{\mathrm{D}_i}, \forall i \in \mathcal{N}_{\mathrm{AH}} \quad (4.4)$$

$$\underline{Q}_{\mathrm{WF}_i} - \lambda_{\mathrm{c}} Q_{\mathrm{D}_i} \le \mathrm{Tr}\{\overline{\mathbf{Y}}_i^{\mathrm{AH}} \boldsymbol{W}_{\mathrm{AH}}^{\mathrm{C}}\} - Q_{\mathrm{C}_i}^{\mathrm{C}} \le \overline{Q}_{\mathrm{WF}_i} - \lambda_{\mathrm{c}} Q_{\mathrm{D}_i}, \forall i \in \mathcal{N}_{\mathrm{AH}} \quad (4.5)$$

where $\underline{P}_{\mathrm{WF}_i}, \overline{P}_{\mathrm{WF}_i}, \underline{Q}_{\mathrm{WF}_i}$ and $\overline{Q}_{\mathrm{WF}_i}$ are the lower and upper bounds on the i-th OWF active/reactive power generations; P_{D_i} and Q_{D_i} are the active and reactive load of bus i; The variable matrix associated with critical point is defined as $\boldsymbol{W}_{\mathrm{AH}}^{\mathrm{C}} := \boldsymbol{X}_{\mathrm{AH}}^{\mathrm{C}} \boldsymbol{X}_{\mathrm{AH}}^{\mathrm{C}\ \mathrm{T}}$; $Q_{c_i}^{\mathrm{C}}$ is the reactive power support associated with critical point.

The bus voltages and transmission line capacity are constrained by (4.6)-(4.9),

$$\left|\underline{V}_i\right|^2 \le \mathrm{Tr}\{\mathbf{M}_i^{\mathrm{AH}} \boldsymbol{W}_{\mathrm{AH}}\} \le \left|\overline{V}_i\right|^2, \forall i \in \mathcal{N}_{\mathrm{AH}} \tag{4.6}$$

$$\left|\underline{V}_i\right|^2 \le \mathrm{Tr}\{\mathbf{M}_i^{\mathrm{AH}} \boldsymbol{W}_{\mathrm{AH}}^{\mathrm{C}}\} \le \left|\overline{V}_i\right|^2, \forall i \in \mathcal{N}_{\mathrm{AH}} \tag{4.7}$$

$$\mathrm{Tr}\{\mathbf{Y}_{lm}^{\mathrm{AH}} \boldsymbol{W}_{\mathrm{AH}}\}^2 + \mathrm{Tr}\{\overline{\mathbf{Y}}_{lm}^{\mathrm{AH}} \boldsymbol{W}_{\mathrm{AH}}\}^2 \le \left|\overline{S}_{lm}\right|^2, (l,m) \in \boldsymbol{\Omega}_{\mathrm{Line}} \tag{4.8}$$

$$\mathrm{Tr}\{\mathbf{Y}_{lm}^{\mathrm{AH}} \boldsymbol{W}_{\mathrm{AH}}^{\mathrm{C}}\}^2 + \mathrm{Tr}\{\overline{\mathbf{Y}}_{lm}^{\mathrm{AH}} \boldsymbol{W}_{\mathrm{AH}}^{\mathrm{C}}\}^2 \le \left|\overline{S}_{lm}\right|^2, (l,m) \in \boldsymbol{\Omega}_{\mathrm{Line}} \tag{4.9}$$

The model of AC-DC converter with AC filter bus f, AC bus m and DC bus s is shown in Fig. 4-3. The converter is modeled as the VSC, which connects AC grid and HVDC network. Some assumptions are made in modeling VSC [130].

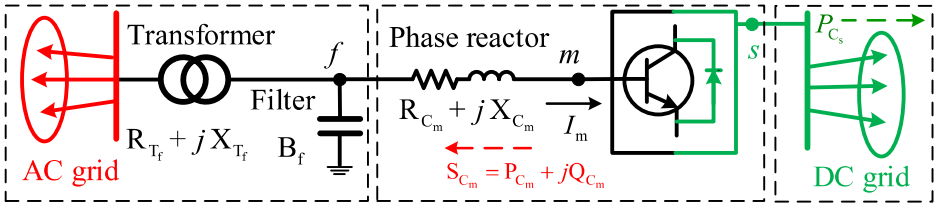

Fig. 4-3 The model of AC-DC converter.

The voltage magnitude can be modulated from AC side to DC side by the VSC with a modulation factor γ_{mo},

$$\mathrm{Tr}\{\mathbf{M}_m^{\mathrm{AH}} \boldsymbol{W}_{\mathrm{AH}}\} \le \gamma_{\mathrm{mo}}^2 \mathrm{Tr}\{\mathbf{M}_s^{\mathrm{AH}} \boldsymbol{W}_{\mathrm{AH}}\}, \ \forall m \in \mathcal{N}_{\mathrm{AC}}^{\mathrm{Conv}}, \forall s \in \mathcal{N}_{\mathrm{DC}}^{\mathrm{Conv}} \tag{4.10}$$

$$\mathrm{Tr}\{\mathbf{M}_m^{\mathrm{AH}} \boldsymbol{W}_{\mathrm{AH}}^{\mathrm{C}}\} \le \gamma_{\mathrm{mo}}^2 \mathrm{Tr}\{\mathbf{M}_s^{\mathrm{AH}} \boldsymbol{W}_{\mathrm{AH}}^{\mathrm{C}}\}, \ \forall m \in \mathcal{N}_{\mathrm{AC}}^{\mathrm{Conv}}, \forall s \in \mathcal{N}_{\mathrm{DC}}^{\mathrm{Conv}} \tag{4.11}$$

where γ_{mo} is the maximum modulation factor; $\mathcal{N}_{\mathrm{DC}}^{\mathrm{Conv}}$ is the set of DC side VSC

buses.

The active power balance of the VSC between AC bus m and DC bus s is,

$$P_m^{\text{Conv}} + P_s^{\text{Conv}} + P_{\text{Loss}}^{\text{Conv}} = 0 \tag{4.12}$$

where P_m^{Conv} and P_s^{Conv} denote the active power injected into AC bus m and DC bus s; $P_{\text{Loss}}^{\text{Conv}}$ denotes the power loss of the VSC; $P_{\text{Loss}}^{\text{Conv}}$ can be approximately described by a quadratic function of AC current magnitude $|I_m|$,

$$P_{\text{Loss}}^{\text{Conv}} = a_{\text{Lo}} + b_{\text{Lo}} |I_m| + c_{\text{Lo}} |I_m|^2 \tag{4.13}$$

where $a_{\text{Lo}}, b_{\text{Lo}}$ and c_{Lo} are the constant, linear and quadratic coefficients [130].

The active power balance constraint of VSC (4.12) can be transformed into SDP form,

$$\text{Tr}\{\mathbf{Y}_m^{\text{AH}} \boldsymbol{W}_{\text{AH}}\} + P_{\text{D}_m} + \text{Tr}\{\mathbf{Y}_s^{\text{AH}} \boldsymbol{W}_{\text{AH}}\} + P_{\text{D}_s} + \text{Tr}\{\mathbf{C}_i^{\text{Conv}} \boldsymbol{I}_m\} = 0 \tag{4.14}$$

$$\text{Tr}\{\mathbf{Y}_m^{\text{AH}} \boldsymbol{W}_{\text{AH}}^{\text{C}}\} + \lambda_{\text{c}} P_{\text{D}_m} + \text{Tr}\{\mathbf{Y}_s^{\text{AH}} \boldsymbol{W}_{\text{AH}}^{\text{C}}\} + \lambda_{\text{c}} P_{\text{D}_s} + \text{Tr}\{\mathbf{C}_i^{\text{Conv}} \boldsymbol{I}_m^{\text{C}}\} = 0 \tag{4.15}$$

The element in the second row and the second column of variable matrix $\boldsymbol{I}_i$ is defined as $\boldsymbol{I}_i^a$. The current magnitude of VSC $|I_m|$ from filter bus f to AC bus m can be obtained,

$$\boldsymbol{I}_m^a = |I_m|^2 = (R_{Cm}^2 + X_{Cm}^2)^{-1} \text{Tr}\{\mathbf{M}_{mf}^{\text{AH}} \boldsymbol{W}_{\text{AH}}\} \tag{4.16}$$

$$\boldsymbol{I}_m^{\text{a,C}} = |I_m^{\text{C}}|^2 = (R_{Cm}^2 + X_{Cm}^2)^{-1} \text{Tr}\{\mathbf{M}_{mf}^{\text{AH}} \boldsymbol{W}_{\text{AH}}^{\text{C}}\} \tag{4.17}$$

Similarly, $\boldsymbol{I}_i^b$ represents the element in the second row and first column of variable matrix $\boldsymbol{I}_i$. Obviously, $\boldsymbol{I}_i^b$ and $\boldsymbol{I}_i^{b,\text{C}}$ are constrained by,

$$\boldsymbol{I}_m^b \geq 0, \ \forall i \in \mathcal{N}_{\text{AC}}^{\text{Conv}} \tag{4.18}$$

$$\boldsymbol{I}_m^{b,\text{C}} \geq 0, \ \forall i \in \mathcal{N}_{\text{AC}}^{\text{Conv}} \tag{4.19}$$

The transferable apparent power constraint of VSC can be presented with the maximum current limit of VSC $|I_m^{\max}|$,

$$(\mathrm{Tr}\{\mathbf{Y}_m^{\mathrm{AH}}\boldsymbol{W}_{\mathrm{AH}}\}+P_{D_m})^2+(\mathrm{Tr}\{\overline{\mathbf{Y}}_m^{\mathrm{AH}}\boldsymbol{W}_{\mathrm{AH}}\}+Q_{D_m})^2\le(I_m^{\max})^2\mathrm{Tr}\{\mathbf{M}_m^{\mathrm{AH}}\boldsymbol{W}_{\mathrm{AH}}\} \tag{4.20}$$

$$(\mathrm{Tr}\{\mathbf{Y}_m^{\mathrm{AH}}\boldsymbol{W}_{\mathrm{AH}}^{\mathrm{C}}\}+\lambda_{\mathrm{c}}P_{D_m})^2+(\mathrm{Tr}\{\overline{\mathbf{Y}}_m^{\mathrm{AH}}\boldsymbol{W}_{\mathrm{AH}}^{\mathrm{C}}\}+\lambda_{\mathrm{c}}Q_{D_m})^2\le(I_m^{\mathrm{C,max}})^2\mathrm{Tr}\{\mathbf{M}_m^{\mathrm{AH}}\boldsymbol{W}_{\mathrm{AH}}^{\mathrm{C}}\} \tag{4.21}$$

In general, the reactive power limit of VSC is proportional to the rated apparent power,

$$-\gamma_{\mathrm{re}}^{\mathrm{b}}S_{C_m}^{\mathrm{rated}}\le\mathrm{Tr}\{\overline{\mathbf{Y}}_m^{\mathrm{AH}}\boldsymbol{W}_{\mathrm{AH}}\}\le\gamma_{\mathrm{re}}^{\mathrm{c}}S_{C_m}^{\mathrm{rated}} \tag{4.22}$$

$$-\gamma_{\mathrm{re}}^{\mathrm{b}}S_{C_m}^{\mathrm{rated}}\le\mathrm{Tr}\{\overline{\mathbf{Y}}_m^{\mathrm{AH}}\boldsymbol{W}_{\mathrm{AH}}^{\mathrm{C}}\}\le\gamma_{\mathrm{re}}^{\mathrm{c}}S_{C_m}^{\mathrm{rated}} \tag{4.23}$$

where $\gamma_{\mathrm{re}}^{\mathrm{b}}$ and $\gamma_{\mathrm{re}}^{\mathrm{c}}$ are the positive constants associated with reactive power limits; $S_{C_m}^{\mathrm{rated}}$ is the rated apparent power of the VSC connected to AC bus m.

The transmission line capacity constraint (4.8)-(4.9) and transferable apparent power constraint of VSC (4.20)-(4.21) are expressed as the quadratic formulas of matrix variable $\boldsymbol{W}_{\mathrm{AH}}/\boldsymbol{W}_{\mathrm{AH}}^{\mathrm{C}}$. In order to obtain the system voltage control program (SVCP) linear in $\boldsymbol{W}_{\mathrm{AH}}/\boldsymbol{W}_{\mathrm{AH}}^{\mathrm{C}}$, the quadratic constraints (4.8)-(4.9) and (4.20)-(4.21) can be reformulated to form the linear matrix inequality constraints. Then the second-order dependence on the matrix variable $\boldsymbol{W}_{\mathrm{AH}}/\boldsymbol{W}_{\mathrm{AH}}^{\mathrm{C}}$ is reduced to linear terms,

$$\begin{bmatrix}\left(I_m^{\max}\right)^2\mathrm{Tr}\{\mathbf{M}_m^{\mathrm{AH}}\boldsymbol{W}_{\mathrm{AH}}\} & \mathrm{Tr}\{\mathbf{Y}_m^{\mathrm{AH}}\boldsymbol{W}_{\mathrm{AH}}\}+P_{D_m} & \mathrm{Tr}\{\overline{\mathbf{Y}}_m^{\mathrm{AH}}\boldsymbol{W}_{\mathrm{AH}}\}+Q_{D_m}\\ \mathrm{Tr}\{\mathbf{Y}_m^{\mathrm{AH}}\boldsymbol{W}_{\mathrm{AH}}\}+P_{D_m} & 1 & 0\\ \mathrm{Tr}\{\overline{\mathbf{Y}}_m^{\mathrm{AH}}\boldsymbol{W}_{\mathrm{AH}}\}+Q_{D_m} & 0 & 1\end{bmatrix}\succeq 0 \tag{4.24a}$$

$$\begin{bmatrix}\left(I_m^{C,\max}\right)^2\mathrm{Tr}\{\mathbf{M}_m^{\mathrm{AH}}\boldsymbol{W}_{\mathrm{AH}}^{C}\} & \mathrm{Tr}\{\mathbf{Y}_m^{\mathrm{AH}}\boldsymbol{W}_{\mathrm{AH}}^{C}\}+\lambda_{\mathrm{c}}P_{D_m} & \mathrm{Tr}\{\overline{\mathbf{Y}}_m^{\mathrm{AH}}\boldsymbol{W}_{\mathrm{AH}}^{C}\}+\lambda_{\mathrm{c}}Q_{D_m}\\ \mathrm{Tr}\{\mathbf{Y}_m^{\mathrm{AH}}\boldsymbol{W}_{\mathrm{AH}}^{C}\}+\lambda_{\mathrm{c}}P_{D_m} & 1 & 0\\ \mathrm{Tr}\{\overline{\mathbf{Y}}_m^{\mathrm{AH}}\boldsymbol{W}_{\mathrm{AH}}^{C}\}+\lambda_{\mathrm{c}}Q_{D_m} & 0 & 1\end{bmatrix}\succeq 0 \tag{4.24b}$$

$$\begin{bmatrix} \left|S_{lm}^{\max}\right|^2 & \mathrm{Tr}\{\mathbf{Y}_{lm}^{\mathrm{AH}}\boldsymbol{W}_{\mathrm{AH}}\} & \mathrm{Tr}\{\overline{\mathbf{Y}}_{lm}^{\mathrm{AH}}\boldsymbol{W}_{\mathrm{AH}}\} \\ \mathrm{Tr}\{\mathbf{Y}_{lm}^{\mathrm{AH}}\boldsymbol{W}_{\mathrm{AH}}\} & 1 & 0 \\ \mathrm{Tr}\{\overline{\mathbf{Y}}_{lm}^{\mathrm{AH}}\boldsymbol{W}_{\mathrm{AH}}\} & 0 & 1 \end{bmatrix} \succeq 0 \tag{4.25}$$

The constraints (4.9) and (4.21) with $\boldsymbol{W}_{\mathrm{AH}}^{\mathrm{C}}$ are similar to (4.24) and (4.25). The non-convex constraints $\boldsymbol{W}_{\mathrm{AH}} = \boldsymbol{X}_{\mathrm{AH}}\boldsymbol{X}_{\mathrm{AH}}^{\mathrm{T}}$, $\boldsymbol{W}_{\mathrm{AH}}^{\mathrm{C}} = \boldsymbol{X}_{\mathrm{AH}}^{\mathrm{C}}(\boldsymbol{X}_{\mathrm{AH}}^{\mathrm{C}})^{\mathrm{T}}$, $\boldsymbol{I}_m = \boldsymbol{T}_m\boldsymbol{T}_m^{\mathrm{T}}$, and $\boldsymbol{I}_m^{\mathrm{C}} = \boldsymbol{T}_m^{\mathrm{C}}(\boldsymbol{T}_m^{\mathrm{C}})^{\mathrm{T}}$ can be expressed by,

$$\boldsymbol{W}_{\mathrm{AH}} \succeq 0,\ \boldsymbol{I}_{\mathrm{m}} \succeq 0,\ \ \forall m \in \mathcal{N}_{\mathrm{AC}}^{\mathrm{Conv}} \tag{4.26}$$

$$\mathrm{rank}\left(\boldsymbol{W}_{\mathrm{AH}}\right) = 1,\ \mathrm{rank}\left(\boldsymbol{I}_{\mathrm{m}}\right) = 1 \tag{4.27}$$

$$\boldsymbol{W}_{\mathrm{AH}}^{\mathrm{C}} \succeq 0,\ \boldsymbol{I}_{\mathrm{m}}^{\mathrm{C}} \succeq 0,\ \forall m \in \mathcal{N}_{\mathrm{AC}}^{\mathrm{Conv}} \tag{4.28}$$

$$\mathrm{rank}\left(\boldsymbol{W}_{\mathrm{AH}}^{\mathrm{C}}\right) = 1,\ \mathrm{rank}\left(\boldsymbol{I}_{\mathrm{m}}^{\mathrm{C}}\right) = 1 \tag{4.29}$$

Due to the presence of rank-one constraints (4.27) and (4.29), the system voltage control program is non-convex. The semidefinite relaxation can be obtained by removing rank-one constraints (4.27) and (4.29), relaxing the non-linear non-convex voltage control program to a convex semidefinite program. It has been shown in [129] that rank-one constraints of matrix variables $\boldsymbol{W}$ and $\boldsymbol{I}$ can be removed without affecting the global optimum of the solution for most power networks. Thus, the program can be shown in a more compact form,

$$\mathrm{SVCP}\ \begin{cases} \text{Minimize} & \text{Total objective function (4.1)} \\ \text{Constraints} & \text{(4.2)-(4.11), (4.14)-(4.19), (4.22)-(4.26), (4.28)} \end{cases}$$

The voltage control program can be solved by using MATLAB with YALMIP as an interface and MOSEK as a solver [130]. By addressing the optimization problem, the optimization matrix variable $\boldsymbol{W}_{\mathrm{AH}}$ is optimized for each control period. According to optimal matrix variable $\boldsymbol{W}_{\mathrm{AH}}^{\mathrm{opt}}$, the optimal boundary variables for wind power generations of several OWFs $\mathrm{Tr}\{\mathbf{Y}_j^{\mathrm{AH}}\boldsymbol{W}_{\mathrm{AH}}^{\mathrm{opt}}\}$ and $\mathrm{Tr}\{\overline{\mathbf{Y}}_j^{\mathrm{AH}}\boldsymbol{W}_{\mathrm{AH}}^{\mathrm{opt}}\}, j \in \boldsymbol{\Omega}_{\mathrm{WF}}$ are generated. With the distributed calculation framework, the boundary optimization variables can be exchanged between grid controller and OWF controllers, and the central communication can be eliminated. The communication topology is shown in Fig. 4-4.

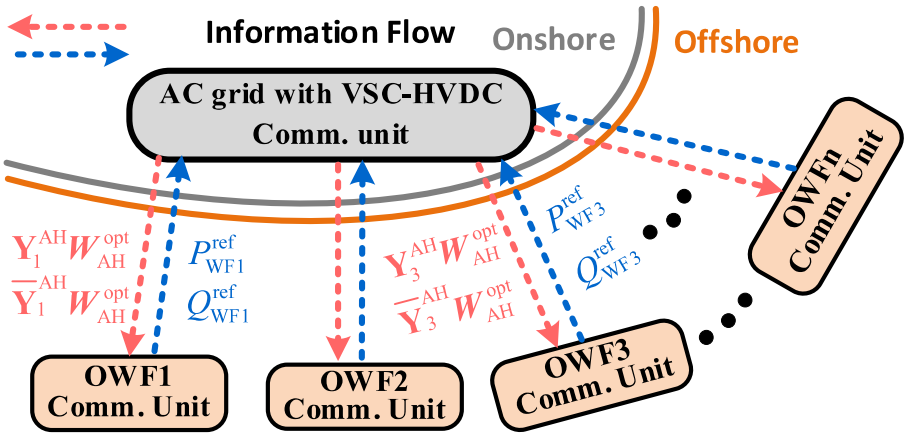

Fig. 4-4 The communication topology.

4.4 Offshore Wind Farm Formulation

The optimization problem is formulated to coordinately optimize active and reactive power outputs of all WTs and active power outputs of the distributed ESSs inside OWFs while considering the cut-in/cut-out wind conditions. The aim is to achieve optimal voltage regulation, minimize power losses and ESS fair utilization inside OWF collection systems. Meanwhile, the boundary variable values are required to exchange between two side controllers until the variables converge the common value under ADMM framework. The dynamic processes of WTs and ESSs are also taken into account by the OPC [142].

4.4.1 Modeling of Distributed ESSs

The distributed ESSs have an ability of releasing active power to support WF tracking TSO demand when several WTs are cut out. The topology of the DC-DC converter and the corresponding control structure is shown in Fig. 4-5.

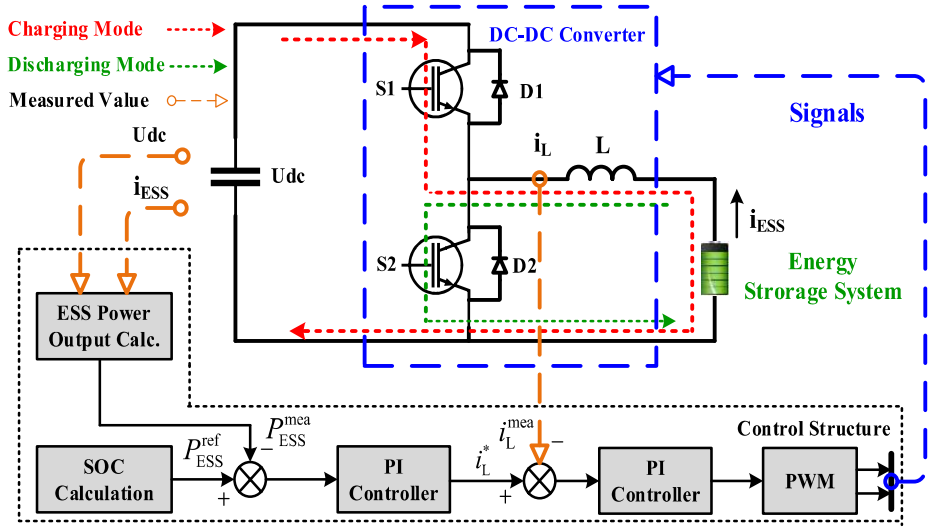

Fig. 4-5 The control structure and topology of DC-DC converter.

The buck or boost status of the DC-DC converter is decided by the two insulated gate bipolar transistors (IGBT) switches S1 and S2. In ESS charging mode, the converter operates in buck mode. The charging power flows from DC side to ESS with current i_{ESS}. In ESS discharging mode, the converter operates in boost mode. The direction of discharging power flow is from ESS to DC side with current i_{ESS}. The processes of charging and discharging are shown by red and green dash lines in Fig. 4-5, respectively. The energy stored in the ESS can be expressed by [142],

$$C_{\mathrm{ESS}} = C_{\mathrm{ESS},0} - \int P_{\mathrm{ESS}} dt \tag{4.30}$$

where $C_{\mathrm{ESS},0}$ and C_{ESS} are the initial and current energy stored in the ESS; P_{ESS} is the charge or discharge power of the ESS.

The double loop control structure of the DC-DC converter consists of two PI controllers. For the outer loop, the ESS power output reference $P_{\mathrm{ESS}}^{\mathrm{ref}}$ is compared with the product of measured value U_{dc} and i_{ESS}. The current reference of the inner loop can be calculated by the PI controller according to the error between $P_{\mathrm{ESS}}^{\mathrm{ref}}$ and $P_{\mathrm{ESS}}^{\mathrm{mea}}$. Generally, the dynamic process of the inner loop can be expressed as a first-order lag function. The duty cycle of the IGBT can be generated by the PI controller in the inner loop [142]. Thus, the DC-DC converter control loop can be simplified as Fig. 4-6.

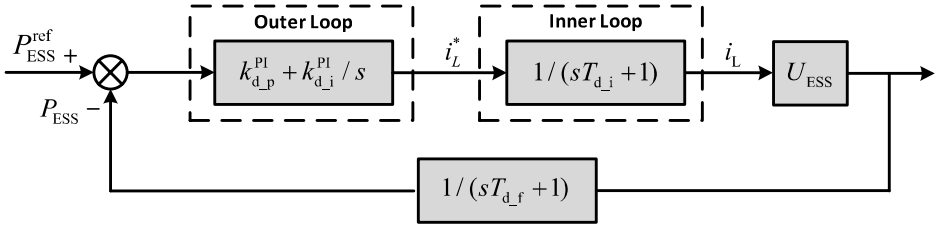

Fig. 4-6 The DC-DC converter control loop.

The incremental model of the DC-DC converter can be summarized as,

$$\Delta \dot{C}_{ESS} = -P_{ESS,0} - \Delta P_{ESS} \tag{4.31}$$

$$\Delta i_L = (k_{d\_p}^{PI} + \frac{k_{d\_i}^{PI}}{s}) \frac{1}{sT_{d\_i}+1} (\Delta P_{ESS}^{ref} - \Delta P_{ESS}) \tag{4.32}$$

$$\Delta P_{ESS} = \frac{1}{sT_{d\_f}+1} U_{ESS} \Delta i_L \tag{4.33}$$

$$\Delta P_{ESS}^{int} = \frac{\Delta P_{ESS}^{ref} - \Delta P_{ESS}}{s} \tag{4.34}$$

where $P_{ESS,0}$ is the initial value of ESS charge or discharge power; $k_{d\_p}^{PI}$ and $k_{d\_i}^{PI}$ are the proportional and integral gains of outer PI controller; T_{d_i} and T_{d_f} are the time constants of inner loop and active power filter in DC-DC converter, respectively.

According to (4.31)-(4.34), the state space model of ESSs can be presented as,

$$\Delta \dot{x}_E = \boldsymbol{A}_E \Delta x_E + \boldsymbol{B}_E \Delta u_E + \boldsymbol{E}_E \tag{4.35}$$

$$\Delta y_E = \boldsymbol{C}_E \Delta x_E \tag{4.36}$$

where

$$\Delta x_E = \left[\Delta C_{ESS}, \Delta P_{ESS}, \Delta P_{ESS}^{int}, \Delta i_L \right]^T$$

$$\Delta u_E = \Delta P_{ESS}^{ref}$$

$$\Delta y_{\mathrm{E}} = \Delta C_{\mathrm{ESS}}$$

$$\boldsymbol{A}_{\mathrm{E}} = \begin{bmatrix} 0 & -1 & 0 & 0 \\ 0 & -\dfrac{1}{\mathrm{T}_{\mathrm{d\_f}}} & 0 & \dfrac{U_{\mathrm{ESS}}}{\mathrm{T}_{\mathrm{d\_f}}} \\ 0 & -1 & 0 & 0 \\ 0 & -\dfrac{k_{\mathrm{d\_p}}^{\mathrm{PI}}}{\mathrm{T}_{\mathrm{d\_i}}} & \dfrac{k_{\mathrm{d\_i}}^{\mathrm{PI}}}{\mathrm{T}_{\mathrm{d\_i}}} & -\dfrac{1}{\mathrm{T}_{\mathrm{d\_i}}} \end{bmatrix}$$

$$\boldsymbol{B}_{\mathrm{E}} = \begin{bmatrix} 0 \\ 0 \\ 1 \\ \dfrac{k_{\mathrm{d\_p}}^{\mathrm{PI}}}{\mathrm{T}_{\mathrm{d\_i}}} \end{bmatrix}$$

$$\boldsymbol{E}_{\mathrm{E}} = \begin{bmatrix} -P_{\mathrm{ESS},0} \\ 0 \\ 0 \\ 0 \end{bmatrix}$$

$$\boldsymbol{C}_{\mathrm{E}} = \begin{bmatrix} 1 \\ 0 \\ 0 \\ 0 \end{bmatrix}^{\mathrm{T}}$$

4.4.2 Modeling of OWF Collection System

Suppose the current measurable values and references of active/reactive power for each WT are $P_{\mathrm{WT}}(t_0)$ / $Q_{\mathrm{WT}}(t_0)$ and $P_{\mathrm{WT}}^{\mathrm{ref}}$ / $Q_{\mathrm{WT}}^{\mathrm{ref}}$. Generally, the WT control system dynamic response is modeled as [94],

$$\Delta P_{\mathrm{WT}} = \frac{1}{1 + s\mathrm{T}_{\mathrm{WT}}^{\mathrm{P}}} \Delta P_{\mathrm{WT}}^{\mathrm{ref}} \tag{4.37}$$

$$\Delta Q_{\mathrm{WT}} = \frac{1}{1 + s\mathrm{T}_{\mathrm{WT}}^{\mathrm{Q}}} \Delta Q_{\mathrm{WT}}^{\mathrm{ref}} \tag{4.38}$$

where $T_{\mathrm{WT}}^{\mathrm{P}}$ and $T_{\mathrm{WT}}^{\mathrm{Q}}$ are the time constants [74].

Thus, the continuous state space of the OWF collection system incorporating N_{WT} WTs with N_{ESS} distributed ESSs is,

$$\Delta \dot{x}_{\mathrm{OWF}} = \boldsymbol{A}_{\mathrm{OWF}} \Delta x_{\mathrm{OWF}} + \boldsymbol{B}_{\mathrm{OWF}} \Delta u_{\mathrm{OWF}} + \boldsymbol{E}_{\mathrm{OWF}} \tag{4.39}$$

$$\Delta y_{\mathrm{OWF}} = \boldsymbol{C}_{\mathrm{OWF}} \Delta x_{\mathrm{OWF}} \tag{4.40}$$

where

$$\Delta x_{\mathrm{OWF}} = [\underbrace{\Delta C_{\mathrm{ESS}}^{\mathrm{sum}}, \Delta P_{\mathrm{ESS}}^{\mathrm{sum}}, \Delta P_{\mathrm{ESS,int}}^{\mathrm{sum}}, \Delta i_{\mathrm{L}}^{\mathrm{sum}}}_{\Delta x_{\mathrm{E}}^{\mathrm{sum}}}, \underbrace{\Delta P_{\mathrm{WT_1}}, \ldots, \Delta P_{\mathrm{WT_{N_{WT}}}}}_{\Delta x_{\mathrm{WT}}^{\mathrm{P}}},$$
$$\underbrace{\Delta Q_{\mathrm{WT_1}}, \Delta Q_{\mathrm{WT_2}}, \ldots, \Delta Q_{\mathrm{WT_{N_{WT}}}}}_{\Delta x_{\mathrm{WT}}^{\mathrm{Q}}}, \underbrace{\Delta x_{\mathrm{E}}^{1}, \Delta x_{\mathrm{E}}^{2}, \ldots, \Delta x_{\mathrm{E}}^{\mathrm{N_{ESS}}}}_{\Delta x_{\mathrm{E}}}]^{\mathrm{T}},$$

$$\Delta u_{\mathrm{OWF}} = [\underbrace{\Delta P_{\mathrm{ESS,sum}}^{\mathrm{ref}}}_{\Delta u_{\mathrm{ESS}}^{\mathrm{total}}}, \underbrace{\Delta P_{\mathrm{WT_1}}^{\mathrm{ref}}, \ldots, \Delta P_{\mathrm{WT_{N_{WT}}}}^{\mathrm{ref}}}_{\Delta u_{\mathrm{WT}}^{\mathrm{Pref}}}, \underbrace{\Delta Q_{\mathrm{WT_1}}^{\mathrm{ref}}, \ldots, \Delta Q_{\mathrm{WT_{N_{WT}}}}^{\mathrm{ref}}}_{\Delta u_{\mathrm{WT}}^{\mathrm{Qref}}},$$
$$\underbrace{\Delta P_{\mathrm{ESS_1}}^{\mathrm{ref}}, .., \Delta P_{\mathrm{ESS_{N_{ESS}}}}^{\mathrm{ref}}}_{\Delta u_{\mathrm{ESS}}}]^{\mathrm{T}},$$

$$\Delta y_{\mathrm{OWF}} = [\Delta C_{\mathrm{ESS}}^{\mathrm{sum}}, \Delta P_{\mathrm{WT_1}}, .., \Delta P_{\mathrm{WT_{N_{WT}}}}, \Delta Q_{\mathrm{WT_1}}, .., \Delta Q_{\mathrm{WT_{N_{WT}}}},$$
$$\Delta C_{\mathrm{ESS}}^{1}, .., \Delta C_{\mathrm{ESS}}^{\mathrm{N_{ESS}}}]^{\mathrm{T}},$$

$$\boldsymbol{A}_{\mathrm{OWF}} = \begin{bmatrix} \boldsymbol{A}_{\mathrm{E}} & & & & & \\ & \boldsymbol{A}_{\mathrm{WT}}^{\mathrm{P}} & & & & \\ & & \boldsymbol{A}_{\mathrm{WT}}^{\mathrm{Q}} & & & \\ & & & \boldsymbol{A}_{\mathrm{E_1}} & & \\ & & & & \ddots & \\ & & & & & \boldsymbol{A}_{\mathrm{E_{N_{WT}}}} \end{bmatrix},$$

$$\boldsymbol{B}_{\mathrm{OWF}}=\begin{bmatrix}\boldsymbol{B}_{\mathrm{E}} & & & & & \\ & \boldsymbol{B}_{\mathrm{WT}}^{\mathrm{P}} & & & & \\ & & \boldsymbol{B}_{\mathrm{WT}}^{\mathrm{Q}} & & & \\ & & & \boldsymbol{B}_{\mathrm{E}_1} & & \\ & & & & \ddots & \\ & & & & & \boldsymbol{B}_{\mathrm{E}_{N_{\mathrm{WT}}}}\end{bmatrix},$$

$$\boldsymbol{C}_{\mathrm{OWF}}=\begin{bmatrix}\boldsymbol{C}_{\mathrm{E}} & & & & & \\ & \boldsymbol{I}_{N_{\mathrm{WT}}}^{\mathrm{P}} & & & & \\ & & \boldsymbol{I}_{N_{\mathrm{WT}}}^{\mathrm{Q}} & & & \\ & & & \boldsymbol{C}_{\mathrm{E}_1} & & \\ & & & & \ddots & \\ & & & & & \boldsymbol{C}_{\mathrm{E}_{N_{\mathrm{WT}}}}\end{bmatrix},$$

$$\boldsymbol{E}_{\mathrm{OWF}}=[\boldsymbol{E}_{\mathrm{E}},\boldsymbol{O}_{N_{\mathrm{WT}}\times 1}^{\mathrm{P}},\boldsymbol{O}_{N_{\mathrm{WT}}\times 1}^{\mathrm{Q}},\boldsymbol{E}_{\mathrm{E}_1},..,\boldsymbol{E}_{\mathrm{E}_{N_{\mathrm{WT}}}}]^{\mathrm{T}},$$

with

$$\boldsymbol{A}_{\mathrm{WT}}^{\mathrm{P}}=\begin{bmatrix}-1/\mathrm{T}_{\mathrm{WT}_1}^{\mathrm{P}} & & \\ & \ddots & \\ & & -1/\mathrm{T}_{\mathrm{WT}_{N_{\mathrm{WT}}}}^{\mathrm{P}}\end{bmatrix},$$

$$\boldsymbol{A}_{\mathrm{WT}}^{\mathrm{Q}}=\begin{bmatrix}-1/\mathrm{T}_{\mathrm{WT}_1}^{\mathrm{Q}} & & \\ & \ddots & \\ & & -1/\mathrm{T}_{\mathrm{WT}_{N_{\mathrm{WT}}}}^{\mathrm{Q}}\end{bmatrix},$$

$$\boldsymbol{B}_{\mathrm{WT}}^{\mathrm{P}}=\begin{bmatrix}1/\mathrm{T}_{\mathrm{WT}_1}^{\mathrm{P}} & & \\ & \ddots & \\ & & 1/\mathrm{T}_{\mathrm{WT}_{N_{\mathrm{WT}}}}^{\mathrm{P}}\end{bmatrix},$$

$$\boldsymbol{B}_{\mathrm{WT}}^{\mathrm{Q}}=\begin{bmatrix} 1/\mathrm{T}_{\mathrm{WT_1}}^{\mathrm{Q}} & & \\ & \ddots & \\ & & 1/\mathrm{T}_{\mathrm{WT_{N_{WT}}}}^{\mathrm{Q}} \end{bmatrix}.$$

where $C_{\mathrm{ESS}}^{\mathrm{sum}}$ is sum of the stored energy in the ESSs; $P_{\mathrm{ESS}}^{\mathrm{sum}}$ and $i_{\mathrm{L}}^{\mathrm{sum}}$ are the sum of charge/discharge power/current in the ESSs; $P_{\mathrm{ESS,int}}^{\mathrm{sum}}$ is the sum of $P_{\mathrm{ESS}}^{\mathrm{int}}$; $P_{\mathrm{ESS,sum}}^{\mathrm{ref}}$ is the total active power output reference of the ESSs. Thus, the continuous model (4.39)-(4.40) can be transformed into the discrete model with the sampling time $\triangle \mathrm{T_P}$,

$$\Delta x_{\mathrm{OWF}}(k+1)=\boldsymbol{A}_{\mathrm{OWF}}^{\mathrm{d}}\Delta x_{\mathrm{OWF}}(k)+\boldsymbol{B}_{\mathrm{OWF}}^{\mathrm{d}}\Delta u_{\mathrm{OWF}}(k)+\boldsymbol{E}_{\mathrm{OWF}}^{\mathrm{d}} \tag{4.41}$$

$$\Delta y_{\mathrm{OWF}}(k)=\boldsymbol{C}_{\mathrm{OWF}}\Delta x_{\mathrm{OWF}}(k) \tag{4.42}$$

where $\boldsymbol{A}_{\mathrm{OWF}}^{\mathrm{d}}$, $\boldsymbol{B}_{\mathrm{OWF}}^{\mathrm{d}}$, and $\boldsymbol{E}_{\mathrm{OWF}}^{\mathrm{d}}$ are discrete state space matrixes [142].

4.4.3 Priority List-based Cutting-in Sequence for WTs

The WT can operate within the range of wind speed from 4 m/s (cut-in) to 25 m/s (cut-out). Due to the simplicity, easy of operation, and short computing time, priority list method is used to determine the sequence of cutting-in for WTs [156]. In this paper, the active power adjusting capacity, adjusting rate, and malfunction rate are combined to determine the cut-in sequence of WTs.

The active power adjusting capacity index K_{Pa}^{i} is,

$$K_{\mathrm{Pa}}^{i}=1.0+(P_{\mathrm{MPPT}}^{i}/P_{\mathrm{rated}}^{i}-p\%)m_{\mathrm{Pa}} \tag{4.43}$$

where P_{MPPT}^{i} and P_{rated}^{i} are the power output with MPPT mode and the rated power of i-th WT; $p\%$ is the base value associated with adjusting capacity; m_{Pa} is the correlation coefficient of power adjusting capacity offset [156].

Adjusting rate index K_{V}^{i} is,

$$K_{\mathrm{V}}^{i}=1.0+(P_{\mathrm{V}}^{i}/P_{\mathrm{rated}}^{i}-q\%)m_{\mathrm{V}} \tag{4.44}$$

where P_{V}^{i} is the average power changes respond to control period per unit time; $q\%$ is the base value associated with adjusting rate; m_{V} is the correlation coefficient of adjusting rate offset [156].

Malfunction rate index K_{Mf}^{i} is,

$$K_{\mathrm{Mf}}^{i} = 1.0 + (M_{\mathrm{f}}^{i} / M_{\mathrm{f\_given}}^{i}) m_{\mathrm{Mf}} \tag{4.45}$$

where M_{f}^{i} is the failure rate in a period of time; $M_{\mathrm{f\_given}}^{i}$ is the given maximum failure rate; m_{Mf} is the correlation coefficient of adjusting rate offset. Thus, the cut-in property index is,

$$K_{\text{Cut-in}}^{i} = w_{\mathrm{Pa}} K_{\mathrm{Pa}}^{i} + w_{\mathrm{V}} K_{\mathrm{V}}^{i} + w_{\mathrm{Mf}} K_{\mathrm{Mf}}^{i} \tag{4.46}$$

where w_{Pa}, w_{V}, and w_{Mf} are weighting factors. Obviously, the larger $K_{\mathrm{Cut-in}}^{i}$, the higher cut-in priority. The cut-in priority sequence of WTs can be calculated rapidly before each control action.

4.4.4 Formulation of OPC-based Voltage Control Program for OWF Collection Systems with Distributed ESSs

The coordinated control strategy owns two-stage control process inside OWF collection systems with distributed ESSs.

4.4.4.1 The Objectives in the First Stage

The first two objectives are voltage regulation for terminal voltages of MV/WT buses. The subzone voltage condition can be reflected by the corresponding MV bus. The third objective is to minimize the power losses inside OWF. The fourth objective is to maintain the power reference of each WT close to the PD-based reference. The last objective is to keep the sum of stored energy close to the medium level inside ESSs.

$$\begin{aligned} \min & \left\| \Delta \boldsymbol{V}_{\mathrm{MV}}^{\mathrm{pre}} \right\|_{\mathrm{W_{MV}}}^{2} + \left\| \Delta \boldsymbol{V}_{\mathrm{WT}}^{\mathrm{pre}} \right\|_{\mathrm{W_{WT}}}^{2} + \left\| \boldsymbol{P}_{\mathrm{Loss}}^{\mathrm{pre}} \right\|_{\mathrm{W_{LO}}}^{2} \\ & + \left\| \Delta \boldsymbol{P}_{\mathrm{WT}}^{\mathrm{pd}} \right\|_{\mathrm{W_{PD}}}^{2} + \left\| \Delta C_{\mathrm{ESS,sum}}^{\mathrm{pre}} \right\|_{\mathrm{W_{ESS}}}^{2} \end{aligned} \tag{4.47}$$

where $w_{MV}, w_{MT}, w_{LO}, w_{PD}$ and w_{ESS} are the weighting factors for five objectives; $\triangle \boldsymbol{V}_{MV}^{pre} = \left[\triangle V_{MV_1}^{pre}, .., \triangle V_{MV_{N_{MV}}}^{pre}\right]^T$; $\triangle \boldsymbol{V}_{WT}^{pre} = \left[\triangle V_{WT_1}^{pre}, .., \triangle V_{WT_{N_{WT}}}^{pre}\right]^T$; $\triangle \boldsymbol{P}_{WT}^{pd} = \left[\triangle P_{WT_1}^{pd}, .., \triangle P_{WT_{N_{WT}}}^{pd}\right]^T$. The above predictive values can be presented as,

$$\Delta V_{MV_i}^{pre}(k) = V_{MV_i}(t_0) + \frac{\partial V_{MV_i}}{\partial P_{WT}} \Delta P_{WT}(k) + \frac{\partial V_{MV_i}}{\partial Q_{WT}} \Delta Q_{WT}(k) - V_{MV_i}^{rated} \tag{4.48}$$

$$\Delta V_{WT_i}^{pre}(k) = V_{WT_i}(t_0) + \frac{\partial V_{WT_i}}{\partial P_{WT}} \Delta P_{WT}(k) + \frac{\partial V_{WT_i}}{\partial Q_{WT}} \Delta Q_{WT}(k) - V_{WT_i}^{rated} \tag{4.49}$$

$$P_{Loss}^{pre}(k) = P_{Loss}^{OWF}(t_0) + \frac{\partial P_{Loss}^{OWF}}{\partial P_{WT}} \Delta P_{WT}(k) + \frac{\partial P_{Loss}^{OWF}}{\partial Q_{WT}} \Delta Q_{WT}(k) \tag{4.50}$$

$$\Delta P_{WT_i}^{pd}(k) = P_{WT_i}(t_0) + \Delta P_{WT_i}(k) - (P_{WT_i}^{avi} / \sum_i P_{WT_i}^{avi}) P_{OWF}^{ref} \tag{4.51}$$

$$\Delta C_{ESS,sum}^{pre}(k) = C_{ESS}^{sum}(t_0) + \Delta C_{ESS}^{sum}(k) - C_{ESS,mid}^{sum} \tag{4.52}$$

where $V_{MV_i}(t_0)/V_{WT_i}(t_0)$ are the measurements of the i-th MV/WT terminal bus voltage at the current time t_0; $V_{MV_i}^{rated}/V_{MT_i}^{rated}$ are the rated values of the i-th MV/WT terminal bus voltages; $\partial P_{Loss}^{OWF}/\partial P_{WT}$ and $\partial P_{Loss}^{OWF}/\partial Q_{WT}$ are the partial derivatives of active power losses with respect to active/reactive power outputs of WT; $P_{WT_i}^{avi}$ is the available wind power of i-the WT; $C_{ESS,mid}^{sum}$ is the medium level of total stored energy in ESSs; $\partial V/\partial P$ and $\partial V/\partial Q$ are the voltage sensitivity coefficients with respect to the active and reactive power injections. The voltage sensitivity coefficients can be rapidly calculated based on SCADA measurements of terminal voltages and phase angles inside OWFs [74].

4.4.4.2 The Constraints in the First Stage

The total available charge/discharge power P_{ESS}^{sum} is limited by,

$$-P_{ESS,sum}^{charge,max} \le P_{ESS}^{sum} \le P_{ESS,sum}^{discharge,max} \tag{4.53}$$

where $P_{ESS,sum}^{charge,max}/P_{ESS,sum}^{discharge,max}$ are the sum of available charge/discharge power inside all ESSs. The energy management of ESSs can be referred to [142].

The available power of WT is constrained by,

$$0 \le P_{\mathrm{WT}_i}(k) \le P_{\mathrm{WT}_i}^{\mathrm{avi}} \tag{4.54}$$

$$\underline{Q}_{\mathrm{WT}_i}(k) \le Q_{\mathrm{WT}_i}(k) \le \overline{Q}_{\mathrm{WT}_i}(k) \tag{4.55}$$

4.4.4.3 The Objectives in the Second Stage

The objective is to achieve the fair utilization among all ESSs while tracking the total power reference from the first stage,

$$\min \sum_{i=1}^{|\mathcal{N}_{\mathrm{T}}|} \left\| C_{\mathrm{ESS}}^{i} - C_{\mathrm{ESS}}^{\mathrm{avr}} \right\|^2 \tag{4.56}$$

4.4.4.4 The Constraints in the Second Stage

The total charge/discharge power of all ESSs is required to track the reference $P_{\mathrm{ESS}}^{\mathrm{sum}}$ from the first stage,

$$\sum_{i=1}^{N_{\mathrm{ESS}}} P_{\mathrm{ESS}_i}^{\mathrm{ref}} = P_{\mathrm{ESS}}^{\mathrm{sum}} \tag{4.57}$$

Similarly, the available charge/discharge power of each ESS is limited by,

$$-P_{\mathrm{ESS}_i}^{\mathrm{charge,max}} \le P_{\mathrm{ESS}_i}^{\mathrm{ref}} \le P_{\mathrm{ESS}_i}^{\mathrm{discharge,max}} \tag{4.58}$$

The OPC-based voltage control program inside OWF with distributed ESSs can be reformulated as a QP program and solved by QP solver. The optimization problem of each OWF is addressed in a distributed manner, and the optimal power output reference for each OWF can be generated. With the distributed process framework, the boundary information of each OWF can be exchanged with grid controller.

4.5 ADMM-based Solution for DOVC Program

The whole system comprises AC gird with VSC-HVDC including OWFs equipped with distributed ESSs. Considering the OWF owns several hundreds of WTs with ESSs, the optimal voltage control (OVC) program is a large-scale optimization problem with large-scale constraints. To address heavy computational burden, an ADMM-based solution method is proposed to solve the OVC program. The ADMM decomposes the convex global optimization problem into sub-problems of

the grid and each OWF with ESSs, which are small-scale and efficiently solved. Since the OVC program is decoupled, the objectives (4.1), (4.47) and (4.56) can be distributed to the grid and each OWF controllers, and processed in parallel while guaranteeing global optimal solution. The OVC program can be reformulated as,

$$\begin{aligned}
&\min \sum_{i=1}^{|\mathcal{N}_{\mathrm{AH}}|} \mathrm{Tr}\{\mathbf{Y}_i^{\mathrm{AH}} \boldsymbol{W}_{\mathrm{AH}}\}_{\mathrm{w_{PL}}} - \left(\lambda_{\mathrm{c}} - \lambda_{\mathrm{rated}}\right)_{\mathrm{w_{VO}}} + \sum_{i=1}^{|\mathcal{N}_{\mathrm{AH}}|} \left(\mathrm{C} * Q_{\mathrm{C}_i}\right)_{\mathrm{W_{QS}}} \\
&+ \left\|\Delta \boldsymbol{V}_{\mathrm{MV}}^{\mathrm{pre}}\right\|_{\mathrm{w_{MV}}}^2 + \left\|\Delta \boldsymbol{V}_{\mathrm{WT}}^{\mathrm{pre}}\right\|_{\mathrm{w_{WT}}}^2 + \left\|\boldsymbol{P}_{\mathrm{Loss}}^{\mathrm{pre}}\right\|_{\mathrm{w_{LO}}}^2 \\
&+ \left\|\Delta \boldsymbol{P}_{\mathrm{WT}}^{\mathrm{pd}}\right\|_{\mathrm{w_{PD}}}^2 + \left\|C_{\mathrm{ESS}}^{\mathrm{sum}} - C_{\mathrm{ESS,mid}}^{\mathrm{sum}}\right\|_{\mathrm{w_{ESS}}}^2 \qquad (4.59) \\
&\text{subject to } (4.2)-(4.11),(4.14)-(4.19),(4.22)-(4.26),(4.28), \\
&\qquad (4.53)-(4.55),(4.57)-(4.58), \boldsymbol{x}-\boldsymbol{z}=0.
\end{aligned}$$

where $\boldsymbol{x}$ and $\boldsymbol{z}$ are the boundary optimization variable vectors associated with the active/reactive power outputs of each OWF. Thus, the argumented Lagrangian can be obtained,

$$\begin{aligned}
&\min \sum_{i=1}^{|\mathcal{N}_{\mathrm{AH}}|} \mathrm{Tr}\{\mathbf{Y}_i^{\mathrm{AH}} \boldsymbol{W}_{\mathrm{AH}}\}_{\mathrm{w_{PL}}} - \left(\lambda_{\mathrm{c}} - \lambda_{\mathrm{rated}}\right)_{\mathrm{w_{VO}}} + \sum_{i=1}^{|\mathcal{N}_{\mathrm{AH}}|} \left(\mathrm{C} * Q_{\mathrm{C}_i}\right)_{\mathrm{W_{QS}}} \\
&+ \left\|\Delta \boldsymbol{V}_{\mathrm{MV}}^{\mathrm{pre}}\right\|_{\mathrm{w_{MV}}}^2 + \left\|\Delta \boldsymbol{V}_{\mathrm{WT}}^{\mathrm{pre}}\right\|_{\mathrm{w_{WT}}}^2 + \left\|\boldsymbol{P}_{\mathrm{Loss}}^{\mathrm{pre}}\right\|_{\mathrm{w_{LO}}}^2 + \left\|\Delta \boldsymbol{P}_{\mathrm{WT}}^{\mathrm{pd}}\right\|_{\mathrm{w_{PD}}}^2 \qquad (4.60) \\
&+ \left\|C_{\mathrm{ESS}}^{\mathrm{sum}} - C_{\mathrm{ESS,mid}}^{\mathrm{sum}}\right\|_{\mathrm{w_{ESS}}}^2 + \boldsymbol{y}^{\mathrm{T}}(\boldsymbol{x}-\boldsymbol{z}) + \frac{\rho}{2}(\boldsymbol{x}-\boldsymbol{z})^2
\end{aligned}$$

where $\boldsymbol{y}$ is the dual variable vectors; ρ is the penalty for the boundary optimization variables in the system being different from the ones in OWFs.

The initial $\boldsymbol{z}$, $\boldsymbol{x}$, and $\boldsymbol{y}$ are set to zero. r is defined as the step of iteration. The OVC program can be solved iteratively including the following steps:

i) The gird controller solves the optimization problem of the AC grid with VSC-HVDC by using the augmented Lagrangian with the system constraints, and it updates system boundary variable vector $\boldsymbol{z}$,

$$\begin{aligned}\boldsymbol{z}(r+1)=\arg\min \sum_{i=1}^{|\mathcal{N}_{\mathrm{AH}}|}\mathrm{Tr}\{\mathbf{Y}_i^{\mathrm{AH}}\boldsymbol{W}_{\mathrm{AH}}\}_{\mathrm{w_{PL}}}-\left(\lambda_{\mathrm{c}}-\lambda_{\mathrm{rated}}\right)_{\mathrm{w_{VO}}}+\\ \sum_{i=1}^{|\mathcal{N}_{\mathrm{AH}}|}\left(\mathrm{C}*Q_{\mathrm{C}_i}\right)_{\mathrm{W_{QS}}}+\boldsymbol{y}^{\mathrm{T}}(r)(\boldsymbol{z}-\boldsymbol{x}(r))+\frac{\rho}{2}\left\|\boldsymbol{z}-\boldsymbol{x}(r)\right\|^2\end{aligned} \tag{4.61}$$

subject to (4.2)-(4.11), (4.14)-(4.19), (4.22)-(4.26), (4.28).

The augmented Lagrangian (4.61) is expressed as a quadratic of $\boldsymbol{z}$. It means that (4.61) includes the quadratic part of optimization matrix $\boldsymbol{W}_{\mathrm{AH}}$. However, the formula should be linear with $\boldsymbol{W}_{\mathrm{AH}}$ in SDP program. Thus, (4.61) can be replaced with (4.62)-(4.64) by using Schur complement with auxiliary variables α_i^{P} and α_i^{Q}, $i \in \boldsymbol{\Omega}_{\mathrm{WF}}$,

$$\begin{aligned}\boldsymbol{z}(r+1)=\arg\min \sum_{i=1}^{|\mathcal{N}_{\mathrm{AH}}|}\mathrm{Tr}\{\mathbf{Y}_i^{\mathrm{AH}}\boldsymbol{W}_{\mathrm{AH}}\}_{\mathrm{w_{PL}}}-\left(\lambda_{\mathrm{c}}-\lambda_{\mathrm{rated}}\right)_{\mathrm{w_{VO}}}\\ +\sum_{i=1}^{|\mathcal{N}_{\mathrm{AH}}|}\left(\mathrm{C}*Q_{\mathrm{C}_i}\right)_{\mathrm{W_{QS}}}+\sum_{i=1}^{|\Omega_{\mathrm{WF}}|}(\alpha_i^{\mathrm{P}}+\alpha_i^{\mathrm{Q}})]\end{aligned} \tag{4.62}$$

$$\begin{bmatrix}\boldsymbol{y}_i^{\mathrm{P}}\mathrm{Tr}\{\mathbf{Y}_i^{\mathrm{AH}}\boldsymbol{W}_{\mathrm{AH}}\}+a_i^{\mathrm{P}} & \sqrt{\rho/2}\mathrm{Tr}\{\mathbf{Y}_i^{\mathrm{AH}}\boldsymbol{W}_{\mathrm{AH}}\}+b_i^{\mathrm{P}}\\ \sqrt{\rho/2}\mathrm{Tr}\{\mathbf{Y}_i^{\mathrm{AH}}\boldsymbol{W}_{\mathrm{AH}}\}+b_i^{\mathrm{P}} & -1\end{bmatrix}\preceq 0,\ i\in\boldsymbol{\Omega}_{\mathrm{WF}}. \tag{4.63}$$

$$\begin{bmatrix}\boldsymbol{y}_i^{\mathrm{Q}}\mathrm{Tr}\{\overline{\mathbf{Y}}_i^{\mathrm{AH}}\boldsymbol{W}_{\mathrm{AH}}\}+a_i^{Q} & \sqrt{\rho/2}\mathrm{Tr}\{\overline{\mathbf{Y}}_i^{\mathrm{AH}}\boldsymbol{W}_{\mathrm{AH}}\}+b_i^{Q}\\ \sqrt{\rho/2}\mathrm{Tr}\{\overline{\mathbf{Y}}_i^{\mathrm{AH}}\boldsymbol{W}_{\mathrm{AH}}\}+b_i^{\mathrm{Q}} & -1\end{bmatrix}\preceq 0,\ i\in\boldsymbol{\Omega}_{\mathrm{WF}}. \tag{4.64}$$

subject to (4.2)-(4.11), (4.14)-(4.19), (4.22)-(4.26), (4.28).

with $a_i^{\mathrm{P}} := -\alpha_i^{\mathrm{P}} - \boldsymbol{y}_i^{\mathrm{P}}\boldsymbol{x}_i^{\mathrm{P}}(r)$,

$b_i^{\mathrm{P}} := -\sqrt{\rho/2}\boldsymbol{x}_i^{\mathrm{P}}(r)$,

$a_i^{\mathrm{Q}} := -\alpha_i^{\mathrm{Q}} - \boldsymbol{y}_i^{\mathrm{Q}}\boldsymbol{x}_i^{\mathrm{Q}}(r)$,

$b_i^{\mathrm{Q}} := -\sqrt{\rho/2}\boldsymbol{x}_i^{\mathrm{Q}}(r)$.

ii) After updating the system variables $\boldsymbol{z}$, each OWF controller solves its augmented Lagrangian with local constraints in parallel, and updates $\boldsymbol{x}$. For i-th OWF controller,

$$\begin{aligned}\boldsymbol{x}_i(r+1) = \arg\min & \left\|\Delta \boldsymbol{V}_{\mathrm{MV}}^{\mathrm{pre}}\right\|_{\mathrm{w_{MV}}}^2 + \left\|\Delta \boldsymbol{V}_{\mathrm{WT}}^{\mathrm{pre}}\right\|_{\mathrm{w_{WT}}}^2 + \left\|\boldsymbol{P}_{\mathrm{Loss}}^{\mathrm{pre}}\right\|_{\mathrm{w_{LO}}}^2 + \left\|\Delta \boldsymbol{P}_{\mathrm{WT}}^{\mathrm{pd}}\right\|_{\mathrm{w_{PD}}}^2 \\ & + \left\|C_{\mathrm{ESS}}^{\mathrm{sum}} - C_{\mathrm{ESS,mid}}^{\mathrm{sum}}\right\|_{\mathrm{w_{ESS}}}^2 + \boldsymbol{y}_i^{\mathrm{T}}(r)(\boldsymbol{z}_i(r+1) - \boldsymbol{x}_i) + \frac{\rho}{2}\left\|\boldsymbol{z}_i(r+1) - \boldsymbol{x}_i\right\|^2\end{aligned} \tag{4.65}$$

subject to (4.53)-(4.55), (4.57)-(4.58).

iii) Update the dual variables $\boldsymbol{y}$ in OWF controllers,

$$\boldsymbol{y}_i(r+1) = \boldsymbol{y}_i(r) + \rho[\boldsymbol{z}_i(r+1) - \boldsymbol{x}_i(r+1)] \tag{4.66}$$

With the large-scale OVC program decomposed, the central controller is eliminated without loss of global optimal control performance. For each controller, the task is only a small-scale constrained optimization problem, and the burden is not heavy.

4.6 Case Study

4.6.1 Test System

The control performance of the proposed DOVC scheme is tested on the modified IEEE 30-bus system with VSC-HVDC including two OWFs with 64×5 MW WTs equipped with distributed ESSs. The proposed DOVC scheme is carried out every 5 s. In order to examine the control performance of the DOVC scheme, two control methods are used to make comparisons: a) centralized optimal voltage control (COVC); b) conventional centralized PD method.

4.6.2 Control Performance

The total simulation time is 250s. During t = 0 ~ 80 s, the dispatch command is set as 106 MW. During t = 80 ~ 155 s, the command gradually increases to 140 MW. During t = 155 ~ 180 s, the command is set as 140 MW. After t = 180 s, the command gradually decreases to 106 MW. Each of two WTs shares the same wind condition in each OWF. The wind speeds of the first four representative groups for WT1 ~ WT8 in OWF1 are shown in Fig. 4-7.

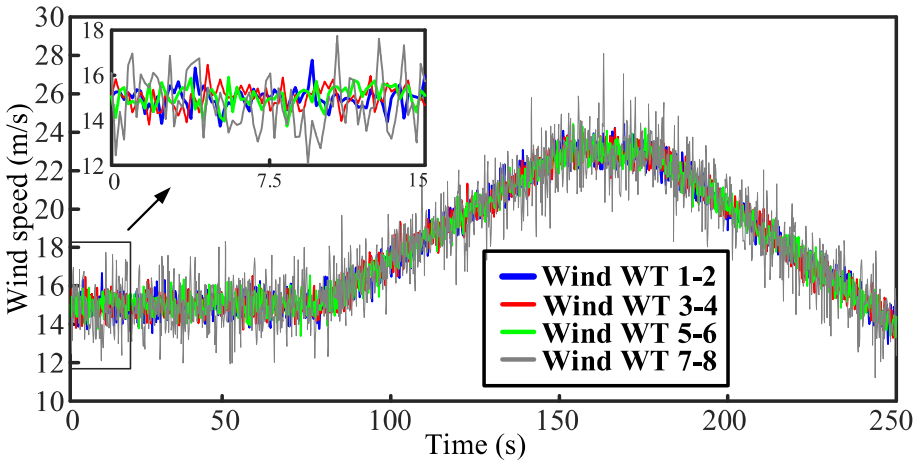

Fig. 4-7 The representative wind speeds of WT1-WT8 in OWF1.

The SOCs of representative ESSs in OWF1 with DOVC scheme is shown in Fig. 4-8. In order to keep the health and life of ESSs, the range of SOC constraints is set as [0.3, 0.7]. The initial SOC of ESS 4, 6, 8, 10, 12, 14, 20, 24, 26, 28, and 32 is set as 0.43, 0.48, 0.42, 0.54, 0.46, 0.47, 0.52, 0.53, 0.49, 0.51, and 0.49, respectively. The remaining initial SOCs of ESSs are all set as 0.5. Considering different initial SOCs, all SOCs of ESSs can converge to a common value (0.50) during t = 0 ~ 30 s. At t = 160 s and 175 s, the WT8 is cut out because wind speed of WT8 is beyond 25 m/s. At these two time points, the active power output of WT8 decreases to 0 MW, as Fig. 4-9 shown. Meanwhile, the corresponding ESS8 delivers power to maintain the terminal bus voltage stable.

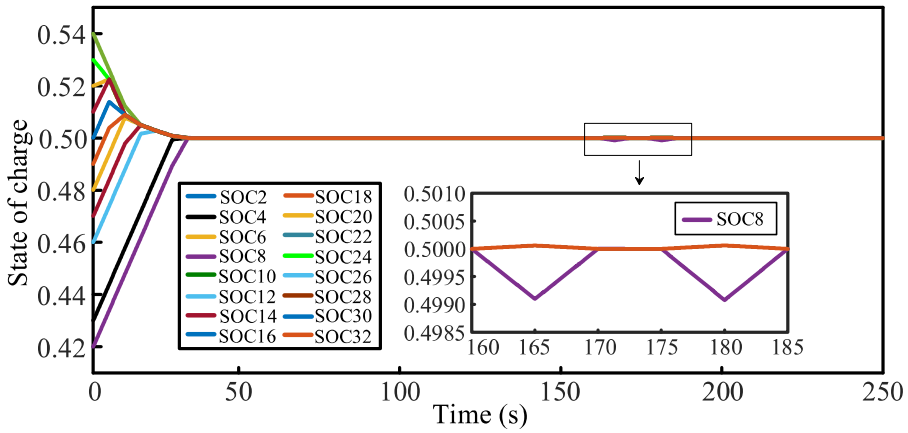

Fig. 4-8 The SOCs of representative ESSs.

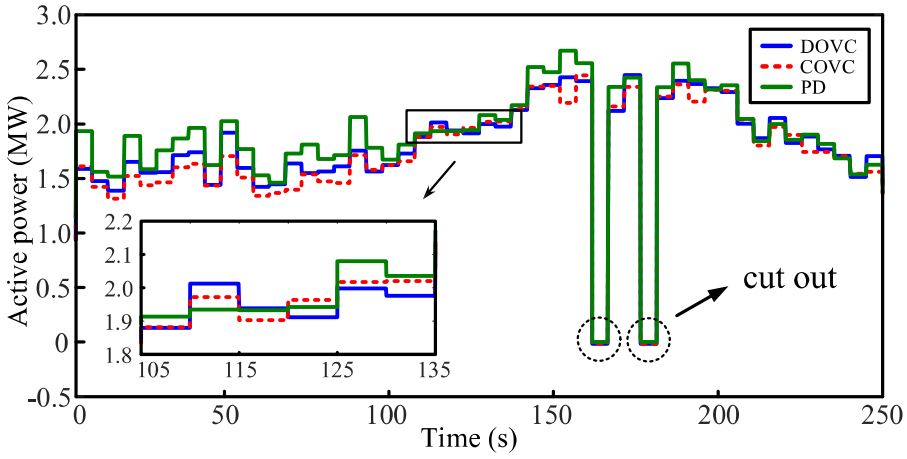

Fig. 4-9 WT8 output active power in OWF1.

The energy stored in ESS32 is shown in Fig. 4-10. The DOVC and COVC schemes can keep the energy stored in ESS32 close to the medium energy level. However, the energy stored in ESS32 with PD method fluctuates between 42.5 MJ and 48.5 MJ, of which the SOC is farther away from the medium level.

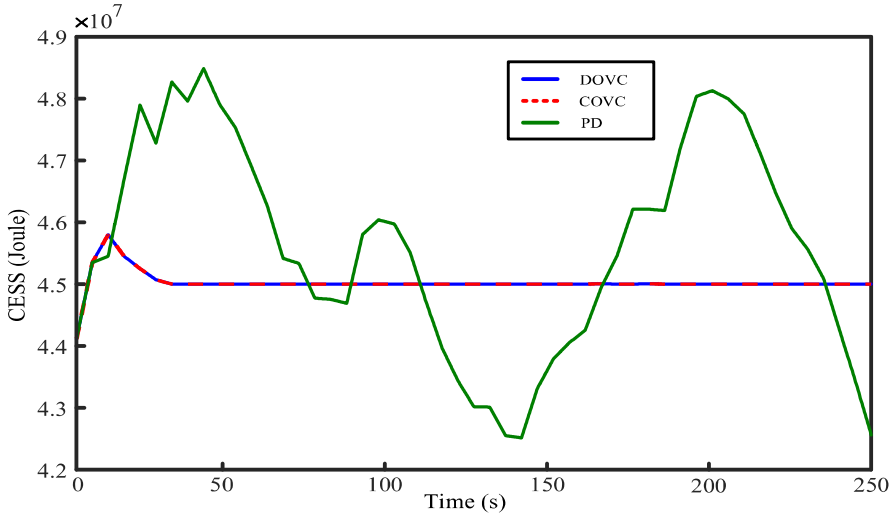

Fig. 4-10 The energy stored in ESS32 in OWF1.

The control performance of the boundary bus voltage between the grid and OWF1 is shown in Fig. 4-11. It can be seen that the proposed distributed DOVC scheme owns the similar control performance as the centralized COVC scheme. As Fig. 4-11 - Fig. 4-13 shown, from t = 0 ~ 155 s, the boundary bus voltage can be maintained at 1.008 p.u., and then gradually increases to 1.012 p.u. with the active and reactive power output of OWF1 increased by 30 MW and 9 Mvar, respectively. After t = 180 s, the boundary bus voltage decreases to 1.008 p.u., with the active and reactive power output decreased by 33 MW and 9.4 Mvar, respectively. Meanwhile, the PD control method can also keep the voltage within the feasible range. However, compared with the DOVC and COVC schemes, the boundary bus with PD control method experiences the much more voltage fluctuations.

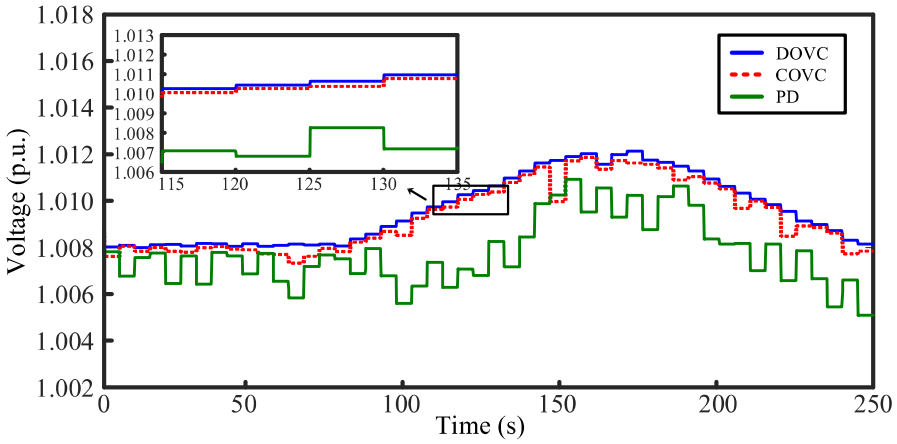

Fig. 4-11 The boundary bus voltage in OWF1.

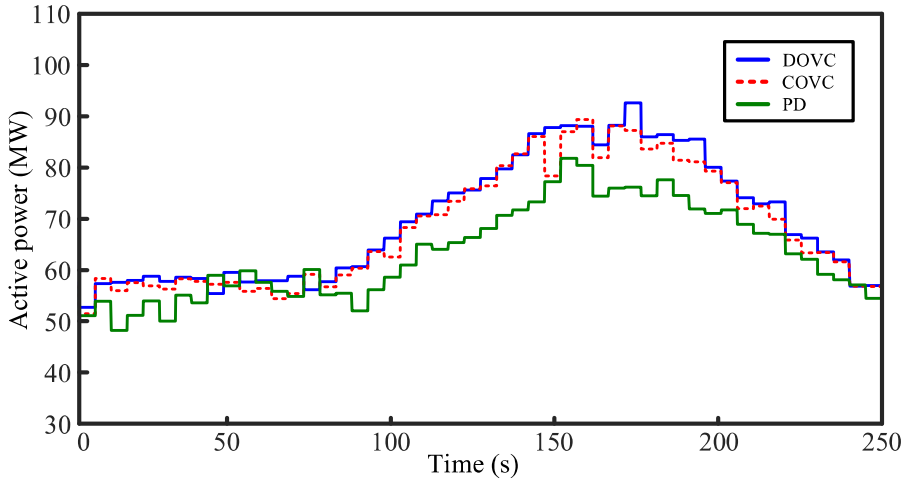

Fig. 4-12 The OWF1 active power output.

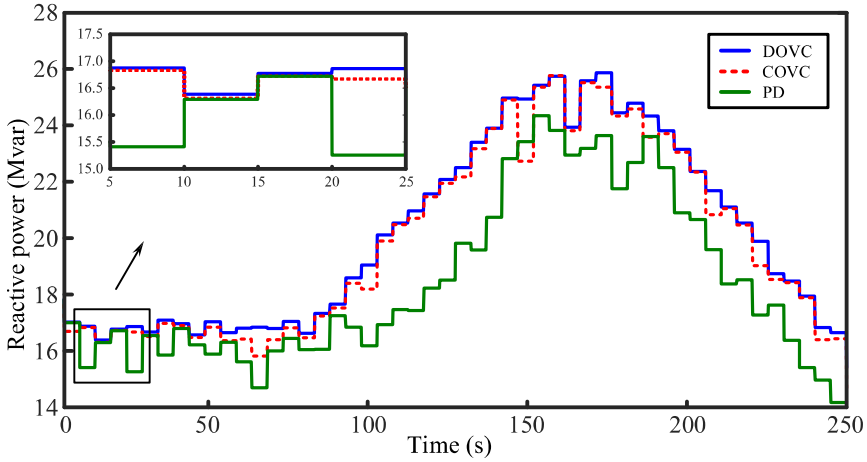

Fig. 4-13 The OWF1 reactive power output.

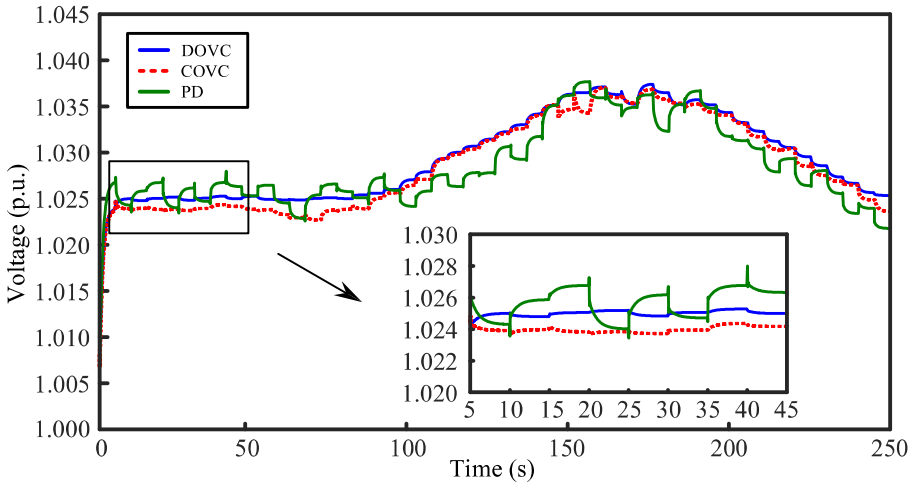

Fig. 4-14 The MV bus 1 voltage in OWF1.

The control performance of the MV bus 1 voltage is shown in Fig. 4-14 - Fig. 4-15. It can be seen that the DOVC scheme has the very similar voltage control performance with the COVC (less than 0.001 p.u.), and regulates the voltage with smaller fluctuations than PD control method. From t = 5 ~ 45 s, the maximal fluctuation of the MV bus voltage with the DOVC and COVC is 0.00035 p.u. Meanwhile, the maximal fluctuation with PD method is 0.0046 p.u. It means that the DOVC and COVC schemes own much smaller voltage fluctuation and better voltage regulation.

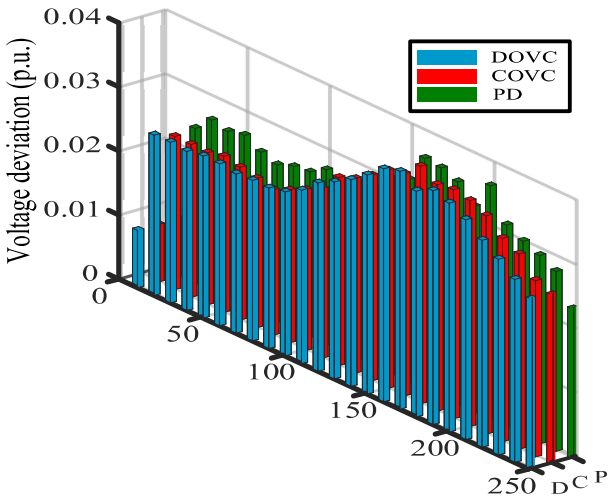

Fig. 4-15 Voltage control performance of MV bus 1 in OWF1.

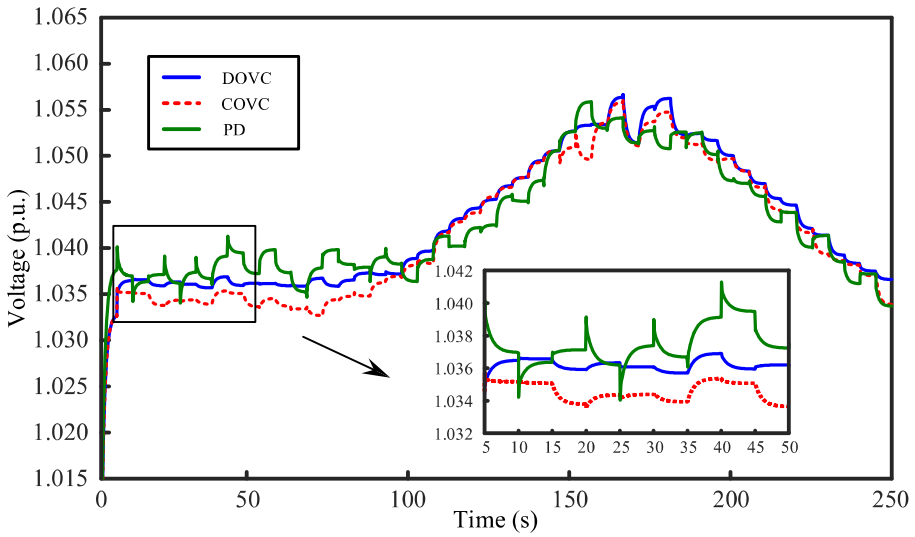

Fig. 4-16 WT32 terminal voltage in OWF1.

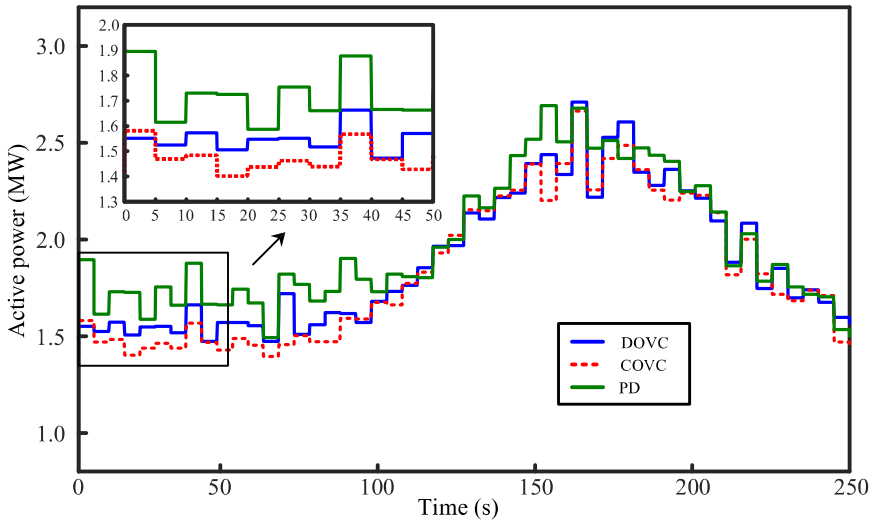

Fig. 4-17 WT32 output active power in OWF1.

Due to the furthest position along the feeder, WT32 is selected as the representative WT to show the voltage performance in Fig. 4-16 - Fig. 4-19. The maximal voltage difference between the DOVC and COVC is less than 0.003 p.u. As Fig. 4-16 - Fig.

4-18 shown, the WT32 terminal bus voltage with DOVC and COVC increases from 1.035 p.u. to 1.055 p.u., with the active and reactive power output of WT32 increased by 1.15 MW and 0.3 Mvar, respectively. For the whole control period, the WT32 terminal bus voltage can be regulated within the feasible range, and experiences the much smaller fluctuations and deviations than PD method. As Fig. 4-17 - Fig. 4-18 shown, the active and reactive power outputs of WT32 with the DOVC and COVC schemes are much smoother than PD method. Obviously, the proposed DOVC and COVC own better voltage control performance.

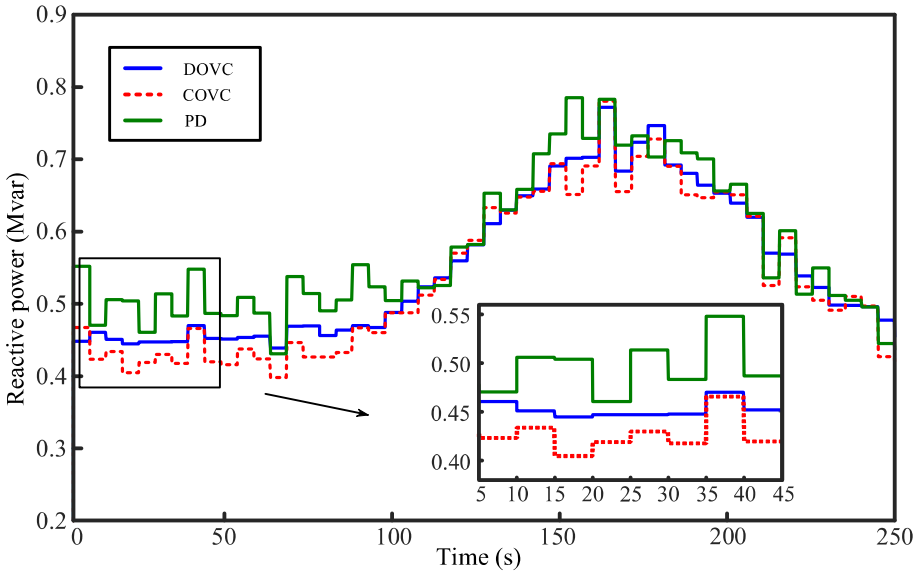

Fig. 4-18 WT32 output reactive power in OWF1.

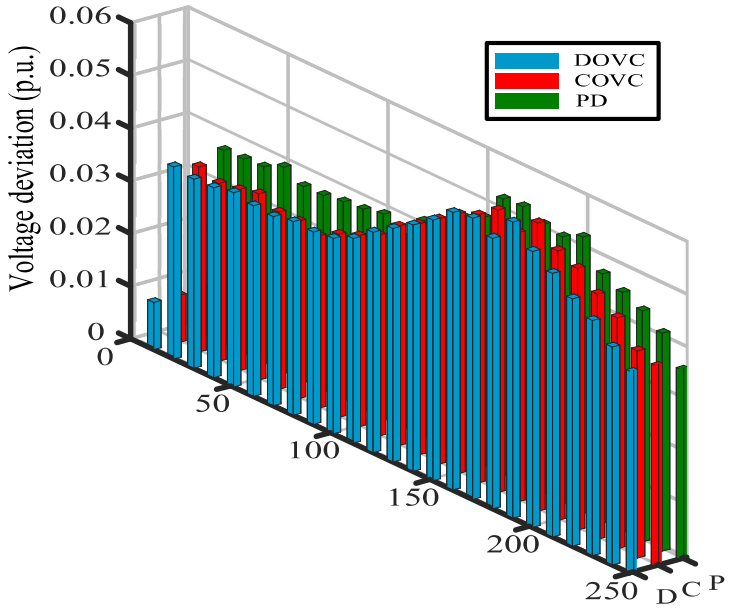

Fig. 4-19 Voltage control performance of WT32 terminal bus in OWF1.

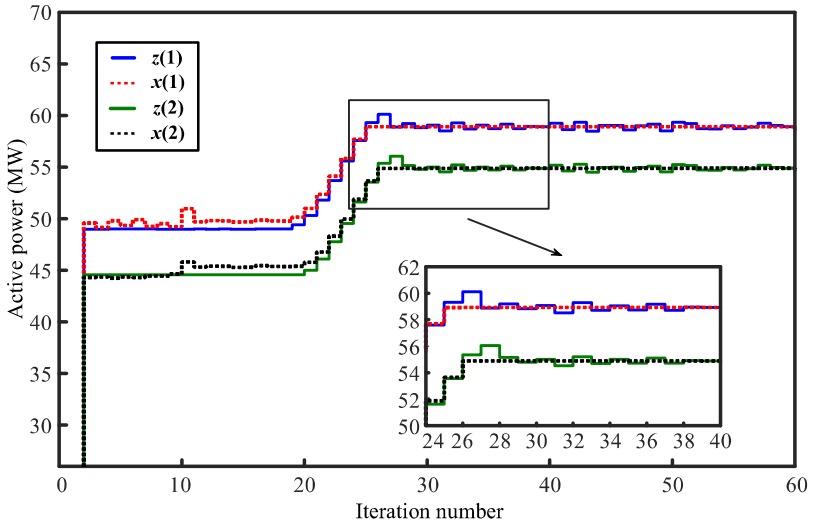

Fig. 4-20 Convergence performance of active power output in OWFs (t=25s).

The convergence performance of the DOVC scheme is shown in Fig. 4-20 - Fig. 4-21. The boundary variables of the active and reactive power outputs in grid-side

controller and OWF-side controllers are selected to illustrate the convergence performance. As Fig. 4-20 shown, the grid boundary variables ($z(1)$, $z(2)$) and OWF boundary variables ($x(1)$, $x(2)$) with the active power outputs converge to 58.92 MW, and 54.88 MW after 29 iterations. It can be seen that, after 27 iterations, the boundary variables with reactive power outputs $z(3)$/$z(4)$ and $x(3)$/$x(4)$ converge to the common values and keep steady in Fig. 4-21. The convergence performance is acceptable.

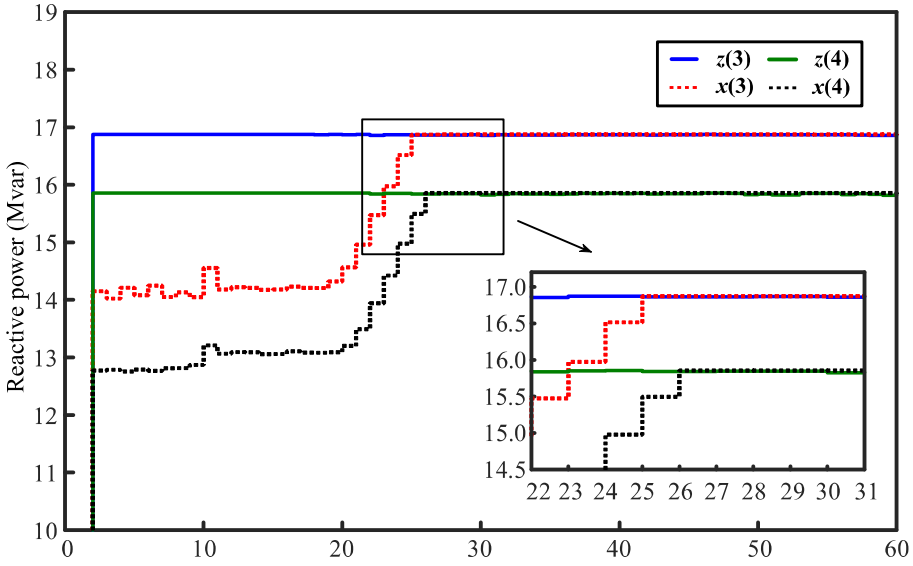

Fig. 4-21 Convergence performance of reactive power output in OWFs (t=25s).

4.7 Summary

This chapter proposes an ADMM-based DOVC strategy for AC grid with VSC-HVDC including the coupled large-scale OWFs equipped with distributed ESSs. The SDP relaxation technique with Schur complement is adopted to AC grid with VSC-HVDC optimization subproblem, which efficiently solves nonconvexity and nonlinearity issues of optimal power distribution. Meanwhile, the OPC-based voltage control method is developed to minimize voltage deviations of terminal buses, and achieve ESS fair utilization inside OWFs. In addition, an ADMM-based distributed framework is developed to decompose the strongly coupled gird and OWFs. The grid and OWF controllers can operate in parallel only with a limited amount of updated variables exchanged, implying better information privacy. Case

studies show the proposed DOVC scheme owns superiority on the voltage regulation for AC grid with VSC-HVDC including OWFs equipped with ESSs.

CHAPTER 5.

CONCLUSIONS AND FUTURE WORK

5.1 Conclusions

In this thesis, the distributed optimal voltage control strategy has been developed for AC grid with VSC-HVDC and several large-scale OWFs including distributed ESSs. The distributed voltage control strategy is proposed to minimize voltage fluctuations and deviations of the terminal buses, reduce the power losses, achieve the optimal active and reactive power distribution, and realize the fair ESS utilization without loss of global optimality in the whole system. In addition, the voltage control performance and information privacy have been both improved.

- The distributed active and reactive power control scheme based on ADMM for regional AC grid with WFs is proposed in this thesis. In the proposed control scheme, the non-convex OPF of TS is relaxed with a convex relaxation while the wind power collection system is modeled by branch flow model. The proposed scheme can achieve the global optimal active and reactive power control of the system in order to reduce power losses of TS while taking TSO demand into consideration, and meanwhile minimize the voltage fluctuations of the terminal buses as well as power losses of wind power collection systems. In addition, the large-scale power control problem can be decomposed by ADMM. With the limited boundary data exchanged, the sub-optimization problems can be solved in TS and WF controllers while guaranteeing global optimal solution. The computational burden is reduced and the central controller is eliminated. The simulation results show the proposed scheme can develop the coordination of TS and WFs to achieve optimal active and reactive power control of the whole system.

- The distributed optimal voltage control method for AC grid with DC connection including large-scale OWFs is developed in this thesis. In the proposed voltage control method, the MPC-based OPF program of AC grid with DC connection is formulated, and the semidefinite relaxation is used to relax OPF model. At the same time, the voltage control problem based on MPC inside OWF is generated while taking the dynamic process of WT into consideration. The proposed voltage control method is to achieve global optimal power distribution to minimize power losses of AC grid with DC connection while maintaining the terminal bus voltage within a feasible range and keeping a low level of power losses in OWF. The centralized scheme may face the drawbacks regarding the calculation burden, communication burden, privacy data disclosure, etc. Thus, this method is designed with a distributed manner, in which the calculation burden of each controller is reduced and the protection of privacy data is enhanced. The simulation results show the proposed distributed voltage control method achieves the same voltage control performance as centralized method, and owns better voltage control performance than other control methods such as PD, OPC, etc.

- The distributed optimal voltage control strategy in AC grid with VSC-HVDC including OWFs equipped with ESSs is developed in this thesis. The current voltage control strategy may not be as effective in the grid coupled with OWFs in the situations of the cut-out wind speed conditions. Thus, this proposed strategy takes the cut-out wind speed of WT, the dynamic behaviors of WT and ESS into consideration. The proposed strategy aims to achieve optimal power distribution in AC grid with VSC-HVDC, while coordinating the WTs and ESSs to achieve optimal voltage management inside OWFs. In addition, the fair utilization of distributed ESS is also achieved. In order to reduce the computation burden of each controller, ADMM is used to decompose the large-scale coupled voltage control problem. Then, the sub-problems can be solved in each controller in parallel guaranteeing the global optimality. The simulation results show the proposed voltage control strategy can achieve the optimal voltage regulation, and minimize power losses of AC grid with VSC-HVDC, while minimizing the voltage deviations and power losses, and achieving ESS fair utilization in OWFs.

5.2 Future Work

Some research questions have been raised by the current work of the Ph.D. thesis, and these questions should be addressed in future:

- The proposed voltage control strategy is achieved by the deterministic optimization and control methods in the thesis. The deterministic optimization method cannot take the uncertainty of the large-scale offshore wind power into consideration. Thus, the future work should investigate a distributed stochastic voltage control strategy to handle the uncertainty of the AC-DC grid with WFs by using the probabilistic data.

- In the thesis, the wind power collection system just includes wind turbines and energy storage systems. With the rapid development of wind farm, wind-hydrogen system has been attracted much attention. Thus, the future work may develop a voltage control method for the grid and large-scale wind-hydrogen system to take full advantage of the offshore wind power, and achieve the voltage management in the whole system.

- In the thesis, the distributed calculation scheme is proposed. However, the proposed strategy cannot consider the communication error and delay during the information exchange. In the future work, the communication error and delay can be modeled to improve control performance of the proposed strategy.

- In the thesis, the proposed voltage control strategy is with offline fashion. Due to the increasing number and size of offshore wind farm, it may be better to develop an online voltage control method in order to handle the voltage fluctuations of terminal buses in real time.

- In the thesis, local distribution of OWF is realized by an AC network. Considering the higher distance than 100 km, the VSC-HVDC is a more suitable solution to integrate large-scale OWFs, which are far away from onshore. This solution has the advantages such as flexible control ability, lower size of converters, etc. Therefore, it is necessary to develop a coordinated voltage control strategy to achieve the optimal voltage regulation in grid coupled with VSC-HVDC connected large-scale OWFs.

- In the thesis, each WF and grid owns a controller, which can solve the sub-optimization problem of each WF and grid. The sub-optimization problem is a small-scale one with constraints, and its computational burden is not heavy. In fact, with the rapid increase of WF projects, more and more WF clusters are connected to grid. Each WF cluster consists of large-scale WFs, and the optimization problem of each WF cluster is not small-scale. Therefore, it is necessary to develop a distributed calculation scheme to handle the large-scale WF clusters without loss of global optimality.

- In the thesis, the proposed voltage control method is effective in WF, which is with radial collection system. It is because there is a unique solution of sensitivity coefficient with respect to power injection in radial collection system. However, radial configuration is the simplest one in several configurations for a collection system. The existing configurations include radial, single return, single-sided ring, etc. Therefore, the voltage control method should be developed to adapt to different configurations of a collection system in WFs.

APPENDIX A

SOLUTION METHOD

The solution method based on ADMM in Chapter 2 is presented in Table A-1.

Table A-1 Steps of solution method for the whole system

1: Input the data of TSO active power command $P_{\mathrm{d}}^{\mathrm{TSO}}$, available wind power $P_{\mathrm{WFs}}^{\mathrm{avi}}$, system parameters $\boldsymbol{Y}_{\mathrm{TS}}$, measurements of WFs, etc.
2: Set step of iteration r=0, primal and dual tolerances θ.
3: Initialize optimization variables, and dual variables λ_k^P, λ_k^Q.
4: The TS controller solves augmented Lagrangian (2.40)-(2.42) with the constraints (2.19)-(2.24), (2.37). Then optimization variables of TS can be updated.
5: After updating TS optimization variables, WF controller can process augmented Lagrangian (2.43) with the constraints (2.27)-(2.30), (2.37). Then optimization variables of WF can be updated.
6: Update dual variables λ_k^P, λ_k^Q by (2.44)-(2.45).
7: Check convergence performance by tolerance θ. If the residuals are less than θ, then iteration process can be stopped. Otherwise, the iteration process will continue.

APPENDIX B

SIMULATION PARAMETERS

The parameters of the system in Chapter 2 are presented inTable B-1.

Table B-1 The parameters of system

Description	**Value**
WF1 rated capacity	160 MW
WF2 rated capacity	160 MW
WT rated capacity	5 MW
Number of WTs in WF1	32
Number of WTs in WF2	32
Number of feeders in WF1	4
Number of feeders in WF2	4
Time of carrying out	5 s

The parameters of the system in Chapter 3 are presented in Table B-2.

Table B-2 The parameters of the whole system

Description	**Value**
OWFa rated capacity	480 MW
OWFb rated capacity	480 MW
OWFc rated capacity	480 MW
WT rated capacity	5 MW
WT active power control time constant $T_{\mathrm{WT}}^{\mathrm{P}}$	1 s
WT reactive power control time constant $T_{\mathrm{WT}}^{\mathrm{Q}}$	1 s
Sample time ΔT_{p}	5 s
Control period T_{c}	5 s
A prediction horizon T_{p}	25 s
Horizon of OPF calculation	25 s

BIBLIOGRAPHY

[1] Energy Strategy 2050. The Danish Government, Copenhagen. [online]. Available: https://moodle.polymtl.ca/plugifile.php/413972/mod_page/content/70/Denmark_Energy%20Strategy%20for%202050_2011.pdf

[2] Global Energy Review 2021. International Energy Agency, Paris. [online]. Available: https://www.iea.org/reports/global-energy-review-2021/renewables.

[3] Global Wind Report 2021. Global Wind Energy Council, Brussels. [online]. Available: https://gwec.net/wp-content/uploads/2021/03/GWEC-Global-Wind-Report-2021.pdf

[4] Z. Li, Q. Guo, H. Sun, and J. Wang, "Coordinated transmission and distribution AC optimal power flow," *IEEE Trans. Smart Grid*, vol. 9, no. 2, pp. 1228-1240, Mar. 2018.

[5] J. Yang, W. Feng, X. Hou, Q. Xia, X. Zhang and P. Wang, "A distributed cooperative control algorithm for optimal power flow and voltage regulation in DC power system," *IEEE Trans. Power Delivery*, vol. 35, no. 2, pp. 892-903, Apr. 2020.

[6] J. Liu, X. Huang and Z. Li, "Multi-time scale optimal power flow strategy for medium-voltage DC power grid considering different operation modes," *J. Modern Power Syst. Clean Energy*, vol. 8, no. 1, pp. 46-54, Jan. 2020.

[7] Z. Yang, H. Zhong, Q. Xia, and C. Kang, "A novel network model for optimal power flow with reactive power and network losses," *Elect. Power Syst. Res.*, vol. 144, pp. 63-71, Mar. 2017.

[8] A. F. Attia, R. A. El Sehiemy, and H. M. Hasanien, "Optimal power flow solution in power systems using a novel sine-cosine algorithm," *Int. J. Electr. Power Energy Syst.*, vol. 99, pp. 331-343, Jun. 2018.

[9] U. Khaled, A. M. Eltamaly, and A. Beroual, "Optimal power flow using particle swarm optimization of renewable hybrid distributed generation," *Energies*, vol. 10, no. 7, Jul. 2017.

[10] G. Chen, H. Zhang, H. Hui, N. Dai and Y. Song, "Scheduling thermostatically controlled loads to provide regulation capacity based on a learning-based optimal power flow model," *IEEE Trans. Sustain. Energy*, DOI:

10.1109/TSTE.2021.3100846.
[11] D. Gayme and U. Topcu, "Optimal power flow with large-scale storage integration," *IEEE Trans. Power Syst.*, vol. 28, no. 2, pp. 709-717, May 2013.
[12] D. Kourounis, A. Fuchs and O. Schenk, "Toward the next generation of multiperiod optimal power flow solvers," *IEEE Trans. Power Syst.*, vol. 33, no. 4, pp. 4005-4014, Jul. 2018.
[13] M. Lubin, Y. Dvorkin and L. Roald, "Chance constraints for improving the security of AC optimal power flow," *IEEE Trans. Power Syst.*, vol. 34, no. 3, pp. 1908-1917, May. 2019.
[14] Panda A, Tripathy M, Barisal A K, Prakash T, "A modified bacteria foraging based optimal power flow framework for hydro-thermal-wind generation system in the presence of STATCOM," *Energy*, vol. 124, pp. 720-740, Apr. 2017.
[15] T. Mühlpfordt, T. Faulwasser, and V. Hagenmeyer, "A generalized framework for chance-constrained optimal power flow," *Sustain. Energy, Grids Netw.*, vol. 16, pp. 231-242, Dec. 2018.
[16] T. Mühlpfordt, L. Roald, V. Hagenmeyer, T. Faulwasser and S. Misra, "Chance-constrained AC optimal power flow: a polynomial chaos approach," *IEEE Trans. Power Syst.*, vol. 34, no. 6, pp. 4806-4816, Nov. 2019.
[17] A. Mešanović, U. Münz and C. Ebenbauer, "Robust optimal power flow for mixed AC/DC transmission systems with volatile renewables," *IEEE Trans. Power Syst.*, vol. 33, no. 5, pp. 5171-5182, Sept. 2018.
[18] E. Dall'Anese, K. Baker and T. Summers, "Chance-constrained AC optimal power flow for distribution systems with renewables," *IEEE Trans. Power Syst.*, vol. 32, no. 5, pp. 3427-3438, Sept. 2017.
[19] Y. Guo, K. Baker, E. Dall'Anese, Z. Hu and T. H. Summers, "Data-based distributionally robust stochastic optimal power flow—Part I: methodologies," *IEEE Trans. Power Syst.*, vol. 34, no. 2, pp. 1483-1492, Mar. 2019.
[20] Y. Guo, K. Baker, E. Dall'Anese, Z. Hu and T. H. Summers, "Data-based distributionally robust stochastic optimal power flow—Part II: case studies," *IEEE Trans. Power Syst.*, vol. 34, no. 2, pp. 1493-1503, Mar. 2019.
[21] P. P. Biswas, P. N. Suganthan, and G. A. J. Amaratunga, "Optimal power flow solutions incorporating stochastic wind and solar power," *Energy Convers. Manage.*, vol. 148, pp. 1194-1207, Sep. 2017.
[22] R. Mieth and Y. Dvorkin, "Data-driven distributionally robust optimal power flow for distribution systems," *IEEE Control Syst. Lett.*, vol. 2, no. 3, pp. 363-368, Jul. 2018.
[23] R. Dobbe, O. Sondermeijer, D. Fridovich-Keil, D. Arnold, D. Callaway and C. Tomlin, "Toward distributed energy services: decentralizing optimal power flow with machine learning," *IEEE Trans. Smart Grid*, vol. 11, no. 2, pp. 1296-1306, Mar. 2020.
[24] K. Turitsyn, P. Sulc, S. Backhaus, and M. Chertkov, "Options for control

of reactive power by distributed photovoltaic generators," *Proc. IEEE*, vol. 99, no. 6, pp. 1063-1073, Jun. 2011.

[25] A. Keane, L. F. Ochoa, E. Vittal, C. J. Dent, and G. P. Harrison, "Enhanced utilization of voltage control resources with distributed generation," *IEEE Trans. Power Syst.*, vol. 26, no. 1, pp. 252-260, Feb. 2011.

[26] P. M. S. Carvalho, P. F. Correia, and L. A. F. M. Ferreira, "Distributed reactive power generation control for voltage rise mitigation in distribution networks," *IEEE Trans. Power Syst*., vol. 23, no. 2, pp. 766-772, May. 2008.

[27] N. H. Awad, M. Z. Ali, R. Mallipeddi, and P. N. Suganthan, "An efficient differential evolution algorithm for stochastic OPF based active-reactive power dispatch problem considering renewable generators," *Appl. Soft Comput*., vol. 76, pp. 445-458, Mar. 2019.

[28] A.-A. A. Mohamed, Y. S. Mohamed, A. A. M. El-Gaafary, and A. M. Hemeida, "Optimal power flow using moth swarm algorithm," *Electr. Power Syst. Res.*, vol. 142, pp. 190-206, Jan. 2017.

[29] E. Naderi, H. Narimani, M. Fathi, M.R. Narimani, "A novel fuzzy adaptive configuration of particle swarm optimization to solve large-scale optimal reactive power dispatch," *Appl. Soft Comput*., vol. 53, pp. 441-456, Apr. 2017.

[30] K. Pandiarajan, C.K. Babulal, "Fuzzy harmony search algorithm based optimal power flow for power system security enhancement," *Int. J. Electr. Power Energy Syst.*, vol. 78, pp. 72-79, 2016.

[31] A. H. Khazali and M. Kalantar, "Optimal reactive power dispatch based on harmony search algorithm," *Int. J. Elect. Power Energy Syst*., vol. 33, no. 3, pp. 684-692, Mar. 2011.

[32] B. Mandal and P. K. Roy, "Optimal reactive power dispatch using quasioppositional teaching learning based optimization," *Int. J. Electr. Power Energy Syst.*, vol. 53, pp. 123-134, Dec. 2013.

[33] M. Mehdinejad, B. Mohammadi-Ivatloo, R. Dadashzadeh-Bonab, and K. Zare, "Solution of optimal reactive power dispatch of power systems using hybrid particle swarm optimization and imperialist competitive algorithms," *Int. J. Electr. Power Energy Syst.*, vol. 83, pp. 104-116, Dec. 2016.

[34] M. Khanabadi, Y. Fu and C. Liu, "Decentralized transmission line switching for congestion management of interconnected power systems," *IEEE Trans. Power Syst.*, vol. 33, no. 6, pp. 5902-5912, Nov. 2018.

[35] X. Li and Q. Xia, "Stochastic optimal power flow with network reconfiguration: congestion management and facilitating grid integration of renewables," *IEEE PES T&D Conference & Exposition*, Chicago, IL, USA, Apr. 2020.

[36] Y. Xu, H. Sun, H. Liu, and Q. Fu, "Distributed solution to DC power flow with congestion management," *Int. J. Elect. Power. Energy Syst*., vol. 98, pp. 73-82, Feb. 2018.

[37] R. Peesapati, V. K. Yadav and N. Kumar, "Transmission congestion management considering multiple and optimal capacity DGs," *J. Modern Power Syst. Clean Energy*, vol. 5, no. 5, pp. 713-724, Sep. 2017.

[38] M. Pourakbari-Kasmaei, J.R.S. Mantovani, M. Rashidinejad, M.R. Habibi, J. Contreras, "Carbon footprint allocation among consumers and transmission losses," *2017 IEEE Int. Conf. Environ. Electr. Eng.*, Milan, Italy, Jul. 2017.

[39] L. Yang, J. Luo, Y. Xu, Z. Zhang and Z. Dong, "A distributed dual consensus ADMM based on partition for DC-DOPF with carbon emission trading," *IEEE Trans. Ind. Informat.*, vol. 16, no. 3, pp. 1858-1872, Mar. 2020.

[40] X. Han, J. Qiu, L. Sun, W. Shen, M. Yuan, D. Yuan, "Low-carbon energy policy analysis based on power energy system modeling," *Energy Convers. Econ.* Oct. 2020. https://doi.org/10.1049/enc2.12005

[41] S. Ida Evangeline and P. Rathika, "A real-time multi-objective optimization framework for wind farm integrated power systems," *J. Power Sources,* vol. 498, Jun. 2021.

[42] J. B. Hmida, T. Chambers, and J. Lee, "Solving constrained optimal power flow with renewables using hybrid modified imperialist competitive algorithm and sequential quadratic programming," *Electr. Power Syst. Res.,* vol. 177, Dec. 2019.

[43] X. Wang, Y. Gong and C. Jiang, "Regional carbon emission management based on probabilistic power flow with correlated stochastic variables," *IEEE Trans. Power Syst.*, vol. 30, no. 2, pp. 1094-1103, Mar. 2015.

[44] S. Galvani and S. R.Marjani, "Optimal power flow considering predictability of power systems," *Electr. Power Syst. Res.,* vol. 171, pp. 66-73, 2019.

[45] A. K. Pathak, M. P. Sharma, and M. Bundele, "A critmodernical review of voltage and reactive power management of wind farms," *Renew. Sustain. Energy Rev.*, vol. 51, pp. 460-471, Nov. 2015.

[46] C. Han *et al*., "STATCOM impact study on the integration of a large wind farm into a weak loop power system," *IEEE Trans. Energy Convers.*, vol. 23, no. 1, pp. 226-233, Mar. 2008.

[47] W. Qiao, G. K. Venayagamoorthy, and R. G. Harley, "Real-time implementation of a STATCOM on a wind farm equipped with doubly fed induction generators," *IEEE Trans. Ind. Appl.*, vol. 45, no. 1, pp. 98-107, Jan. 2009.

[48] T. M. Masaud and P. Sen, "Study of the implementation of statcom on DFIG-based wind farm connected to a power system," *Proc. IEEE PES ISGT*, pp. 1-7, Apr. 2012.

[49] S. M. Muyeen, M. H. Ali, R. Takahashi, T. Murata, and J. Tamura, "Wind generator output power smoothing and terminal voltage regulation by using STATCOM/ESS," *Proc. IEEE PowerTech. 2007 Conf*., Lausanne, Switzerland, pp. 1232-1237, Jul. 2007.

[50] M. N. Slepchenkov, K. M. Smedley and J. Wen, "Hexagram-converter-

based STATCOM for voltage support in fixed-speed wind turbine generation systems," *IEEE Trans. Ind. Electron.*, vol. 58, no. 4, pp. 1120-1131, Apr. 2011.

[51] N. A. Lahacani, D. Aouzellag, and B. Mendil, "Static compensator for maintaining voltage stability of wind farm integration to a distribution network," *Renew. Energy*, vol. 35, no. 11, pp. 2476-2482, Nov. 2010.

[52] C. Wessels, N. Hoffmann, M. Molinas and F. W. Fuchs, "StatCom control at wind farms with fixed-speed induction generators under asymmetrical grid faults," *IEEE Trans. Ind. Electron.*, vol. 60, no. 7, pp. 2864-2873, Jul. 2013.

[53] Y. Zhang, Y. Wang, D. Zhang, X. Chen and C. Gong, "Broadband impedance shaping control scheme of MMC-based STATCOM for improving the stability of the wind farm," *IEEE Trans. Power Electron.*, vol. 36, no. 9, pp. 10278-10292, Sept. 2021.

[54] A. A. Tamimi, A. Pahwa and S. Starrett, "Effective wind farm sizing method for weak power systems using critical modes of voltage instability," *IEEE Trans. Power Syst.*, vol. 27, no. 3, pp. 1610-1617, Aug. 2012.

[55] H. Rezaie and M. H. Kazemi-Rahbar, "Enhancing voltage stability and LVRT capability of a wind-integrated power system using a fuzzy-based SVC," *Int. J., Eng. Sci. Technol.*, vol. 22, no. 3, pp. 827-839, Jun. 2019.

[56] H. Samet, S. Ketabipoor, M. Afrasiabi, S. Afrasiabi, and M. Mohammadi, "Deep learning forecaster based controller for SVC: wind farm flicker mitigation," *IEEE Trans. Ind. Informat.*, pp. 1-1, Sep. 2020.

[57] S. M. Muyeen, S. Shishido, M. H. Ali, R. Takahashi, T. Murata, and J. Tamura, "Application of energy capacitor system (ECS) to wind power generation," *Wind Energy*, vol. 11, no. 4, pp. 335-350, Dec. 2007.

[58] H. V. Pham, J. L. Rueda and I. Erlich, "Online optimal control of reactive sources in wind power plants," *IEEE Trans. Sustain. Energy*, vol. 5, no. 2, pp. 608-616, Apr. 2014.

[59] V. S. Pappala, M. Wilch, S. N. Singh, and I. Erlich, "Reactive power management in offshore wind farms by adaptive PSO," in *Proc. 14th Int. Conf. Intelligent System Appl. Power Syst.*, Kaohsiung, Taiwan, 2007, pp. 1-8.

[60] L. Zhang, B. Liu, H. Shen, and X. Qin, "Voltage control strategy with stepped controllable shunt reactor in large-scale wind power system," in *Proc. IEEE Power Engineering and Automation Conf.*, Wuhan, China, 2011, pp. 78-81.

[61] H. T. Nguyen, G. Yang, A. H. Nielsen and P. H. Jensen, "Combination of synchronous condenser and synthetic inertia for frequency stability enhancement in low-inertia systems," *IEEE Trans. Sustain. Energy*, vol. 10, no. 3, pp. 997-1005, Jul. 2019.

[62] H. T. Nguyen, G. Yang, A. H. Nielsen and P. H. Jensen, "Hardware- and software-in-the-loop simulation for parameterizing the model and control

of synchronous condensers," *IEEE Trans. Sustain. Energy*, vol. 10, no. 3, pp. 1593-1602, Jul. 2019.

[63] J. Jia, G. Yang and A. H. Nielsen, "A review on grid-connected converter control for short-circuit power provision under grid unbalanced faults," *IEEE Trans. Power Del.*, vol. 33, no. 2, pp. 649-661, Apr. 2018.

[64] G. Yang, "Review of European offshore wind development practice and future technological outlook," in Chinese, *Autom. Electr. Power Syst.*, accepted, in press.

[65] J. Jia, G. Yang, A. H. Nielsen, and P. R. Hansen, "Impact of VSC control strategies and incorporation of synchronous condensers on distance protection under unbalanced faults," *IEEE Trans. Ind. Electron.*, vol. 66, no. 2, pp. 1108-1118, Feb. 2019.

[66] J. Jia, G. Yang, A. H. Nielsen, and V. Gevorgian, "Investigation on the combined effect of VSC-based sources and synchronous condensers under grid unbalanced faults," *IEEE Trans. Power Del.*, vol. 34, no. 5, pp. 1898-1908, Oct. 2019.

[67] H. T. Nguyen, C. Guerriero, G. Yang, C. J. Boltonand, T. Rahman, and P. H. Jensen, "Talega syncon - power grid support for renewable-based systems," in *Proc. IEEE Southeastcon*, Huntsville, AL, USA, 2019.

[68] H. T. Nguyen, G. Yang, A. H. Nielsen, P. H. Jensen, and B. Pal, "Applying synchronous condenser for damping provision in converter-dominated power system," *J. Modern Power Syst. Clean Energy*, vol. 9, pp. 639-647, Sept. 2020.

[69] G. Xu, L. Xu, D. J. Morrow and D. Chen, "Coordinated DC voltage control of wind turbine with embedded energy storage system," *IEEE Trans. Energy Convers.*, vol. 27, no. 4, pp. 1036-1045, Dec. 2012.

[70] K. Li, H. Xu, Q. Ma, and J. Zhao, "Hierarchy control of power quality for wind-battery energy storage system," *IET Power Electron*., vol. 7, no. 8, pp. 2123-2132, Aug. 2014.

[71] G. O. Suvire and P. E. Mercado, "DSTATCOM with flywheel energy storage system for wind energy applications: Control design and simulation," *Electr. Power Syst. Res.*, vol. 80, no. 3, pp. 345-353, Mar. 2010.

[72] Wind Energy Technology Data Update: 2020 Edition. Lawrence Berkeley National Laboratory, Berkeley. [online]. Available: https://moodle.polymtl.ca/plugifile.php/413972/mod_page/content/70/Denmark_Energy%20Strategy%20for%202050_2011.pdf

[73] B. Zhang, W. Hu, P. Hou, J. Tan, M. Soltani, and Z. Chen, "Review of reactive power dispatch strategies for loss minimization in a DFIG-based wind farm," *Energies*, vol. 10, no. 7, p. 856, Jul. 2017.

[74] Y. Guo, H. Gao, Q. Wu, H. Zhao, J. Østergaard and M. Shahidehpour, "Enhanced voltage control of VSC-HVDC-connected offshore wind farms based on model predictive control," *IEEE Trans. Sustain. Energy*, vol. 9,

no. 1, pp. 474-487, Jan. 2018.
[75] Y. Guo, H. Gao, H. Xing, Q. Wu and Z. Lin, "Decentralized coordinated voltage control for VSC-HVDC connected wind farms based on ADMM," *IEEE Trans. Sustain. Energy*, vol. 10, no. 2, pp. 800-810, Apr. 2019.
[76] H. Zhao, Q. Wu, Q. Guo, H. Sun, S. Huang and Y. Xue, "Coordinated voltage control of a wind farm based on model predictive control," *IEEE Trans. Sustain. Energy*, vol. 7, no. 4, pp. 1440-1451, Oct. 2016.
[77] Y. Guo, H. Gao, Q. Wu, H. Zhao, and J. Østergaard, "Coordinated voltage control scheme for VSC-HVDC connected wind power plants," *IET Renew. Power Gener.*, vol. 12, no. 2, pp. 198-206, Nov. 2017.
[78] Y. Guo, H. Gao, Q. Wu, J. Østergaard, D. Yu, and M. Shahidehpour, "Distributed coordinated active and reactive power control of wind farms based on model predictive control," *Int. J. Elect. Power Energy Syst*., vol. 104, pp. 78-88, Jan. 2019.
[79] H. Zhao, Q. Wu, J. Wang, Z. Liu, M. Shahidehpour and Y. Xue, "Combined active and reactive power control of wind farms based on model predictive control," *IEEE Trans. Energy Convers.*, vol. 32, no. 3, pp. 1177-1187, Sept. 2017.
[80] S. Huang, Y. Gong, Q. Wu, F. Rong, "Two-tier combined active and reactive power control for VSC-HVDC connected large-scale wind farm cluster based on ADMM," *IET Renew. Power Gener.*, vol. 14, no. 8, pp.1379-1386, Jun. 2020.
[81] W. Qiao, R. G. Harley and G. K. Venayagamoorthy, "Coordinated reactive power control of a large wind farm and a STATCOM using heuristic dynamic programming," *IEEE Trans. Energy Convers.*, vol. 24, no. 2, pp. 493-503, Jun. 2009.
[82] E. DÍaz-Dorado, C. Carrillo and J. CidrÁs, "Control algorithm for coordinated reactive power compensation in a wind park," *IEEE Trans. Energy Convers.*, vol. 23, no. 4, pp. 1064-1072, Dec. 2008.
[83] W. Guo, F. Liu, J. Si, D. He, R. Harley, and S. Mei, "Approximate dynamic programming based supplementary reactive power control for DFIG wind farm to enhance power system stability," *Neurocomputing*, vol. 170, pp. 417-427, Dec. 2015.
[84] H. Fakham, A. Ahmidi, F. Colas, and X. Guillaud, "Multi-agent system for distributed voltage regulation of wind generators connected to distribution network," in *Proc. IEEE PES Conf. Innovative Smart Grid Technol. Eur.*, Gothenburg, Sweden, pp. 1-6. Oct. 2010.
[85] K. K. Mehmood, C. -H. Kim, S. U. Khan and Z. M. Haider, "Unified planning of wind generators and switched capacitor banks: a multiagent clustering-based distributed approach," *IEEE Trans. Power Syst.*, vol. 33, no. 6, pp. 6978-6988, Nov. 2018.
[86] T. Moger and T. Dhadbanjan, "Fuzzy logic approach for reactive power

coordination in grid connected wind farms to improve steady state voltage stability," *IET Renew. Power Gener.*, vol. 11, no. 2, pp. 351-361, 2016.

[87] X. Chen, L. Wang, H. Sun and Y. Chen, "Fuzzy logic based adaptive droop control in multiterminal HVDC for wind power integration," *IEEE Trans. Energy Convers.*, vol. 32, no. 3, pp. 1200-1208, Sept. 2017.

[88] L. Jerbi, L. Krichen, and A. Ouali, "A fuzzy logic supervisor for active and reactive power control of a variable speed wind energy conversion system associated to a flywheel storage system," *Elect. Power Syst. Res.*, vol. 79, no. 6, pp. 919-925, Jun. 2009.

[89] S. Behera and B. Subudhi, "A complete modeling and simulation of DFIG based wind turbine system using fuzzy logic control," *Front. Energy*, vol. 10, no. 2, pp. 143-154, 2016.

[90] E. Sáiz-Marín, E. Lobato, and I. Egido, "New challenges to wind energy voltage control. Survey of recent practice and literature review," *IET Renew. Power Gener.*, vol. 12, no. 3, pp. 267-278, Feb. 2018.

[91] F. M. Ebrahimi, A. Khayatiyan, and E. Farjah, "A novel optimizing power control strategy for centralized wind farm control system," *Renew. Energy*, vol. 86, no. 2, pp. 399-408, Feb. 2016.

[92] M. J. Hossain, H. R. Pota, M. A. Mahmud and M. Aldeen, "Robust control for power sharing in microgrids with low-inertia wind and PV generators," *IEEE Trans. Sustain. Energy*, vol. 6, no. 3, pp. 1067-1077, Jul. 2015.

[93] F. Baccino, F. Conte, S. Grillo, S. Massucco and F. Silvestro, "An optimal model-based control technique to improve wind farm participation to frequency regulation," *IEEE Trans. Sustain. Energy*, vol. 6, no. 3, pp. 993-1003, Jul. 2015.

[94] S. Huang, Q. Wu, Y. Guo, X. Chen, B. Zhou and C. Li, "Distributed voltage control based on ADMM for large-scale wind farm cluster connected to VSC-HVDC," *IEEE Trans. Sustain. Energy*, vol. 11, no. 2, pp. 584-594, Apr. 2020.

[95] R. Blasco-Gimenez, S. Añó-Villalba, J. Rodríguez-D'Derlée, F. Morant and S. Bernal-Perez, "Distributed voltage and frequency control of offshore wind farms connected with a diode-based HVdc Link," *IEEE Trans. Power Electron.*, vol. 25, no. 12, pp. 3095-3105, Dec. 2010.

[96] X. Yin and X. Zhao, "Deep neural learning based distributed predictive control for offshore wind farm using high fidelity LES data," *IEEE Trans. Ind. Electron.*, vol. 68, no. 4, pp. 3251-3261, Apr. 2021.

[97] Y. Guo, H. Gao, and Q. Wu, "Distributed cooperative voltage control of wind farms based on consensus protocol," *Int. J. Electr. Power Energy Syst.*, vol. 104, pp. 593-602, Jan. 2019.

[98] S. Huang, Q. Wu, Y. Guo, and Z. Lin, "Bi-level decentralised active power control for large-scale wind farm cluster," *IET Renew. Power Gener.*, vol. 12, no. 13, pp. 1486-1492, Oct. 2018.

[99] S. Huang, Q. Wu, J. Zhao and W. Liao, "Distributed optimal voltage control for VSC-HVDC connected large-scale wind farm cluster based on analytical target cascading method," *IEEE Trans. Sustain. Energy*, vol. 11, no. 4, pp. 2152-2161, Oct. 2020.

[100] S. Huang, Q. Wu, W. Liao, G. Wu, X. Li and J. Wei, "Adaptive droop-based hierarchical optimal voltage control scheme for VSC-HVdc connected offshore wind farm," *IEEE Trans. Ind. Informat.* , vol. 17, no. 12, pp. 8165-8176, Dec. 2021.

[101] S. Huang, Q. Wu, Y. Guo and F. Rong, "Hierarchical active power control of DFIG-based wind farm with distributed energy storage systems based on ADMM," *IEEE Trans. Sustain. Energy*, vol. 11, no. 3, pp. 1528-1538, Jul. 2020.

[102] L. Ye *et al*., "Hierarchical model predictive control strategy based on dynamic active power dispatch for wind power cluster integration," *IEEE Trans. Power Syst.*, vol. 34, no. 6, pp. 4617-4629, Nov. 2019.

[103] X. Kong, X. Liu, L. Ma, and K. Y. Lee, "Hierarchical distributed model predictive control of standalone Wind/Solar/Battery power system," *IEEE Trans. Syst., Man, Cybern. Syst.*, vol. 49, no. 8, pp. 1570-1581, Aug. 2019.

[104] W. Bao, Q. Wu, L. Ding, S. Huang and V. Terzija, "A hierarchical inertial control scheme for multiple wind farms with BESSs based on ADMM," *IEEE Trans. Sustain. Energy*, vol. 12, no. 2, pp. 751-760, Apr. 2021.

[105] M. Ghanavati and A. Chakravarthy, "PDE-based modeling and control for power generation management of wind farms," *IEEE Trans. Sustain. Energy*, vol. 10, no. 4, pp. 2104-2113, Oct. 2019.

[106] L. Yuan, K. Meng, and Z. Y. Dong, "Hierarchical control scheme for coordinated reactive power regulation in clustered wind farms," *IET Renew. Power Gener.*, vol. 12, no. 10, pp. 1119-1126, Jul. 2018.

[107] G. Li, H. Ye, "Hierarchical nonlinear model predictive control for frequency support of wind farm," *Int. J. Elect. Power Energy Syst*., vol. 129, Jul. 2021.

[108] Q. Wu, T. Takarics, and V. Akhmatov, "Coordinated voltage and reactive power control scheme of HVAC meshed offshore grid of offshore wind power plant at Kriegers Flak," in *Proc. 8th Renew. Power Gener. Conf.*, Shanghai, China, Oct. 2019.

[109] H. Yassami, F. Bayat, A. Jalilvand, and A. Rabiee, "Coordinated voltage control of wind-penetrated power systems via state feedback control," *Int. J. Electr. Power Energy Syst.*, vol. 93, pp. 384-394, Dec. 2017.

[110] H. Yassami, A. Rabiee, A. Jalilvand, and F. Bayat, "Model predictive control scheme for coordinated voltage control of power systems at the presence of volatile wind power generation," *IET Gener., Transmiss. Distrib.*, vol. 12, no. 8, pp. 1922-1928, 2018.

[111] J. Ouyang, T. Tang, J. Yao, and M. Li, "Active voltage control for DFIG-

based wind farm integrated power system by coordinating active and reactive powers under wind speed variations," *IEEE Trans. Energy Convers.*, vol. 34, no. 3, pp. 1504-1511, Sep. 2019.

[112] J. Liu, Y. Xu, J. Qiu, Z. Dong, and K. Wong, "Non-network solution coordinated voltage stability enhancement with STATCOM and UVLS for wind-penetrated power system," *IEEE Trans. Sustain. Energy.*, vol. 11, no. 3, pp. 1559-1568, Jul. 2020.

[113] Z. Tang, D. J. Hill, and T. Liu, "Two-stage voltage control of subtransmission networks with high penetration of wind power," *Control Eng. Pract.*, vol. 62, pp. 1-10, May. 2017.

[114] Z. Li, Z. Xu, Y. Xie, D. Qi, and J. Zhang, "Two-stage ADMM-based distributed optimal reactive power control method for wind farms considering wake effects," *Global Ener. Interconn.*, vol. 4, no. 3, pp. 251-260, Jun. 2021.

[115] P. Li, L. Song, J. Qu, Y. Huang, X. Xu, X. Lu, and S. Xia, "A two-stage distributionally robust optimization model for wind farms and storage units jointly operated power systems," *IEEE Access*, vol. 9, pp. 111132-111142, Jul. 2021.

[116] S. Huang, P. Li, Q. Wu, F. Li, and F. Rong, "ADMM-based distributed optimal reactive power control for loss minimization of DFIG-based wind farms," *Int. J. Elect. Power Energy Syst*., vol. 118, pp.105827, Jun. 2020.

[117] A. Rabiee and A. Soroudi, "Stochastic multiperiod OPF model of power systems with HVDC-connected intermittent wind power generation," *IEEE Trans. Power Del.*, vol. 29, no. 1, pp. 336-344, Feb. 2014.

[118] A. Panda and M. Tripathy, "Optimal power flow solution of wind integrated power system using modified bacteria foraging algorithm," *Int. J. Elect. Power Energy Syst*., vol. 54, no. 1, pp. 306-314, Jan. 2014.

[119] L. Xie, H. D. Chiang, and S. H. Li, "Optimal power flow calculation of power system with wind farms," in *Proc. IEEE Power Energy Soc. Gen. Meeting*, San Diego, CA, USA, Jul. 2011, pp. 1-6.

[120] M. B. Wafaa and L. A. Dessaint, "Multi-objective stochastic optimal power flow considering voltage stability and demand response with significant wind penetration," *IET Gener., Transm. & Distrib.*, vol. 11, no. 14, pp. 3499-3509, Sept. 2017.

[121] S. M. Mohseni-Bonab, A. Rabiee, and B. Mohammadi-Ivatloo, "Voltage stability constrained multi-objective optimal reactive power dispatch under load and wind power uncertainties: a stochastic approach," *Renew. Energy*, vol. 85, pp. 598-609, Jan. 2016.

[122] P. Hou, W. Hu, B. Zhang, M. Soltani, C. Chen, and Z. Chen, "Optimised power dispatch strategy for offshore wind farms," *IET Renew. Power Gener.*, vol. 10, no. 3, pp. 399-409, Mar. 2016.

[123] B. Zhang, P. Hou, W. Hu, M. Soltani, C. Chen, and Z. Chen, "A reactive power dispatch strategy with loss minimization for a DFIG-based wind

farm," *IEEE Trans. Sust. Energy,* vol. 7, no. 3, pp. 914-923, Jul. 2016.
[124] Q. Zhou, M. Shahidehpour, A. Paaso, S. Bahramirad, A. Alabdulwahab, and A. Abusorrah "Distributed control and communication strategies in networked microgrids," *IEEE Commun. Surveys Tuts.*, vol. 22, no. 4, pp. 2586-2633, Sept. 2020.
[125] Q. Zhou, Z. Tian, M. Shahidehpour, X. Liu, A. Alabdulwahab, and A. Abusorrah, "Optimal consensus-based distributed control strategy for coordinated operation of networked microgrids," *IEEE Trans. Power Syst.*, vol. 35, no. 3, pp. 2452-2462, May 2020.
[126] S. Huang, Q. Wu, W. Bao, N. D. Hatziargyriou, L. Ding, and F. Rong, "Hierarchical optimal control for synthetic inertial response of wind farm based on ADMM," *IEEE Trans. Sust. Energy*, vol. 12, no. 1, pp. 25-35, Jan. 2021.
[127] D. Xu, Q. Wu, B. Zhou, C. Li, L. Bai, and S. Huang, "Distributed multi-energy operation of coupled electricity, heating and natural gas networks," *IEEE Trans. Sust. Energy*, vol. 11, no. 4, pp. 2457-2469, Oct. 2020.
[128] J. Lavaei and S. H. Low, "Zero duality gap in optimal power flow problem," *IEEE Trans. Power Syst.*, vol. 27, no. 1, pp. 92-107, Feb. 2012.
[129] S. Bahrami, F. Therrien, V. W. S. Wong, and J. Jatskevich, "Semidefinite relaxation of optimal power flow for AC-DC grids," *IEEE Trans. Power Syst.*, vol. 32, no. 1, pp. 289-304, Jan. 2017.
[130] A. Venzke and S. Chatzivasileiadis, "Convex relaxations of probabilistic AC optimal power flow for interconnected AC and HVDC grids," *IEEE Trans. Power Syst.*, vol. 34, no. 4, pp. 2706-2718, Jul. 2019.
[131] H. G. Yeh, D. F. Gayme, and S. H. Low, "Adaptive VAR control for distribution circuits with photovoltaic generators," *IEEE Trans. Power Syst.*, vol. 27, no. 3, pp. 1656-1663, Aug. 2012.
[132] S. Cai, Y. Xie, Q. Wu, and Z. Xiang, "Robust MPC-based microgrid scheduling for resilience enhancement of distribution system," *Int. J. Elect. Power Energy Syst.*, vol. 121, pp. 106068, Oct. 2020.
[133] F. Shen, J. C. Lopez, Q. Wu, M. J. Rider, T. Lu, and N. D. Hatziargyriou, "Distributed self-healing scheme for unbalanced electrical distribution systems based on alternating direction method of multipliers," *IEEE Trans. Power Syst.*, vol. 35, no. 3, pp. 2190-2199, May 2020.
[134] R. Li, W. Wei, S. Mei, Q. Hu, and Q. Wu, "Participation of an energy hub in electricity and heat distribution markets: an MPEC approach," *IEEE Trans. Smart Grid,* vol. 10, no. 4. pp. 3641-3653, Jul. 2019.
[135] S. Huang, Q. Wu, Y. Guo, and Z. Lin, "Bi-level decentralized active and reactive power control for large-scale wind farm cluster," *Int. J. Elect. Power Energy Syst.*, vol. 111, pp. 201-215, Oct. 2019.
[136] J. Tan, Q. Wu, M. Zhang, W. Wei, N. Hatziargyriou, F. Liu, and T. Konstantinou, "Wind power scenario generation with non-separable spatio-temporal covariance function and fluctuation-based clustering," *Int. J. Elect.*

Power Energy Syst., vol. 130, pp. 106955, Sep. 2021.
[137] W. Liao, P. Li, Q. Wu, S. Huang, G. Wu, and F. Rong, "Distributed optimal active and reactive power control for wind farms based on ADMM," *Int. J. Elect. Power Energy Syst*., vol. 129, pp. 106799, Jul. 2021.
[138] B. Zhou, H. Duan, Q. Wu, H. Wang, S. W. Or, K. W. Chan, and Y. Meng, "Short-term prediction of wind power and its ramp events based on semi-supervised generative adversarial," *Int. J. Elect. Power Energy Syst*., vol. 125, pp. 106411, Feb. 2021.
[139] K. Meng, W. Zhang, Y. Li, Z. Y. Dong, Z. Xu, K. P. Wong, and Y. Zheng, "Hierarchical SCOPF Considering Wind Energy Integration Through Multiterminal VSC-HVDC Grids," *IEEE Trans. Power Systems*, vol. 32, no. 6, pp. 4211-4221, Nov. 2017.
[140] M. Aragüés-Peflalba, A. Egea-Àlvarez, O. Gomis-Bellmunt, and A. Sumper, "Optimum voltage control for loss minimization in HVDC multi-terminal transmission systems for large offshore wind farms," *Elect. Power Syst. Res.*, vol. 89, pp. 54-63, Aug. 2012.
[141] Fan J, Tong X, and Zhao J, "Unified optimal power flow model for AC/DC grids integrated with natural gas systems considering gas-supply uncertainties," *J. Modern Power Syst. Clean Energy*, vol. 6, no. 6, pp. 1193-1203, Nov. 2018.
[142] S. Huang, Q. Wu, Y. Guo, and F. Rong, "Optimal active power control based on MPC for DFIG-based wind farm equipped with distributed energy storage systems," *Int. J. Elect. Power Energy Syst*., vol. 113, pp. 154-163, Dec. 2019.
[143] Y. Guo, H. Gao and Z. Wang, "Distributed online voltage control for wind farms using generalized fast dual ascent," *IEEE Trans. Power Syst.*, vol. 35, no. 6, pp. 4505-4517, Nov. 2020.
[144] T. Erseghe, "Distributed optimal power flow using ADMM," *IEEE Trans. Power Syst.*, vol. 29, no. 5, pp. 2370-2380, Sept. 2014.
[145] M. Yan, X. AI, J. Wen, Y. He and Y. Zhang, "Decentralized optimization for multi-area optimal transmission switching via iterative ADMM," in *Proc. IEEE Power Energy Soc. Gen. Meeting (PESGM)*, pp. 1-5, Aug. 2018.
[146] A. Turk, Q. Wu, and M. Zhang, "Model predictive control based real-time scheduling for balancing multiple uncertainties in integrated energy system with power-to-x," *Int. J. Elect. Power Energy Syst*., vol. 130, pp. 107015, Sep. 2021.
[147] J. Zhao, Y. Liu, H. Wang, and Q. Wu, "Receding horizon load restoration for coupled transmission and distribution system considering load-source uncertainty," *Int. J. Elect. Power Energy Syst.*, vol. 116, pp. 105517, Mar. 2020.
[148] F. Zhang, A. Fu, L. Ding, and Q. Wu, "MPC based control strategy for bat-

tery energy storage station in a grid with high photovoltaic power penetration," *Int. J. Electr. Power Energy Syst.*, vol. 115, pp. 105448, Feb. 2020.

[149] H. Zhao, Z. Lin, Q. Wu, and S. Huang, "Model predictive control based coordinated control of multi-terminal HVDC for enhanced frequency oscillation damping," *Int. J. Electr. Power Energy Syst.*, vol. 123, pp. 106328, Dec. 2020.

[150] H. Ding, Z. Hu and Y. Song, "Rolling optimization of wind farm and energy storage system in electricity markets," *IEEE Trans. Power Syst.*, vol. 30, no. 5, pp. 2676-2684, Sept. 2015.

[151] P. Wang, Q. Wu, S. Huang, C. Li and B. Zhou, "ADMM-based distributed active and reactive power control for regional AC power grid with wind farms," *J. Modern Power Syst. Clean Energy*, Jun. 2021. Early Access.

[152] S. Xia, Z. Ding, M. Shahidehpour, K. W. Chan, S. Bu and G. Li, "Transient stability-constrained optimal power flow calculation with extremely unstable conditions using energy sensitivity method," *IEEE Trans. Power Syst.*, vol. 36, no. 1, pp. 355-365, Jan. 2021.

[153] Z. Li, H. Sun, Q. Guo, J. Wang, and G. Liu, "Generalized master-slave-splitting method and application to transmission-distribution coordinated energy management," *IEEE Trans. Power Syst.*, vol. 34, no. 6, pp. 5169-5183, Nov. 2019.

[154] C. Zhang, H. Chen, Z. Liang, M. Guo, D. Hua and H. Ngan, "Reactive power optimization under interval uncertainty by the linear approximation method and its modified method," *IEEE Trans. Smart Grid*, vol. 9, no. 5, pp. 4587-4600, Sept. 2018.

[155] C. Zhang, H. Chen, K. Shi, et al., "A multi-time reactive power optimization under interval uncertainty of renewable power generation by an interval sequential quadratic programming method," *IEEE Trans. Sustain. Energy*, vol. 10, no. 3, pp. 1086-1097, Jul. 2019.

[156] W. Teng, H. Wang, and Y. Jia, "Construction and control strategy research of black start unit containing wind farm," in *Proc. IEEE Region 10th Annu. Int. Conf., TENCON*, pp. 1-5, Jan. 2016.

[157] E. Naderi, H. Narimani, M. P. Kasmaei, F. V. Cerna, M. Marzband, and M. Lehtonen, "State-of-the-art of optimal active and reactive power flow: a comprehensive review from various standpoints," *Processes*, vol. 9, no. 8, pp. 1-48, Jul. 2021.